Modeling Temperature Effects on Vector-Borne Disease Dynamics

Fadoua El Moustaid

Dissertation submitted to the faculty of the Virginia Polytechnic Institute and State University in partial fulfillment of the requirements for the degree of
Doctor of Philosophy
In
Biological Sciences

Leah R. Johnson
Dana M. Hawley
Lauren M. Childs
Sally L. Paulson

August 5^{th}, 2019
Blacksburg, VA

Keywords— temperature, vector-borne diseases, mathematical modeling, mosquito density, dengue, bluetongue

Modeling Temperature Effects on Vector-Borne Disease Dynamics

Fadoua El Moustaid

ABSTRACT

Vector-borne diseases (VBDs) cause significant harm to humans, plants, and animals worldwide. For instance, VBDs are very difficult to manage, as they are governed by complex interactions. VBD transmission depends on the pathogen itself, vector-host movement, and environmental conditions. Mosquito-borne diseases are a perfect example of how all these factors contribute to changes in VBD dynamics. Although vectors are highly sensitive to climate, modeling studies tend to ignore climate effects. Here, I am interested in the arthropod small vectors that are sensitive to climate factors such as temperature, precipitation, and drought. In particular, I am looking at the effect of temperature on vector traits for two VBDs, namely, dengue, caused by a virus that infects humans and bluetongue disease, caused by a virus that infects ruminants. First, I collect data on mosquito traits' response to temperature changes, this includes adult traits as well as juvenile traits. Next, I use these traits to model mosquito density, and then I incorporate the density into our mathematical models to investigate the effect it has on the basic reproductive ratio R_0, a measure of how contagious the disease is. I use R_0 to determine disease risk. For dengue, my results show that using mosquito life stage traits response to temperature improves our vector density approximation and disease risk estimates. For bluetongue, I use midge traits response to temperature to show that the suitable temperature for bluetongue risk is between 21.5 °C and 30.7 °C. These results can inform future control and prevention strategies.

Modeling Temperature Effects on Vector-Borne Disease Dynamics

Fadoua El Moustaid

GENERAL AUDIENCE ABSTRACT

Infectious diseases are a type of illness that occurs when microorganisms spread between hosts. Some infectious diseases are directly transmitted and some require indirect transmission such as vector-borne diseases (VBDs). Each VBD requires the presence of a vector for the disease to be transmitted. For example, dengue that puts 40% of the world population at risk, requires mosquitoes to transmit the disease between humans. My research aims to investigate how the main climate factor, temperature, influences the spread of VBDs. I develop mathematical and statistical models that explain the effect of temperature on vector traits of a mosquito-borne disease (dengue) and a midge-borne disease (bluetongue) and investigate modeling formulas to improve our estimates for dengue mosquito densities. My results can be used to inform future prevention and control strategies.

Acknowledgements

First I would like to express my extreme gratitude to Allah Subhanaho Wataala for allowing me to pursue a Ph.D. and helping me get through all the hardship. Second, I want to thank my adviser, Leah Johnson, my co-adviser, Dana Hawley, and my committee members, Lauren Childs, and Sally Paulson for all their support and encouragement. Then, I want to thank my two families, here in Blacksburg, David and Brenda Roberts and in Morocco, my dad, Bouchaib El Moustaid, my mom, Bouchra Lafraoui, and my three sisters, Safa El Moustaid, Zineb El Moustaid, and Hafsa El Moustaid for all their support throughout this journey.

Contents

Chapter 1

Vector-Borne Diseases (VBDs)

1.1 Overview

Infectious diseases are illnesses caused by the transmission of pathogens such as viruses, parasites, and fungi. Infectious diseases can be directly transmitted, for example through host to host contact, or indirectly transmitted through the water or other mechanisms, including insect bites [1]. Infectious disease outbreaks can cause significant harm to the host population and each infectious disease may be disrupted with various preventative measures such as insecticide spraying [2].

An example of indirectly transmitted infectious diseases are vector-borne diseases (VBDs), which are a major threat to human, animal, and plant health [3, 4, 5]. Vectors are typically invertebrates capable of spreading pathogens, protozoa, and worms (Table 1.1). The mechanisms of spread range from vector bites, as in the case of dengue, to vector faeces, as in the case of Chagas' disease. Examples of vectors also include ticks that cause Lyme disease transmission.

Moreover, there are other vectors responsible for VBD transmission to animals and plants such as midges and psyllids (Table 1.1). The biting midges transmit the pathogen that causes bluetongue disease which infects all ruminants. Psyllids spread the pathogen causing Huanglongbing disease that is one of the most damaging citrus plants diseases, known as citrus greening disease. Fruits produced by infected trees are green and bitter which makes them unsuitable for sale. In addition, infected trees eventually die within a

few years from infection [6]. Although these are not human diseases and do not affect our health, they do affect the animal and agriculture industries [6, 7].

VBDs represent more than 17% of all infectious diseases, many of which are human diseases and are considered preventable when appropriate protective measures are applied [8, 9]. The possibility of preventing VBD spread is the main motivation for most modeling efforts invested in VBDs. The better we understand vector-host dynamics, the more we can prevent infection outbreaks [10]. Mosquitoes represent the most targeted vectors for research, as they are responsible for diseases causing a large number of annual deaths. In addition, having limited knowledge of some new emerging diseases such as Zika makes it a necessity to further study mosquito-borne diseases (MBDs). This is especially true since most MBDs are caused by similar vectors, carrying different pathogens and exposed to similar climate conditions . Hence, studying dengue, and how climate factors affect its spread, can give some insight on other MBDs such as Zika.

1.2 Role of climate factors

Prior studies highlight the impact of climate factors on VBDs [11, 12, 13]. Changes in precipitation, seasonal temperature, and rainfall influence the life cycle and behavior of arthropod vectors leading to variation in VBD dynamics [14, 15]. Therefore, understanding the role played by climate factors in directing the spread of VBDs is important, and will guide our modeling methods for investigating VBDs.

Climate factors affect vectors' life cycle and behavior, as well as the distribution of humans and animals, leading to significant variation in transmission seasons [16, 17, 18, 19, 20]. Although studies show the effect of climate factors on vector traits, there is a lack of strong evidence on the way these effects occur [21]. The variation in temperature, rainfall and precipitation not only affect vector traits, but they also affect the pathogens they transmit [22, 23, 24]. All of these components contribute to the complexity of VBD dynamics, making it challenging to determine whether/when and

Vector	**Disease**
Mosquitoes:	
Aedes aegypti	Dengue, yellow fever, chikungunya, Zika virus
Aedes albopictus	Chikungunya, dengue, West Nile virus
Culex quinquefasciatus	Lymphatic filariasis
Anopheles	Malaria, lymphatic filariasis (in Africa)
Haemagogus	Yellow fever
Sandflies	Leishmaniasis
Triatomine bugs	Chagas disease
Ticks	Crimean-Congo haemorrhagic fever, tick-borne encephalitis, typhus, Lyme disease
Fleas	Plague, Murine typhus
Flies (various species)	Human African trypanosomiasis, onchocerciasis
Midges	Bluetongue disease
Citrus psyllid	Huanglongbing (HLB) also called citrus greening

Table 1.1: Examples of important vectors and the corresponding vector-borne diseases they are able to transmit [8]

where transmission will occur. The dynamics of host-vector contact are sensitive to climate-related natural disasters (such as floods) as well as sudden changes in temperatures, rainfall, and humidity. I summarize the impact of these climate factors into two categories, namely, temperature and precipitation.

Temperature Impact: Temperature is a major climate factor affecting the life cycle of both vectors and pathogens. The daily changes in temperature influence the pathogen's growth and development rates within vectors, which influence the success of disease transmission when biting occurs [25]. Seasonal and daily temperature changes, on the other hand, affect the survival and reproduction of vectors. Depending on the vector species, its survival can increase within a specific temperature range and decrease above or below certain temperature thresholds [26, 27, 28, 29]. Moreover, temperature can alter the susceptibility of vectors to certain pathogens, either by reducing their body size or by limiting their activity [30, 31, 32, 33, 34]. The vector blood feeding rate and host contact also vary with temperature, which in turn affects the vector population growth and probability of transmission[33, 35, 36].

Precipitation Impact: Vectors can also be affected by rainfall. The availability of multiple water poolings can lead to an increase in vector breeding sites [24]. However, an excess of rain can cause flooding, which eliminates vector habitats or creates them depending on species, thus leading to a perturbation in their population size. Low rainfall also plays a major role in VBD dynamics. For instance, low rates of rain are the main drivers of dry season malaria and West Nile virus epidemics [37, 38]. Drought causes rivers to dry and slow, therefore forming new habitats for vectors and increasing vector-host interactions as there are fewer sources of water. Moreover, vector survival changes monotonically with humidity, hence transmission seasons tend to be longer in a more humid environment [39].

Temperature and precipitation both have local and global effects on VBDs. Vector traits respond differently to changes in temperature and precipitation. For VBD models to be useful for prediction, they must incorporate the impact of climate factors on the disease. Here I propose to investigate the effects of temperature on dengue and bluetongue.

1.3 Modeling VBDs

Modeling has played an important role in advancing VBD risk management [40]. Moreover, understanding the response of vectors to environmental changes allows us to develop accurate and effective mathematical models [41, 42]. One way to investigate climate factors' effect on vector traits is to include those factors into mathematical models.This can help us project the progress of VBDs and inform public health interventions.

Vector-borne disease dynamics involve multiple complex processes that range from a micro-scale, where vectors interact with pathogens causing the infection, to a macro-scale where both vectors and hosts are affected by global changes in climate. Understanding these mechanisms is difficult, and scientists have used modeling to describe the effect of climate on patterns of VBDs.

Early modeling approaches highlighted the seasonality patterns in vector-borne dynamics and the need for understanding climate effect on VBDs [43]. However, there was a lack of theoretical foundation in the thermal biology of ecthoterms which led modelers to use different ways to understand the relationship between temperature and modeling related components [44, 45, 46, 47]. Since then, vector traits' dependence on temperature has been investigated and used in models [48, 37, 41, 49, 50, 27, 51, 52]. To model temperature effects we should take into account that it has an impact on multiple vector traits. Therefore, introducing a single function that represents temperature in the model (as used in previous models [53, 54]) may not correctly represent the impact of temperature on vector traits. However, it could be a good first step to understand the impact of temperature variation on the model. Moreover, interactions between hosts and vectors have a complex structure and are challenging to study, especially when climate factors are taken into consideration.

When analyzing my models, I will focus on the quantities that can provide information on the epidemic, such as the basic reproductive ratio, denoted (R_0), which is a fundamental concept in epidemiology. It is defined as the number of new infected individuals caused by introducing one infected

individual into an entirely susceptible population [55, 56]. If $R_0 < 1$, this indicates that the disease dies out, while $R_0 > 1$ means that the disease spreads through the susceptible population. This threshold metric is very helpful when deciding suitable control strategies and when exactly should they be applied. When it is possible to accurately predict the value of R_0 we can determine the magnitude of possible new cases given currently infected ones, and therefore get insight on the spread of an infectious disease [57, 58]. However, because of the complexity of models, it is usually very hard to explicitly quantify R_0. With that being said, we can analyze R_0 numerically as a function of the parameters. R_0 is a dimensionless number and can be expressed as follows:

$$R_0 \propto \left(\frac{\text{infection}}{\text{contact}}\right)\left(\frac{\text{contact}}{\text{time}}\right)\left(\frac{\text{time}}{\text{infection}}\right)$$

where the first ratio indicates the probability of infection given infectious contact (transmissibility), the second ratio is the average rate of contact between susceptible and infected individuals, and the last ratio is the duration of infectiousness.

Moreover, R_0 takes different forms depending on the structure of the mathematical model. For example, in Johnson et al. (2015) R_0 has the following form

$$R_0 = \sqrt{\frac{V}{Hd}\frac{a^2 bc \exp(-\mu/\nu)}{\mu}}, \quad \text{with} \quad V = \frac{F \cdot p_{EA} \cdot 1/\rho_A}{\mu^2}$$

where V is the vector density, a is the biting rate, bc is vector competence, μ is the mortality rate of adult vectors, ν is the parasite development rate, H is the host density, d is the host recovery rate, F is the number of eggs produced per female per day, p_{EA} is the probability that an egg will hatch and the larvae will survive to the adult stage, and $1/\rho_A$ is the adult vector development rate (with ρ_A being adult development time). All of these parameters are directly related to vector traits that contribute to variations in R_0, hence they need to accurately reflect the biology governing VBD dynamics. Thus,

predicting R_0 as well as VBD transmission requires understanding of traits corresponding to the vector transmitting the pathogen.

We can combine mathematical models and statistical tools (such as Bayesian Inference) to inform the model parameters with data, hence improve our results. For instance, studying the effect of temperature on malaria vector traits shows that the dependence between traits and temperature is non-linear [26, 59, 60, 61]. Johnson et al. (2015) used a Bayesian approach leading to curves fitting collected data on vector traits. The traits considered include biting rate, vector competence, daily survival probability, parasite and vector development rates, eggs to adult survivorship and eggs per female per day.

Thereafter, all these functions representing different traits contribute to the derivation of R_0. Having an analytical formula of R_0 that reflects the role of temperature allows us to study the indirect effect that temperature has on the spread of VBDs. This means that we can look at how temperature changes lead to fluctuations in R_0 which in turn drive the disease to die out or spread.

1.4 Data sets

Testing our model requires two types of data, case data on reported VBD infections and lab data on vector traits' dependence on environmental factors.

VBD case data

We have access to dengue incidence and environmental data from Iquitos, Peru and San Juan, Puerto Rico from 2000 until 2010. The data include human population size, min and max temperatures, precipitation, El Niño, as well as dengue incidence reported cases. The Iquitos dengue data have been studied before and the results showed that there is no correlation between the reported new cases and temperature [62]. This result can be interpreted using three possible explanations. The first is that the impact of temperature is indirect. Temperature affects vector traits, which in turn elongate transmission seasons and delay incidence peaks. Second, because of this in-

direct interaction, temperature effect is non-linear, and therefore will not be viewed through a simple linear correlation. Lastly, it is possible, although highly unlikely, that temperature was not the main driver in this case and did not have an impact on dengue spread. The same study also showed that performing a prevention strategy (spraying insecticide) in some years led to a significant decrease of incidence peak. However, this did not eradicate the diseases completely; hence, we need to further study how can we possibly make the control and prevention strategies more efficient in the future.

Vector trait data

Vector traits tend to have a hump shaped curve when plotted against temperature (Figure 1.1), and these data can be used to approximate the fitted curves used later on in the mathematical model. I am interested in laboratory experiments measuring vector traits varying with constant temperatures. Ideally, I search for three or more data points capturing a minimum and a maximum temperature and I use a Bayesian model to fit the thermal curve. Because I am only interested in the effect of temperature, I exclude field experiments since the variation in traits is affected by multiple factors.

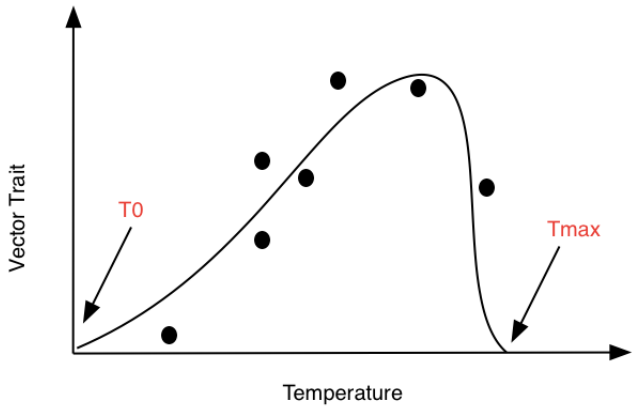

Figure 1.1: An illustration of vector traits' dependence on temperature, where T_0 is the minimum temperature and T_{max} is the maximum temperature for that particular trait.

1.5 Scope of dissertation

For the purpose of my work, I am interested in studying a mosquito-borne disease, dengue, and a midge-borne disease, bluetongue. I will incorporate environmental data in our model through vector traits, specifically those appearing in the R_0 formula. Then, I use reported cases to determine the time lag at which the correlation between R_0 and cases is the strongest. For bluetongue, we do not have access to case data. For validation, I will combine the available midge distribution with our model findings to determine disease risk maps that can help detect bluetongue risk for certain areas.

Here, I look at the dependence of each vector trait on temperature from fitting lab data in a Bayesian framework as done by Johnson et al. (2015). I use this trait based approach because it allows me to study the effect of temperature on traits related to transmission rates. Because these temperature-dependent traits can be included in the models as unimodal thermal responses, I can determine the suitable temperatures at which disease transmission is likely to occur which can provide useful insights to inform control and prevention strategies. In particular, my mathematical model will include parameter functions derived to fit dengue and bluetongue vector traits' response to temperature changes and my main objective is to explain dengue and bluetongue patterns driven by temperature.

My approach requires finding lab data from previous studies. Specifically, I need data on vector traits changing with temperature. My goal is to perform a study similar to Johnson et al. (2017) for the two dengue mosquitoes and bluetongue midges to see how their traits change in an environment with varying temperature.

In Chapter 2, I will present the mathematical model that explains all mosquito life stages dynamics leading to adult mosquito density. The data needed for our model will be collected from the literature and fitted using a Bayesian model in Chapter 3. In Chapter 4, I will model the dynamics of bluetongue disease. Then I summarize my work in Chapter 5.

Chapter 2

Modeling Temperature Effect on Dengue Mosquito *Aedes aegypti*'s Density

Abstract

Mosquito density plays an important role in the spread of mosquito borne diseases such as dengue and Zika. While it remains very challenging to estimate the density of mosquitoes, modelers have tried different methods to represent it in mathematical models. The goal of this paper is to investigate the various ways mosquito density has been quantified as well as to propose a dynamical system model that includes details of mosquito life stages leading to the adult population. We first discuss the mosquito traits involved in deriving mosquito density, especially those that are mostly temperature dependent. Then, we evaluate different forms of mosquito densities based on these traits, and explore the effect of their variation with temperature. Finally, we compare these approximations to *Aedes aegypti* data to discuss the outcomes of each density estimate. Our results show that the regression using the sine function is the best estimate for *Aedes aegypti* abundance data globally. However, the other density forms are better estimates for the local peaks.

Keywords— mathematical modeling, mosquito density, temperature, dengue, mosquito borne disease

2.1 Introduction

Mosquitoes are among the deadliest insects and animals in the world due to all the pathogens they transmit [63, 64]. In particular, dengue is a life-threatening disease caused by dengue virus spread by mosquitoes [65, 66]. Currently, there is no effective vaccine or cure for dengue, hence dengue prevention relies solely on vector control [67]. Thus, improving our current prevention and control strategies can help reduce severity of ongoing outbreaks.

While the research is ongoing to find a cure, the primary goal of modelers is to understand the dynamics of mosquito-borne diseases and to inform future prevention and control strategies [52]. For example, predicting dengue transmission is valuable when deciding the appropriate control measures for a given outbreak [68]. Predicting mosquito density and location is important when implementing an insecticide spraying strategy to prevent an outbreak [69, 70]. These types of prediction require a deep understanding of the ecology of mosquitoes. Thus, mosquitoes are one of the most studied vectors because they transmit multiple mosquito-borne diseases [71].

Because mosquitoes are highly sensitive to climate factors, understanding the role of the environment is important when modeling dengue [72]. In particular, temperature is an important determinant of dengue mosquito density, since it affects the mosquito traits. These traits associated with each of the life stages all contribute to the approximation of the total mosquito density.

The way the total mosquito density has been modeled in the past ignored the underlying characteristics of each stage as well as the role of climate factors. In a review of literature conducted by Legros et. al. [73], they highlighted the importance of further investigating density-dependent for *A. aegypti* and the need for further empirical studies to reduce our uncertainty when estimating mosquito density. In another study, an approximation that depends directly on adult traits has been used [74]. In other cases, a sine formula has been used to estimate mosquito density while taking into account possible seasonal fluctuations as a response to temperature changes [75, 76].

Here we are interested in quantifying female mosquito density as a result of life stages dynamics and compare it to approximated densities that depend directly on mosquito traits. The goal of this paper is to compare four different forms of mosquito density, investigate their response to temperature, and discuss the difference between estimates provided by each form when compared to *A. aegypti* density data.

2.2 Methods

2.2.1 Mosquito life stages

The mosquitoes responsible for spreading dengue are *Aedes aegypti*, the main dengue vector worldwide, and *Aedes albopictus*, mostly a secondary vector (main vector in some asian countries such as India) [77, 72]. They go through three juvenile life stages, egg, larvae, and pupae, before they emerge as adults. The time spent within each juvenile life stage varies between species because of the life history and genetic differences, as well as within species since each of the life stages is sensitive to environmental conditions [66]. The four life stages differ in length and characteristics. For instance, the eggs stage starts when adult females lay their eggs on a wet surface, or in moist soil, as only a small amount of water is required [72]. Eggs will hatch after a few days or can survive for months, which occurs when eggs become dry and prevents them from developing to the next stage [78, 79]. Diapause eggs can survive unfavorable environmental conditions and thus alter the population density throughout the year because these eggs are ready to hatch anytime the environmental conditions become suitable. This in turn can affect the transmission season into starting earlier than expected or lasting a longer period [80].

The larval stage starts when eggs hatch in wet conditions and continue to develop in water. Larvae are filter-feeders and air-breathers. The larval stage is when mosquitoes begin shaping their adult features, such as wings, and develop their initial body size characteristic [72, 79, 81]. This stage has four sub-stages called instars where larvae continue to compete over space and resources often leading to death due to crowding [82]. For this, we include

in our model a density-dependent mortality term to incorporate the loss of individuals during this stage.

The larval stage is followed by the pupal stage. Pupae live and move in water and breath through their respiratory horns. During this stage, the male reproductive organs mature before females (protandry), that is the earlier sexual maturation of males compared to conspecific females [83, 84]. Pupae emerge as adults and mate shortly before flying away, then the females start looking for their first blood meal. Adult female mosquitoes use blood meals from humans and animals for their reproduction. This process enables the transmission of pathogens.

Researchers usually focus on adult mosquito traits when modeling mosquito-borne disease since they are the ones transmitting the pathogen. Because temperature affects mosquito traits at every life stage, we argue that modeling should implement life stages as well. Here, we investigate the effect of temperature on life stages and compare four models estimating mosquito abundance. Figure 2.1 shows a diagram describing the mosquito life cycle from eggs through adult females.

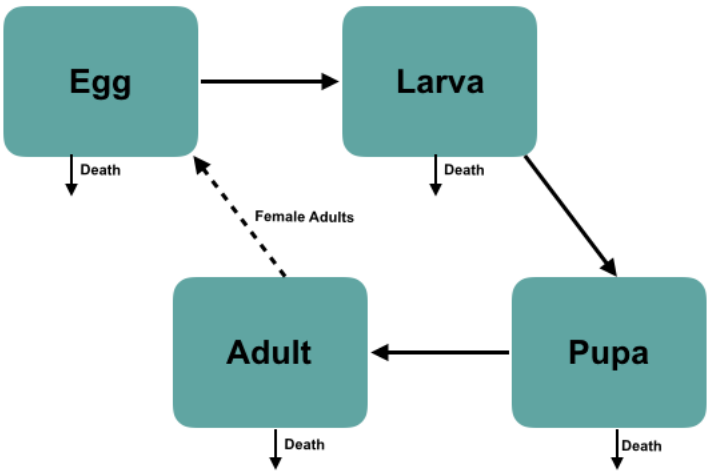

Figure 2.1: A graphical representation of mosquito life cycle including eggs, larvae, pupae, and adults with only female adults providing new eggs to the population. Arrows represent the movement between stages due to development as well as the removal from the stage due to mortality.

2.2.2 Mathematical model

We use a system of ordinary differential equations to describe mosquito vector dynamics at each of the four life stages, namely: eggs (E_g); larvae (L); pupae (P); and adults (A). The model equations follow adult females, but all sexes in earlier stages.

A number of eggs are produced per female per day F, while a proportion of eggs die at a temperature-dependent rate μ_E, a proportion develops to larvae at a temperature-dependent rate $1/\rho_E$ (Equation 2.1). Once larvae develop from eggs, we assume that the larval death depends on two factors: over-crowding at a rate k_j; and temperature at a rate, μ_L. The surviving larval population moves to the pupal stage at a rate $1/\rho_L$ (Equation 2.2). Pupae either die at a temperature-dependent rate, μ_P or develop to the adult stage at a temperature-dependent rate, $1/\rho_P$ (Equation 2.3). Next, we assume that 50% of the pupal population emerge as female adults which either, die at a temperature-dependent rate μ or a temperature-independent rate k, or survive the stage and lay new eggs (Equation 2.4). Thus, our model equations are given by:

$$\frac{dE_g}{dt} = F\ A - (\mu_E + 1/\rho_E)E_g \tag{2.1}$$

$$\frac{dL}{dt} = E_g/\rho_E - \mu_L L(1 + k_j L)) - L/\rho_L \tag{2.2}$$

$$\frac{dP}{dt} = L/\rho_L - (\mu_P + 1/\rho_P)P \tag{2.3}$$

$$\frac{dA}{dt} = 0.5 \times\ P/\rho_P - (\mu + k)A. \tag{2.4}$$

The total female mosquito density is $A(t)$ which is the outcome of the model dynamics at each time t. It is this value that is the focus of our analysis.

2.2.3 Mosquito density

We are interested in comparing four temperature-dependent mosquito density forms. The first form is the outcome of our dynamical model $A(t)$,

denoted, moving forward, as $V_d(t)$ which depends on the progress of each life stage before the adult stage.

The second form is an approximation that assumes a stationary and constant mosquito population but still depends on the life stages traits [74]. We denote V_l the density given by

$$V_l(t) = \frac{F\ p_E\ p_L\ p_P}{(\rho_E + \rho_L + \rho_P)\mu^2} \tag{2.5}$$

where $p_E\ p_L\ p_P$ and $\rho_E + \rho_L + \rho_P$ are mortality rates and development times for eggs, larvae, and pupae, respectively. F and μ are defined as in the dynamical model above.

The third form we will use is an approximation of mosquito density that has been used in other VBD models [26, 59, 27, 17, 85], where density is dependent on adult thermal traits:

$$V_a(t) = \frac{F\ p_{EA}}{\rho_A\ \mu^2} \tag{2.6}$$

where p_{EA} is the probability from eggs to adults, and ρ_A is adult mosquito development time.

Because of the sensitivity of infectious diseases in general and vector-borne diseases in particular to environmental drivers, seasonality has an effect on disease dynamics [14, 52]. Hence, another density form has been used by Bacaer et al. [75, 76] which represents the vector population with seasonal fluctuations. For our fourth form, we use a simplified sine function that captures seasonality as follows:

$$V_s(t) = V_0(1 + 0.5\sin(2\pi t/365)) \tag{2.7}$$

where $V_0 = mean(V(t))$. We note that this density form is the same as the sine form used for temperature, which means that this form has the same temperature fluctuations and does not need to depend on temperature directly. Figure 2.2 shows a spectrum of the four densities based on their trait dependence and their formula.

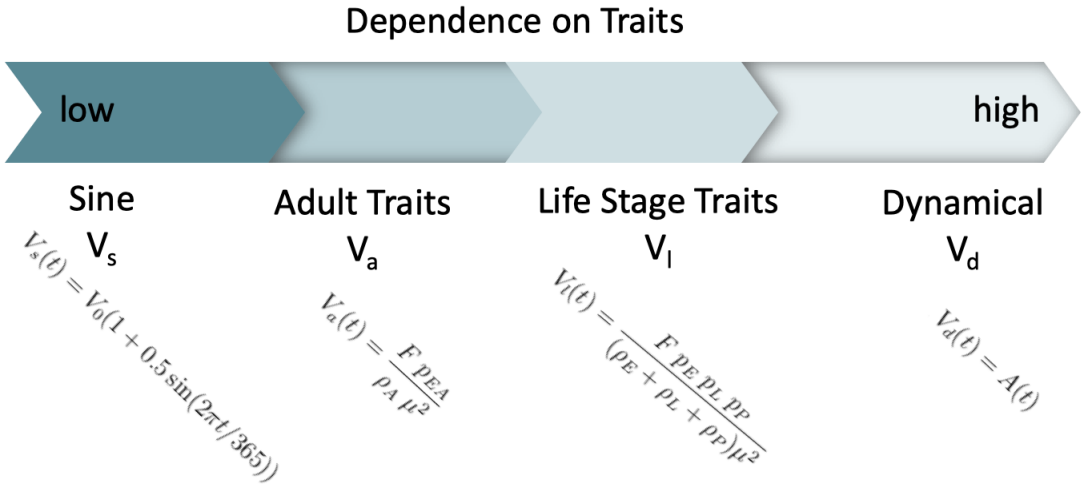

Figure 2.2: Traits' dependence spectrum showing the evaluated density forms ranging from low to high traits' dependence. First, the sine form V_s, second the adult traits density V_a, third the life stages traits density V_l, and the dynamical density V_d is last.

2.2.4 Parameterization and numerical analysis

All the vector traits used in the model are assumed to depend on temperature except the temperature-independent mortality, k for adult mosquitoes and k_j for larvae. The parameters and variables that are temperature-dependent vary according to the following temperature sine function capturing seasonality over a year

$$T(t) = T_0(1 + B\sin(2\pi t/365)) \tag{2.8}$$

where T_0 is the starting temperature and B is the amplitude of the sine wave.

The temperature dependence in traits is represented by unimodal thermal curves previously fit to trait data using a Bayesian method explained in details in [17]. We use humped shaped curves, a Brière or a quadratic, to represent our temperature-dependent mosquito traits. The Brière curve is determined by the equation $\alpha T(T - T_{Min})\sqrt{T_{Max} - T}$, the concave-down quadratic by the equation $qd(T - T_0)(T_m - T_0)$, and the concave-up by the equation $inter - slope\ T + qd\ T^2$. These two forms are a symmetric (quadratic) and asymmetric (Brière) unimodal curves used by Mordecai *et. al.* to fit thermal curves to *A. aegypti* and *A. albopictus* adult mosquito traits using a Bayesian fitting method [17]. The life stage mosquito traits are

fit using a similar method in Chapter 3. Table 2.1 summarizes all the parameters used, their values and references. These curves show trait's response to temperature changes from 0°C to 50°C. The choice between Brière and quadratic forms is based on the pattern that the trait data follow. For the thermal curves function values see Table 2.1 and for the plots of all curves see Appendix A.

We use Matlab software ode solver, ode45, to numerically solve the ode model described by Equations 2.1–2.4. First, we evaluate the model dynamics at one constant temperature T_0 until they reach equilibrium. We use those steady state values as initial conditions for the temperature varying model. Next, we define the temperature function, $T(t)$, with t being days of the year. Then we evaluate each parameter at each temperature using formulas from Table 2.1. The model solution provides the density progress for each life stage including the adult females $V_d(t)$. In addition, we evaluate each of the rest of the densities, $V_l(t)$ and $V_a(t)$ based on the same forcing function $T(t)$, while $V_s(t)$ is evaluated directly.

Throughout our analysis we tune the temperature-independent parameters to obtain useful results. For the dynamical model we adjust k and k_j to make the mean of V_d close to the other densities. For the sine density V_s, we adjust the amplitude and starting density. However, V_l and V_a depend solely on temperature-dependent thermal curves, thus we did not adjust any of their parameters.

2.3 Results

We start our model analysis by exploring the dynamics of full model then compare the outcomes of the total densities. Below is a summary of our results.

2.3.1 Model dynamics

We specify initial densities for each life stage and solve our model numerically as described in the previous section. The juvenile population densities Figure 2.3 (A) increase exponentially as temperature increases to the 26°C - 28°C

Parameter	Description	Function	Value	Units	Refs
lf	Adult mosquito lifespan ($\mu = 1/lf$)	quad	$qd = -0.0011,\ T_m = 36.1065,\ T_0 = 9.1088$	day	[17, 86]
p_{EA}	Survival probability from eggs to adult	quad	$qd = -0.0006,\ T_m = 38.29,\ T_0 = 13.56$	-	[17, 86]
F	Eggs per female per day	Brière	$\alpha = 0.0086,\ T_m = 34.61,\ T_0 = 14.58$	day^{-1}	[87, 52]
ρ_E	Eggs development time	quad	$inter = 87.1722,\ slope = 1.1575,\ qd = 0.0136$	day	fitted in Chapter 3
ρ_L	Larvae development time	quad	$inter = 201.2429,\ slope = 14.0345,\ qd = 0.2310$	day	[87, 52]
ρ_P	Pupae development time	quad	$inter = 20.5074,\ slope = 1.0954,\ qd = 0.0153$	day	[87, 52]
$1/\rho_A$	Mosquito development rate	Brière	$\alpha = 0.0000786,\ T_m = 39.17,\ T_0 = 11.36$	day^{-1}	[17, 86]
p_E	Eggs survival probability ($\mu_E = (1 - p_E)/\rho_E$)	Brière	$\alpha = 0.00077,\ T_m = 30.33,\ T_0 = 9.395$	-	fitted [88]
p_L	Larvae survival probability ($\mu_L = (1 - p_L)/\rho_L$)	Brière	$\alpha = 0.00046,\ T_m = 36.79,\ T_0 = 2.354$	-	fitted in Chapter 3
p_P	Pupae survival probability ($\mu_P = (1 - p_P)/\rho_P$)	Brière	$\alpha = 0.0349,\ T_m = 37.4679,\ T_0 = 9.96278$	-	fitted [88]
k	Temperature-independent mortality rate	-	0.486	day^{-1}	estimated
k_j	Density-dependent mortality rate	-	0.09	day^{-1}	estimated

Table 2.1: Parameters used in the model and in the density forms, their description, function or value used, and reference. The curves associated with the temperature dependent traits are plotted in Appendix A.

range. As temperature approaches its peak of 30°C, the densities' growth rate is reduced. The life stage densities start declining at 29°C before they resume their increase as temperature drops again. The temperature continues to drop and densities reach their minimum. We consider two years to show that although densities seem to be zero, they do not in fact completely fade out. They only get very low and as soon as temperature increases again they grow as we can see during the second-year phase. This is because our temperature curve, with mean temperature of 23°C, ranges between 18.67°C and 30°C. Within this range *A. aegypti* trait values keep the population from dying out.

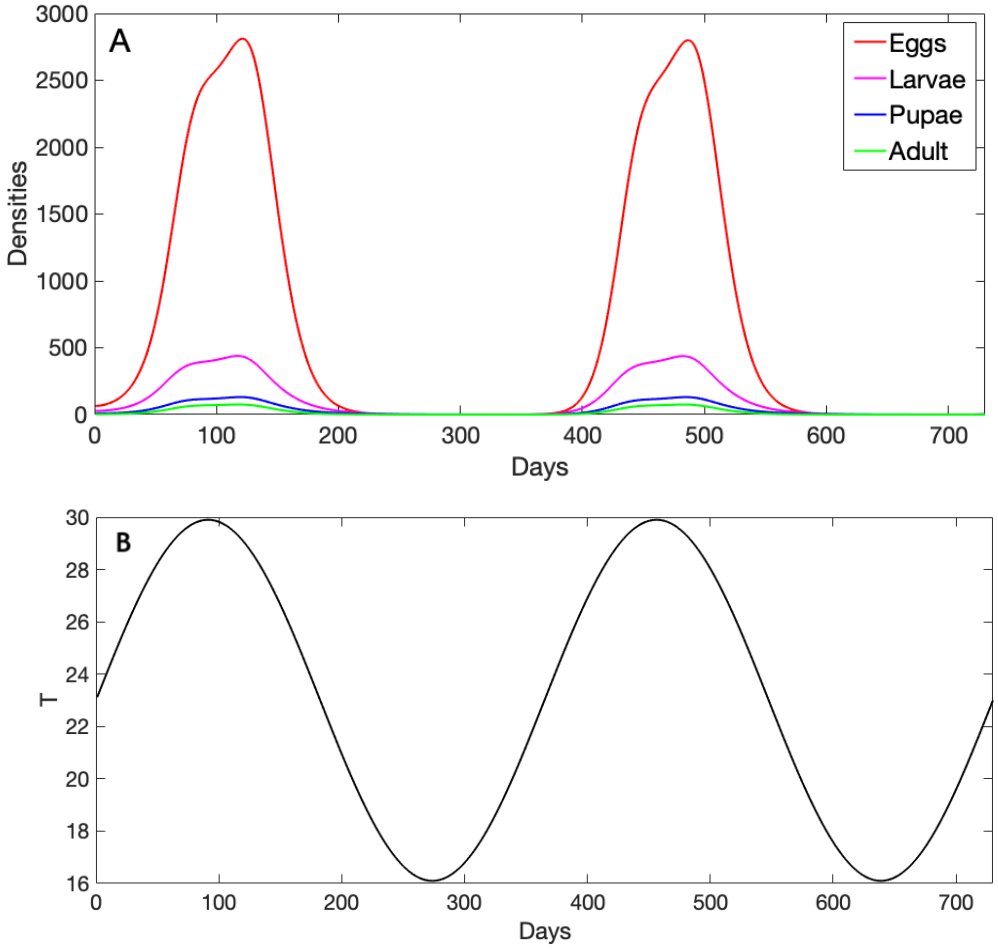

Figure 2.3: (A) Daily mosquito life stages densities evaluated for 730 days (two years). The lines show the numerical solution of our dynamical model for eggs, larvae, pupae and female adults life stages, the parameter values used here are given in Table 2.1. (B) The corresponding daily temperature given by a sine function ($T_0(1 + B\sin(2\pi t/365)$ with $T_0 = 23$ and $B = 0.3$) evaluated at 730 days (two years) used to evaluate our thermal traits incorporated into the dynamical model.

2.3.2 Mosquito density

Now we compare just the adult dynamics across four models. Figures 2.4 and 2.5 show two temperature regimes of all densities. The first regime (Figures 2.4) follows a sine wave that starts at an initial temperature of $T_0 = 23°C$ and ranges from a minimum of 16°C to a maximum of 30°C.

We recall the four densities, namely, V_d the adult female population result from our dynamical model, V_l the life stage trait dependent vector population, V_a the adult trait dependent vector population, and V_s the sine wave approximation of vector population. The results show differences in both values and patterns of these densities.

The values of the four densities differ except between V_l and V_a, which agree when the temperature is below 25°C. This is because of the similarities in their formula. As temperature increases, V_d increases exponentially, while the rest of the curves have a more linear increase at first. We note that the peak of V_d is delayed due to incorporating dynamics for each stage explicitly in the model, whereas the rest of the curves are evaluated directly at each temperature. All three densities, V_d, V_l, V_a decrease as temperatures peaks or approaches a minimum, which reflects the high mortality of vectors at very high and very low temperatures. While V_s decreases as well but not as drastically since it follows the temperature sine wave patterns. As a result, V_s makes qualitatively different density predictions in this scenario.

At peak temperature, we see that the curves (except V_s) decrease at different magnitudes due to differences in their formula, but they all reach local minimums at peak temperature 30°C and low temperature of 16 °C. V_d peaks at temperature of 29°C, V_a at 27°C, and V_l at 26°C. Figure 2.4 C shows the gradients of all four curves to highlight where they increase and decrease. The gradient is the first derivative corresponding to every curve data point, a positive value is an indication that the density increases while a negative value means the density decreases.

The second graph (Figures 2.5) shows patterns of a lower temperature regime where the starting temperature is 18°C with a range of 12°C – 23°C.

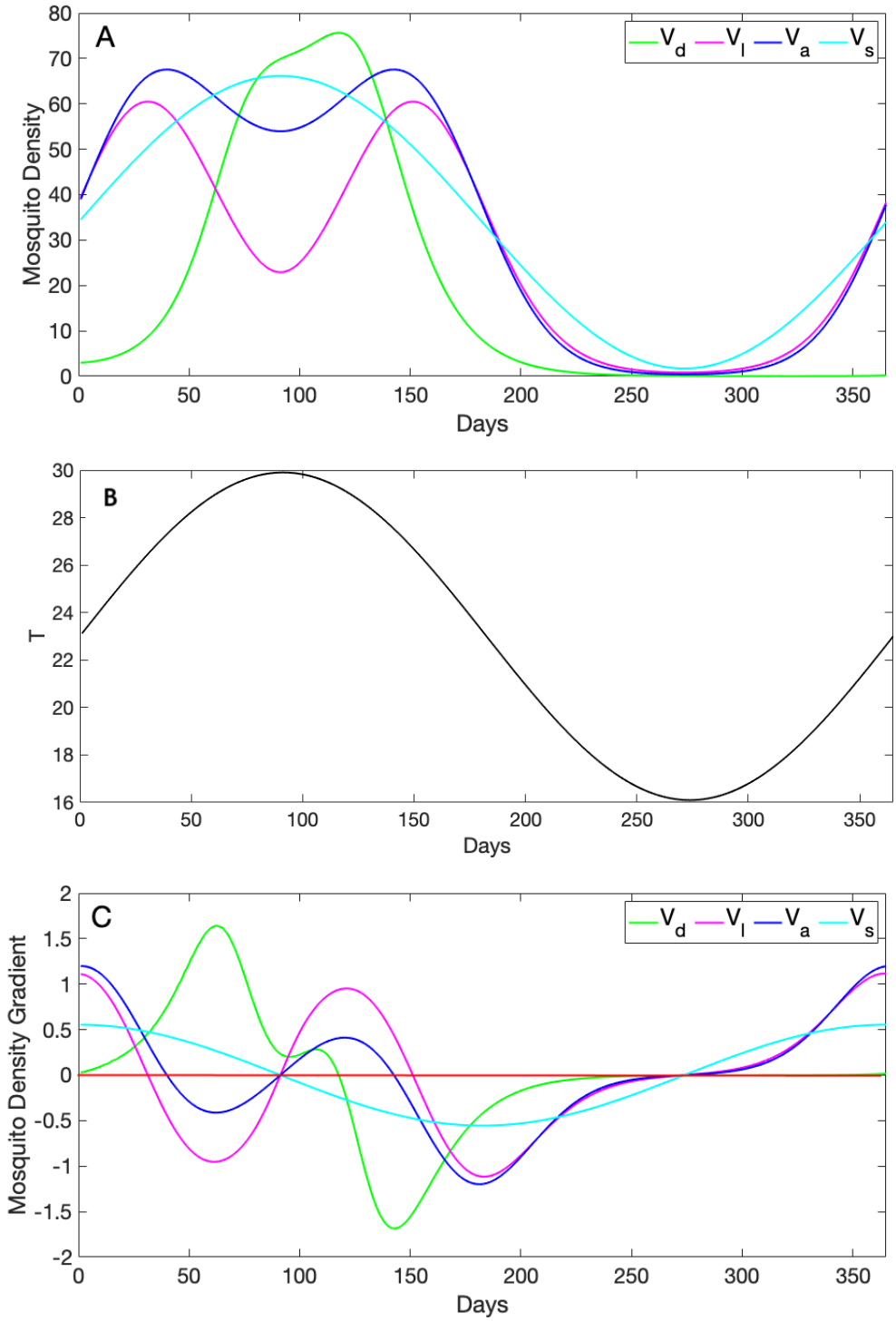

Figure 2.4: (A) Daily adult females mosquito densities approximated using four forms, namely, the sine wave V_s with initial $V_0 = 33$ and amplitude of 0.45, the adult trait dependent form V_a, the life stage trait dependent V_l, and the dynamical density V_d the parameter values used to solve the ode model are given in Table 2.1. (B) Daily temperature given by a sine function ($T_0(1 + B\sin(2\pi t/365$ with $T_0 = 23$ and $B = 0.3$) evaluated at 365 days used to evaluate our thermal traits incorporated into the dynamical model. (C) Densities' first derivatives calculated to show how each curve changes its gradient as it varies with temperature. The red line shows when the gradient is zero, positive gradient values (above the red line) mean that the density increases and negative values of the gradient (below the red line) mean that the curve decreases.

This low range leads all density forms to have global optimums compared to local optimums in the previous regime. As temperature vary, thermal traits take different values, meaning that each regime will have different thermal trait values, thus the variation in total densities. at the low ranges of temperature, thermal curves have a linear dependence to temperature, while at high ranges the thermal curve is hump-shaped leading the local optimums in the densities. Appendix A has plots of all thermal traits from 0°C to 50°C.

Here, the two forms V_a and V_l are similar. V_s has a sine shape with a lower peak compared to V_a and V_l. There is a 20 days lag between V_d the rest of the densities which indicates that solving the model dynamics requires some initial burnin time before the patterns become apparent, but other than that, V_d also shows global optimums. Similarly, Figure 2.5 shows the density gradients at every point indicate when they increase and decrease.

2.4 Validation

To test our density forms, we use data from a study published by Lana et al. [71]. The data are collected by a long term program of entomological surveillance, named "Intelligent Dengue Monitoring System" that is organized by the city of Vitòria in Brazil. The surveillance plan's duration is four years from January 2008 to December 2011. *A. aegypti* mosquitoes were collected weekly from mosquito traps placed in 80 neighborhoods of the city resulting in 208 weeks of *A. aegypti* mosquito abundance. The temperature data were obtained from the International Research Institute for Climate and Society (IRI) platform at Columbia University Land Institute.

We use weekly average temperatures of Vitòria city in Brazil to evaluate *A. aegypti* mosquito traits and solve our dynamical model to obtain V_d. Because of the delayed response shown in V_d dynamics, we define a burning time of 8 weeks to reduce the lag between V_d patterns and *A. aegypti* abundance. In addition, we adjust the temperature-independent model parameters k and k_j to make V_d close to *A. aegypti* abundance.

Next, we evaluate V_l and V_a directly at the weekly average temperature

Density	V_d	V_l	V_a	V_s
Aedes Data	279	255	316	227

Table 2.2: Mean squared error calculated between collected *Aedes* abundance data and our density approximations V_d, V_l, V_a, and V_s.

in Vitòria city. We note that we did not tune any of the parameters in V_l and V_a since they are all temperature-dependent. For the sine wave density V_s, we change the frequency from daily to weekly and use a non-linear regression model to determine V_0 and the amplitude which give the best fit of the *A. aegypti* abundance data, the results show that $V_0 = 36.31$ and the amplitude is 0.35. Figure 2.6 (B) shows weekly temperature data for Vitòria city and Figure 2.6 (A) shows *Aedes* abundance data together with our approximated densities.

To investigate the goodness of our approximations we calculate the mean squared error (MSE) to quantify the difference between each curve and the data (Table 2.2). The smaller the MSE the closer the prediction to the data.

The closest approximation is V_s which is the fitted curve using non-linear regression. The second best is V_l the life stage trait dependent curve followed by the dynamical curve V_d that also incorporates life stages traits. While the highest error is given by our adult trait dependent density V_a.

2.5 Discussion

Vector density is an essential component in vector-borne disease transmission. For instance, a location with high vector density increases the chance for contact with the host, which in turns, increases disease risk and facilitates disease spread [89, 90]. For mosquito-borne diseases such as dengue, Zika and others, understanding mosquito traits and their role in quantifying the density is important for monitoring spread. However, measuring mosquito abundance in the field can be challenging and the role climate factors play in the global distribution and dynamics of mosquitoes including *A. aegypti* remains unclear [91, 92].

In this study, we use four forms to approximate vector density for *A. ae-*

gypti. We propose a spectrum of model formulations based on their dependence on mosquito traits: a simple sine wave form V_s independent of traits; an adult trait dependent form V_a; a life stage trait dependent form V_l; and a density V_d derived from a dynamical model. We solve the model and evaluate the density forms at each daily temperature to compare the resulting patterns. The results show that the densities are more similar in the low mean temperature regime, while more differences appear in the high-temperature regime. For instance, unlike the rest of the density forms, the sine wave does not capture the effect of temperature optimums on thermal traits. The dynamical density form, V_d, shows a delayed response which indicates that the model requires more time to reach a steady state and produce a density suitable for comparison.

To investigate further how the densities perform in a more realistic setting, we use weekly temperature and *A. aegypti* abundance data collected in Vitòria city, Brazil. We implement the sine wave form V_s in a non-linear regression model to fit the abundance data. We evaluate the densities V_a and V_l at the given temperature and solve the model to obtain V_d. We compare the densities to the weekly *A. aegypti* abundance (Figure 2.3). The results show that the regression fit using the sine form provides the smaller mean squared error, meaning that it is the closest estimate to the data. This is obvious because fitting case data should be a close estimate of the data than using temperature to estimate the data. The next best approximation is V_l followed by V_d which highlights the importance of incorporating life stage traits in our models. The highest error is given by the adult trait dependent density, V_a.

Although some of these forms did not come up best, this does not mean that the forms are not useful for a different data case. For example, using the form V_a in the basic reproductive ratio of a malaria system improved the estimate of the observed entomological inoculation rate [26]. This is not surprising given the different biology and life history of *Anopeheles* and *Aedes*. For instance, in our case V_a is the farthest estimate from the data. On the other hand, our model is a representation of growth curves of a population

of mosquitoes going through each life stage, while the data collected is a sum of adult mosquitoes trapped each week. Hence, the dynamical model might be suitable for a different type of data. Usually, we need to approximate density because of lack of abundance data, so making sure our approximation is accurate is necessary. Our work shows similarities and differences between the densities which could be useful when deciding which form to use given a location with certain characteristics. In our example, the life stages vector density V_l and V_d are more suitable for the abundance data in Vitòria city if we are interested in capturing the role of temperature in guiding density dynamics. But if we are only interested in approximating the number of mosquitoes regardless of the effect of temperature, then using a simple sine wave might be sufficient.

The way vector density has been modeled varies depending on modeling assumptions and data type and availability [93, 94, 76, 75]. The temperature has been shown to influence the dynamics of VBD [47, 20, 17]. This is because transmission depends on mosquito traits that are sensitive to temperature as well as other climate factors [52, 95]. Our work investigates the effect of temperature on a dengue mosquito and could be adjusted to study another vector-borne disease.

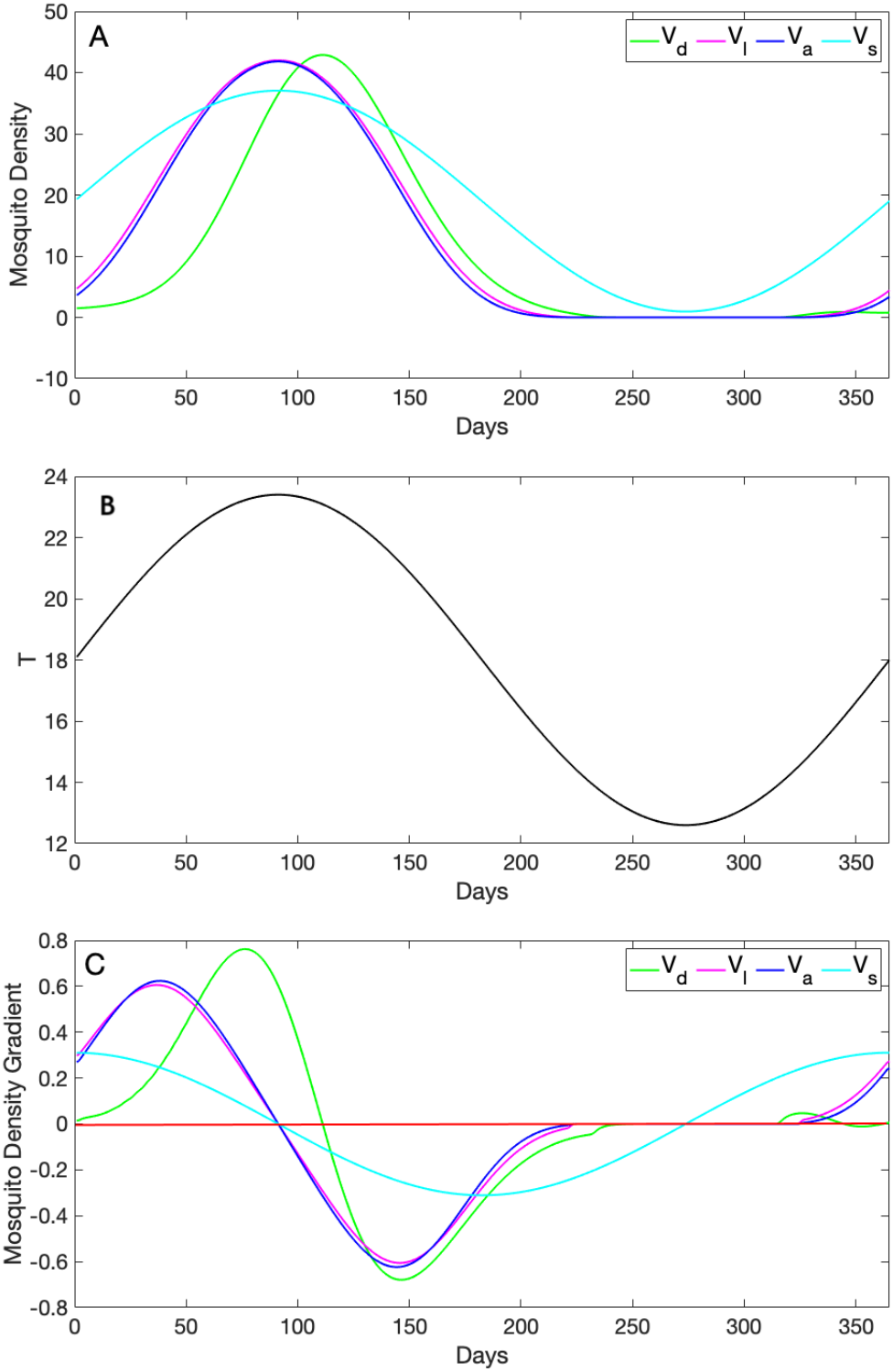

Figure 2.5: (A) Daily adult females mosquito densities approximated using four forms, namely, the sine wave V_s with initial $V_0 = 19$ and amplitude of 0.95, the adult trait dependent form V_a, the life stage trait dependent V_l, and the dynamical density V_d the parameter values used to solve the ode model are given in Table 2.1. (B) Daily temperature given by a sine function ($T_0(1 + B\sin(2\pi t/365)$ with $T_0 = 18$ and $B = 0.3$) evaluated at 365 days used to evaluate our thermal traits incorporated into the dynamical model. (C) Densities' first derivatives calculated to show how each curve changes its gradient as it varies with temperature. The red line shows when the gradient is zero, positive gradient values (above the red line) mean that the density increases and negative values of the gradient (below the red line) mean that the curve decreases.

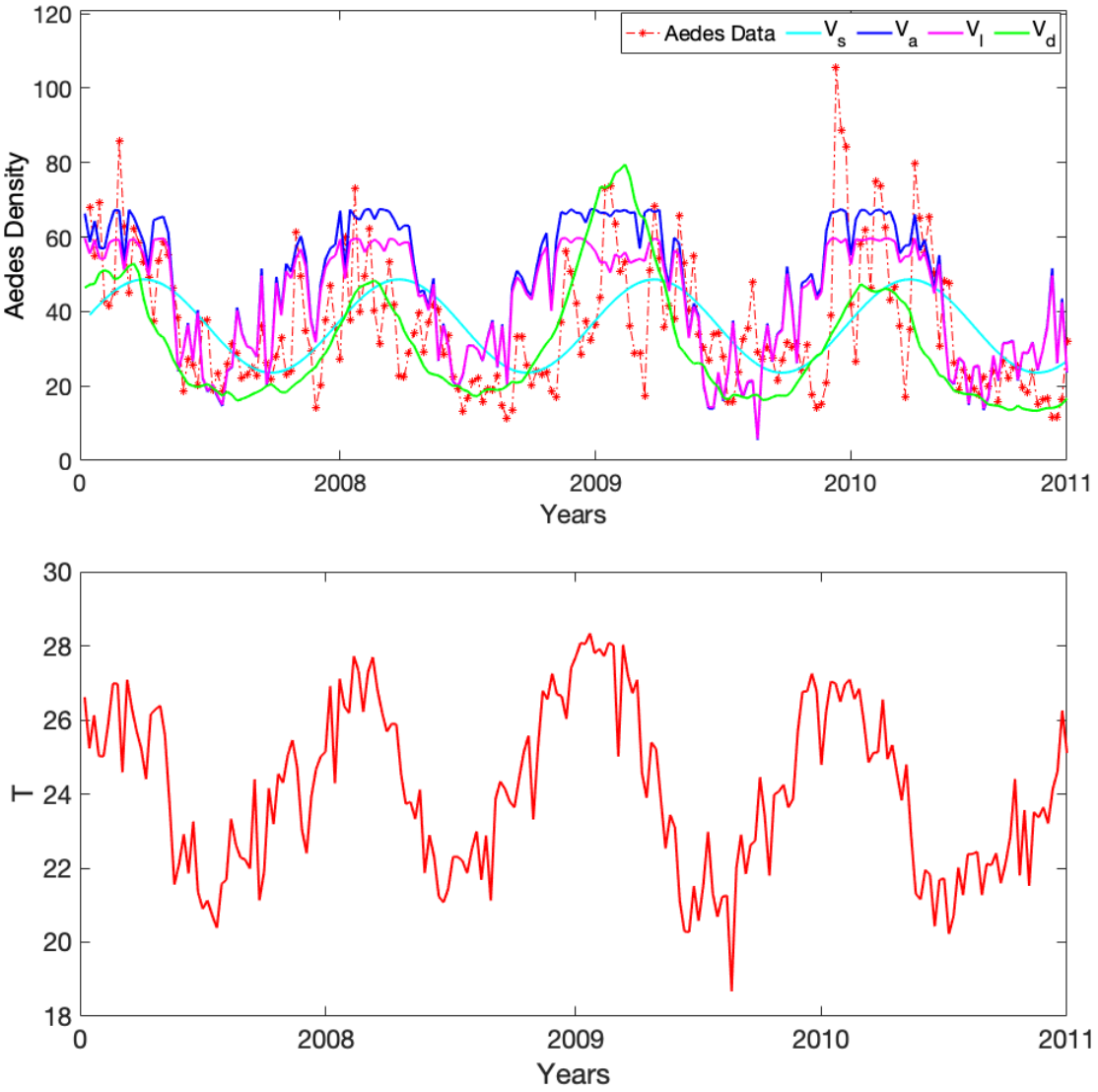

Figure 2.6: (A) Vitòria city's *Aedes* weekly abundance data in red stars and our density estimates evaluated at the weekly temperature in Vitòria city, Brazil. The sine wave density V_s in cyan blue, the adult trait dependent densityV_a in dark blue, the life stage trait dependent density V_l in magenta, and the dynamical density V_d in green. (B) Vitòria city's weekly average temperature during the period of the study. Mosquito and temperature data both from [71]

Chapter 3

Temperature Effect on Mosquito Life Stages and Dengue Transmission

Abstract

Temperature is a major transmission driver for mosquito-borne diseases such as dengue. Mosquitoes are sensitive to temperature changes as it affects their life history traits as well as behavior. Using temperature measures to detect dengue transmission suitability is very useful for dengue predictions. In this paper, we collect dengue mosquitoes' trait data from the literature and use a Bayesian approach to fit traits' thermal curves for all mosquito life stages. We use these thermal curves a deterministic mathematical model to derive a temperature-dependent basic reproductive ratio R_0 across a 0 °C to 50 °C temperature range. In this model, we test two different forms of mosquito densities for comparison. The results show that the R_0 densities are overlapping and fall within each others' HPD intervals, meaning that there is no significant differences between the density forms or the two species *A. aegypti* and *A. albopictus*. Next, we use *A. aegypti* mosquito traits' thermal curves evaluated at average weekly temperature in two locations, Iquitos, Peru and San Juan, Puerto Rico, to calculate the corresponding R_0. Then, we use the R_0 curves to investigate the lag at which the correlation between the basic reproductive ratio R_0 and the total number of weekly dengue cases in these two locations is strongest. The results show that the correlation between R_0 and weekly dengue cases is strongest at 37 weeks for Iquitos and 31 weeks for San Juan.

Keywords— mathematical modeling, mosquito traits, Bayesian analysis, temperature

3.1 Introduction

Dengue is a viral mosquito-borne disease that puts almost half the world's population at risk [96, 97, 89]. Since mosquitoes are arthropods, they are sensitive to climate factors as it affects their ecology [72]. Thus, dengue and other mosquito-borne diseases dynamics are influenced by climate factors as well [3, 98, 99, 100, 101, 102]. Although there are some insights on the effect of climate on mosquito-borne diseases, there is a lot to learn still about diseases' dependence on climate factors and further investigations are required.

Mosquitoes can transmit dengue and other diseases to both humans and animals [72]. This process starts when a mosquito acquires the infection after biting an infected host. Soon after an incubation period, the mosquito becomes infectious and able to infect other hosts. Mosquitoes are specialist vectors in the sense that not every mosquito transmits every pathogen but they are able to transmit multiple pathogens causing different diseases [103]. For instance, *A. aegypti* and *A. albopictus* transmit yellow fever, dengue, chikungunya, and Zika. In addition, *A. albopictus* also transmits nematodes and dog heartworms [104].

Mosquitoes spend a certain number of days at each of the four life stages. During each stage, mosquitoes receive the necessary resources to develop to the next stage until they become adults and begin their reproduction. Furthermore, to identify if a mosquito species is competent to transmit a particular disease, mosquitoes get tested for susceptibility and infectiousness. In animal methods, first, mosquitoes feed on an infected animal host and are allowed the time needed to become infected. Second, mosquitoes get tested for infection to make sure the pathogen is present [105, 106]. Then, mosquitoes can bite an uninfected host which in turn gets tested to check the infectiousness of mosquitoes [106, 105]. Other methods involve mosquito saliva assays which are suitable in the case of a human host [107].

There are two primary vectors responsible for dengue transmission, namely, *Aedes aegypti* and *Aedes albopictus* [108, 109]. In the transmission process of dengue, many mosquito traits are involved, such as the biting rate, mortality

rate, and vector competence. Temperature affects each vector trait responsible for transmission [110, 111]. Therefore, the vector-borne transmission season, which is defined to be the time of the year at which transmission occurs, varies between locations depending on the location's temperature and potentially other climate factors. For example, in Puerto Rico, the low transmission season is between March and June, while the high transmission season is from August until November [112].

Vector-borne disease models tend to focus on the vector's adult stage since adult are the ones transmitting the pathogen [26, 85]. Here, we use dengue mosquito traits' data to fit unimodal thermal curves including traits associated with juvenile life stages. We compare the thermal curve results for both *A. aegypti* and *A. albopictus*. Moreover, we investigate the time lag (in weeks) at which the correlation between our estimated R_0 and weekly dengue cases for San Juan, Puerto Rico and Iquitos, Peru is the strongest. Being able to use modeling to predict this lag can help us better understand the relationship between R_0 estimates and dengue cases and potentially guide our disease risk predictions for future dengue outbreaks.

3.2 Methods

To model dengue transmission we use several mosquito traits to represent what happens in reality. We use laboratory measured traits to approximate our model parameters. For example, we use the duration between female mosquito blood meals and laying eggs, called the gonotrophic cycle [82], to estimate the biting rate which is used in the transmission rate.

Each time a mosquito bites an infected host it has a chance of getting infected. Similarly, when an infected mosquito bites a host, the host is likely to become infected [108]. We assume that the uninfected adult female mosquitoes must come in contact with an infected host for a chance to become infected and vice-versa. Thus, we use vector competence as a product of the probability of mosquitoes getting infected times the probability of mosquitoes becoming infectious.

The mortality rate is either independent of climate factors such as dy-

ing due to predation or it can depend a climate factor such as extremely low and high temperatures. We split mortality into three different forms: adult female mortality, larvae density-dependent mortality, and temperature-dependent mortality for all stages.

Infected mosquitoes take some time before they become infectious. During that time, the virus completes its development and takes a transmissible form. The duration of dengue virus development depends on the virus itself, the mosquito, and environmental factors. We use data on the virus's extrinsic incubation period, the time taken by the pathogen to complete its development within the female mosquito, to derive the pathogen development rate used in the model. Below is a detailed description of data used and the thermal fitting method.

3.2.1 Data description

Here, we describe the data used in our model analysis. First, we explain the thermal trait collection method. Then we describe dengue case data used for validation.

Trait data: we collected temperature-dependent trait data for all life stages of *A. albopictus'* and *A. aegypti'* from published laboratory studies. We included experiments that measure a mosquito trait across three or more constant temperatures. We excluded field studies as they may include additional factors while the lab conditions restrict the predictor only to temperature.

Data were either manually inputted from tables or were from graphs using PlotDigitizer [113]. We extracted data for adult mosquito traits of *A. albopictus* traits, namely, egg-to-adult probability, fecundity, development rate and mortality rate [114, 115, 116, 117]. We obtained *A. albopictus'* fecundity, vector competence, and extrinsic incubation period from [118]. As for the *A. albopictus'* juvenile traits; development times and survival probabilities at the egg, larvae, and pupae stages; we used [114, 119].

For adult trait curves of *A. aegypti*, we used already published results

from [17] and for the juvenile trait data; development time for larvae and pupae and survival probability of eggs and pupae; we used [88, 87]. We were unable to find data for eggs development time and larval survival probability. Instead we used *A. albopictus* thermal fits as an approximation.

Case data we use time series of weekly dengue cases data for two cities, Iquitos, Peru from 2000 - 2009 and San Juan, Puerto Rico from 1990 - 2010. The case data was collected by placing a surveillance network in public and military hospitals and clinics throughout the two towns [120, 62]. The data are comprised of both case and environmental data compiled for easy comparison with dengue cases in these two locations. The environmental data are from multiple sources including ground observations, remote sensing, and reanalysis. For this study, we only use weekly average temperature data for each location. Data were originally compiled for the CDC dengue forcasting project (CITE) and are available at [121].

3.2.2 Temperature-dependent traits

Temperature is an important dengue transmission determinant as it affects several traits associated with mosquitoes [122]. Similar to other ectotherms, mosquito thermal traits increase from zero at a minimum temperature T_0, reach a maximum at a peak temperature, and drop to the minimum again at a maximum temperature T_m [123, 124]. These unimodal thermal responses have been used previously for other mosquito-borne diseases such as malaria [110, 50, 59].

We fit unimodal shaped functions to the trait data. The choice of these unimodal functions depends on the shape of the data and the trait characteristic. Here we use a Brière ($cT(T-T_0)\sqrt{T_m-T}$) for asymmetrical traits or a quadratic form ($qd(T-T_0)(T_m-T)$) for symmetrical traits, to describe the mean thermal trait response [125]. The parameters, T_0, and T_m, in both forms represent the minimum and maximum temperatures for transmission, while c and qd are constants.

Similar to the method published in [59], we fit thermal curves to the data

using a Bayesian approach. We choose an appropriate likelihood distribution describing the collected data, and priors for each of the equation parameters, i.e., c, T_0, and T_m for Brière and qd, T_0, and T_m for quadratic. To model the observed data, we assume a normal distribution for all traits with mean predicted by the unimodal form and precision τ. We truncated the lower limit at zero for all curves and truncated the upper limit at one for all probabilities.

To assure that all mean curves give biologically reasonable predictions, all functions are defined to be zero outside the thermal limits (i.e., below T_0 and above T_m, so that the functions are piece wise continuous). Further, curves describing probabilities, are truncated to disallow values greater than 1. Prior forms were chosen to assure that parameters have the correct sign (positive for c and negative for qd) and to ensure that T_m had a higher range than T_0, further details, including specific distributions for each trait are presented in Appendix B.

We use a Markov Chain Monte Carlo (MCMC) sampling in JAGS/rjags to fit our models. For each fit, we run five MCMC chains with 5000 step burn-in followed by 25000 samples, of which 5000 thinned samples were kept for subsequent analyses. We used these 5000 samples of each parameter to calculate the associated trait thermal curves, resulting in 5000 thermal fits of the trait data. Next, we use the mean of all 5000 posterior distributions as the thermal curve fitting the trait data.

We calculate the the corresponding 95% highest posterior density (HPD) interval which is the smallest interval in which 95% of the distribution lies [126]. The Bayesian analysis was implemented in R [127]. More details on likelihoods and priors used can be found in Appendix B.

3.2.3 Formulation of R_0

We use a previously derived mosquito-borne disease basic reproductive ratio, R_0 [128, 129, 130, 50]. The ratio R_0 describes how contagious the disease is: when $R_0 > 1$, the disease is likely to cause an outbreak, while $R_0 < 1$ means

that the disease is likely to die out. Our derived R_0 is given by

$$R_0(T) = \left(\frac{V(T)\ bc(T)\ a(T)^2}{d\ H\ \mu(T)} \left(\frac{3\nu(T)}{3\nu(T) + \mu(T)} \right)^3 \right)^{1/2}, \tag{3.1}$$

where bc is vector competence, a is the biting rate, μ is the adult mortality rate (the inverse of adult lifespan lf), ν is the parasite development rate (the inverse of the parasite extrinsic incubation period; $\nu = 1/EIP$), d is host recovery rate, and H is the total host population. We do not use any data on host population or recovery rate, hence we choose H and d values so that the product is one to exclude the host effect. The mosquito density V is expressed in two ways, depending on whether we use juvenile traits or adult traits, both forms have been used before [53, 26, 59]. The mathematical formula for each density is given by:

$$V_l(T) = \frac{F(T)\ p_E(T)\ p_L(T)\ p_P(T)}{\mu(T)^2\ (\rho_E(T) + \rho_L(T) + \rho_P(T))} \tag{3.2}$$

$$V_a(T) = \frac{F(T)\ p_{EA}(T)}{\mu(T)^2\ \rho_A(T)} \tag{3.3}$$

where F is a fecundity measure given by the number of eggs per female per day, and $p_E,\ p_L,\ p_P$, are survival probabilities for egg-to-larvae, larvae-to-pupae, and pupae-to-adult. Alternatively, p_{EA} is egg-to-adult survival probability. Similarly, $\rho_E,\ \rho_L,\ \rho_P$, are development times for egg-to-larvae, larvae-to-pupae, and pupae-to-adult, and ρ_A is egg-to-adult development time. We note that the development rate is the inverse of development time $(1/\rho)$.

3.3 Results

3.3.1 Thermal traits

We fit unimodal curves to the collected mosquito data and plot the mean of posterior distributions together with their HPD interval. We note that this is not the full predictive interval, the HPD interval here is just the credible interval for the mean representation of the posterior distributions.

Full trait fits including marginal posteriors of the parameters for each trait are in Appendix B.

Figures 3.1 A, B, and C show development rates $1/\rho_E$, $1/\rho_P$, $1/\rho_A$,. The development rates for these stages are similar for both species and peak between 30 and 35°C for pupae and adults while the peak is between 25 and 30°C for eggs. Pupal development rate peak is the highest (> 0.7) and the peaks for eggs and adults are between 0.2 and 0.5. Figures 3.1 D shows that the adult lifespan, lf for *A. aegypti* is lower than the lifespan of *A. albopictus*, which reaches its peak of 149 days at 22°C.

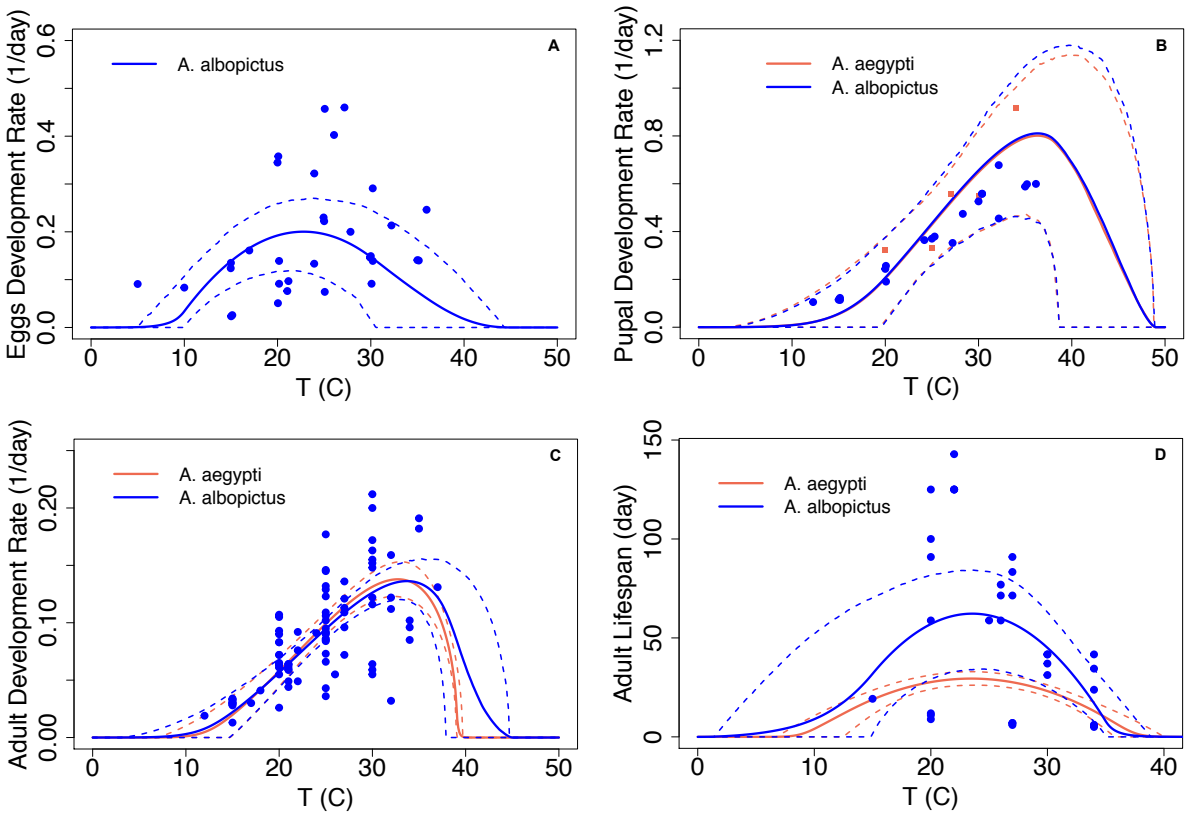

Figure 3.1: Development rate for *Aedes albopictus* eggs ($1/\rho_E$,) also used to approximate the egg development rate of *Aedes aegypti*. Development rates for pupae ($1/\rho_P$) and adults ($1/\rho_A$) and adult lifespan ($1/lf$). Blue colors represent *Aedes albopictus* and coral colors represent *Aedes aegypti*. Solid lines show fitted curves and dashed lines are the corresponding HPD intervals. There is no data for*Aedes aegypti*'s eggs development rate, so we estimate it using *Aedes albopictus* fitted curve.

Figure 3.2 shows development rates for larval instars. Early instars (1 and 2) show that the development rate for *A. albopictus* reaches the peak (>1 and <1.4) at 28°C, while the development rate's peak of *A. aegypti* is not as high (<0.8). However, it seems that higher temperature is tolerated by

A. aegypti instars 1 and 2. For instars 3 and 4, *A. albopictus*'s development rate peaks (>1 for instar 3 and >0.7 for instar 4) at 35°C, while *A. aegypti* reaches the peak (0.6 for instar 3 and 0.3 for instar 4) at 30°C.

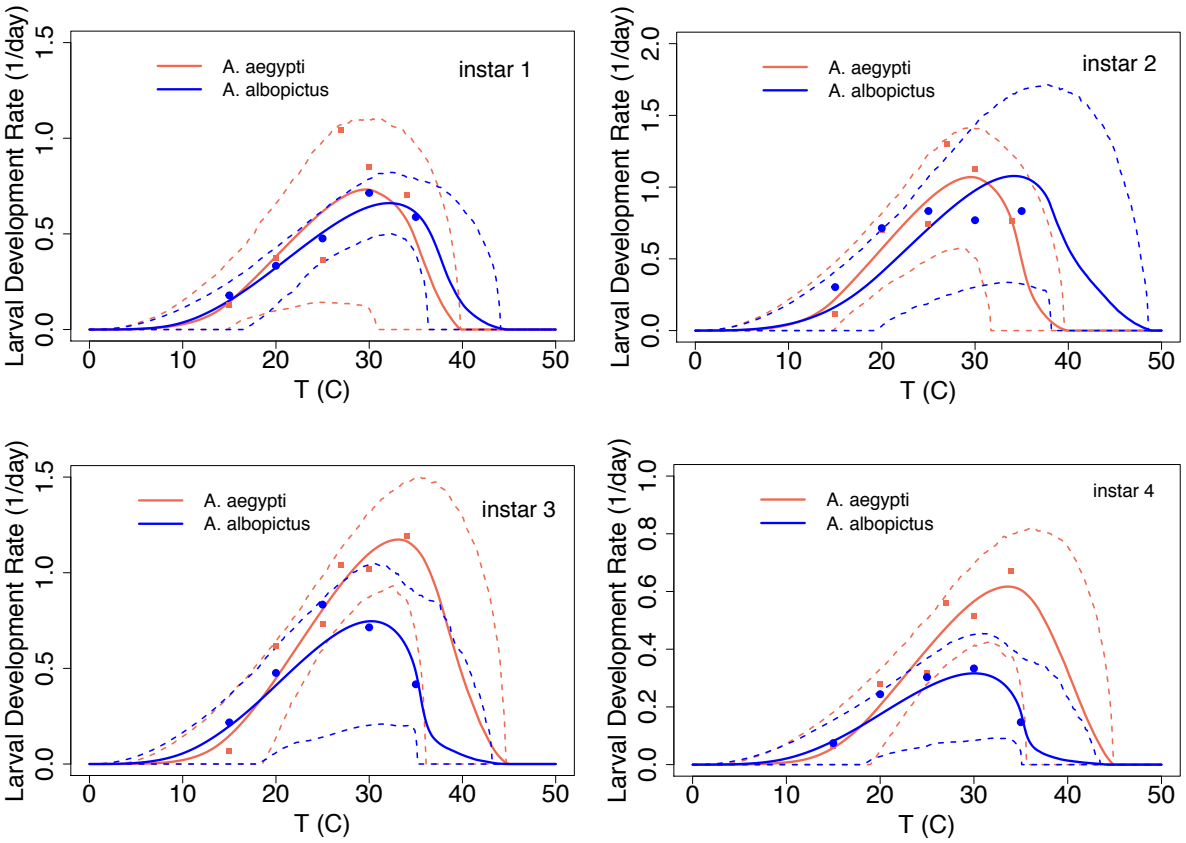

Figure 3.2: Development rates for each of the four larval instars ($1/\rho_L$). Blue colors represent *Aedes albopictus* and coral colors represent *Aedes aegypti*. Solid lines show fitted curves and dashed lines are the corresponding HPD intervals.

Figure 3.3 shows survival probabilities of all stages for both *A. albopictus* and *A. aegypti*. Overall, the survival probability peak (>0.9) is reached within 28-35°C for the first two instars . For instars 3 and 4, the survival probability peaks at 30°C for *A. albopictus* and at 35°C for *A. aegypti*.

Fecundity F peaks between 25 and 35°C at 19 eggs per female per day for *A. albopictus* and at 30°C for *A. aegypti*. The parasite development rate peaks ($\nu = 0.25$) at 30°C for *A. albopictus* and at 40°C for *A. aegypti* (Figure 3.4).

The biting rate a, transmission probability b, and infection probability c all peak at 30°C, with a reaching 1 and b and c reaching 0.8 (see Figure 3.5). We do not have data for *A. aegypti* eggs development rate and larval

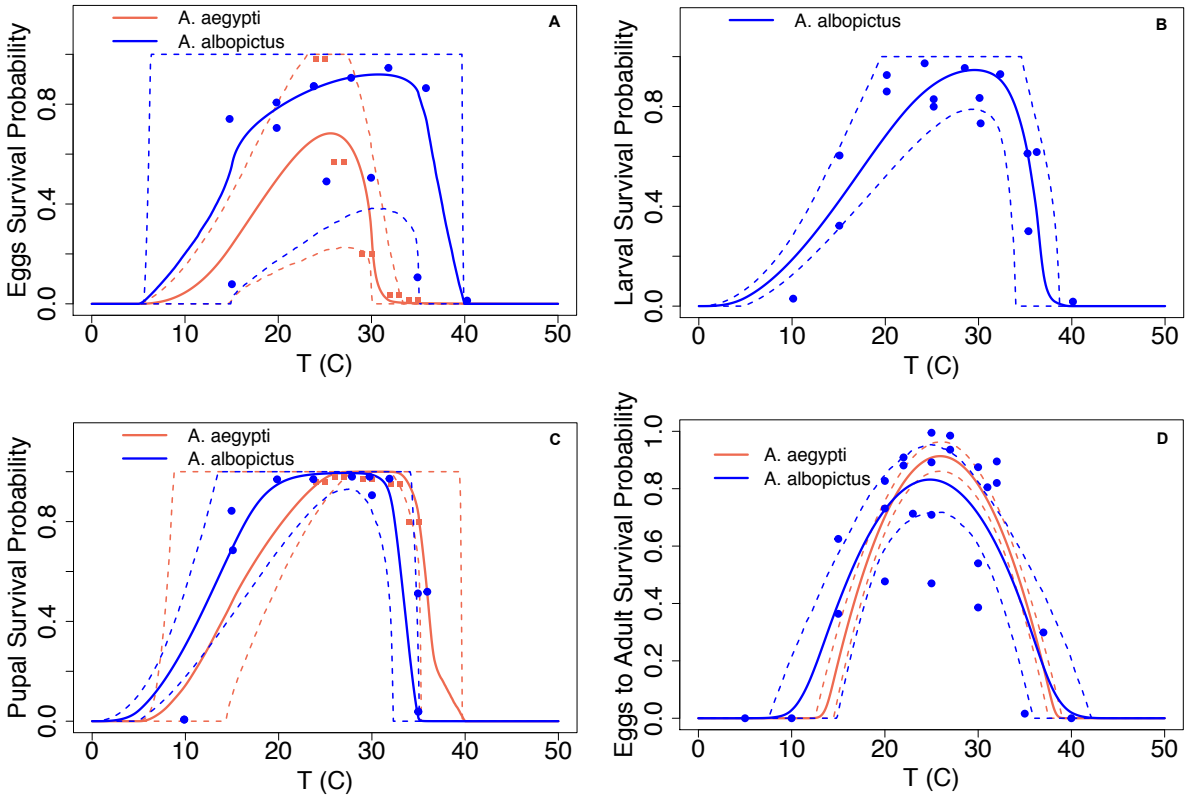

Figure 3.3: Survival probabilities for eggs (p_E), larvae (p_L), pupae (p_P), and eggs to adults (p_{EA}). Blue colors represent *Aedes albopictus* and coral colors represent *Aedes aegypti*. Solid lines show fitted curves and dashed lines are the corresponding HPD intervals. There is no data for*Aedes aegypti*'s larval survival probability, so we estimate it using *Aedes albopictus* fitted curve.

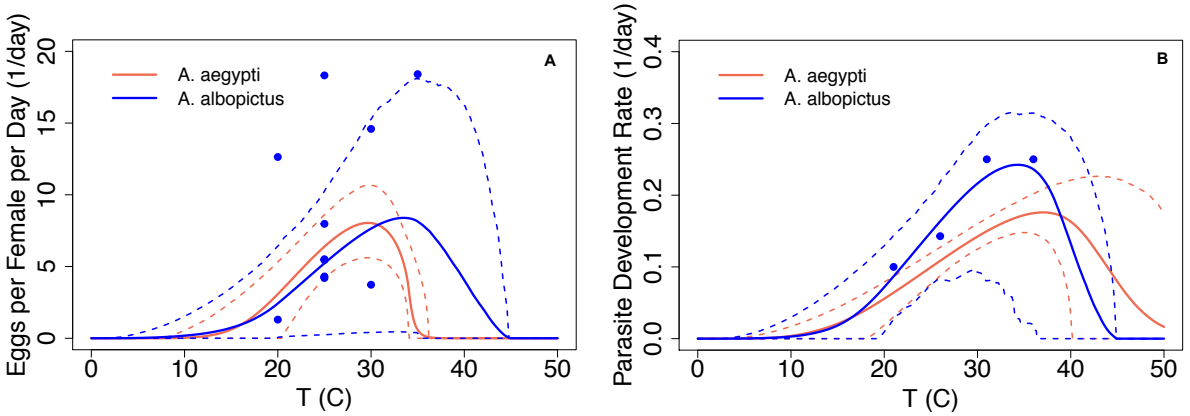

Figure 3.4: Eggs per female per day is a mosquito fecundity measure (F) and parasite development rate (ν) is the inverse of extrinsic incubation period of dengue virus ($\nu = 1/EIP$). Blue colors represent *Aedes albopictus* and coral colors represent *Aedes aegypti*. Solid lines show fitted curves and dashed lines are the corresponding HPD intervals.

survival probability, so in the following analyses we use that of *A. albopictus* as an approximation.

To summarize trait data used in our analysis we use Diagram 3.6 to show

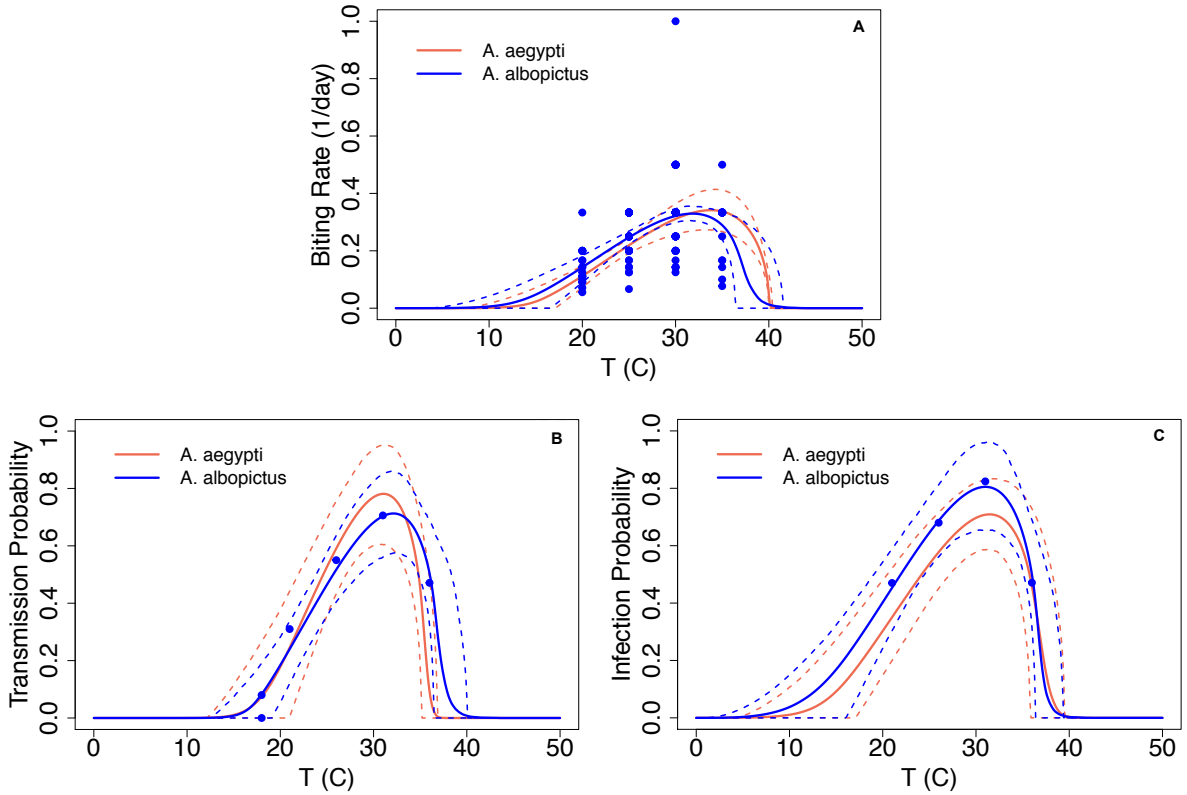

Figure 3.5: Mosquito biting rate(a), transmission probability (b), and infection probability (c). The product of the transmission and infection probabilities is the vector competence (bc). Blue colors represent *Aedes albopictus* and coral colors represent *Aedes aegypti*. Solid lines show fitted curves and dashed lines are the corresponding HPD intervals.

the traits we collected and fit versus what was already published as well as the trait data that we could not find.

3.3.2 Dengue disease risk

We use thermal trait curves of both dengue mosquitoes to derive the mean posterior densities for the adult mosquito population V and the basic reproductive ratio R_0. Figure 3.7 shows the scaled total mosquito densities and scaled R_0 for *A. albopictus* and *A. aegypti* using the two forms given in equations 3.2 and 3.3. The quantities are scaled by dividing the curve and its HPD interval by their maximum value. Leading the curves to range between zero and one, while the HPD interval's upper limit might exceeds one.

Figure 3.7 A shows that the life stage trait dependent form V_l leads to a tighter mosquito density (darker lines) than the adult trait dependent form

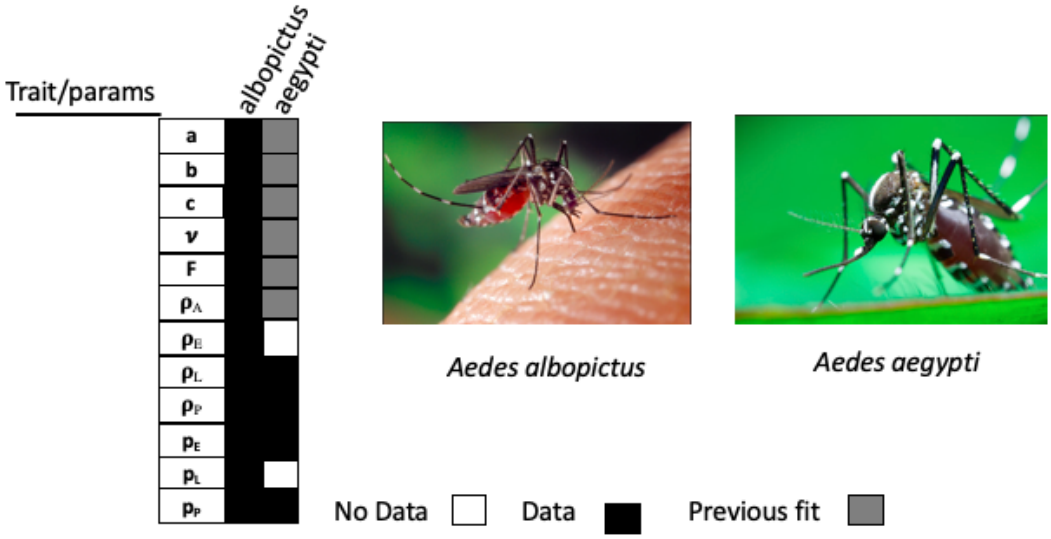

Figure 3.6: This diagram shows pictures of *Aedes albopictus* and *Aedes aegypti* (pictures from www.flikr.com) and the trait data associated with each mosquito. The black squares indicate that we found the data for the specific trait, grey squares means that we used previously fitted thermal curves, while white squares indicate that we were not able to find the trait data.

V_a (lighter lines). The density for *A. aegypti* (shades of blue) peaks at 26°C for V_l and at 29°C for V_a. The density for *A. albopictus* (shades of red) peaks at 27°C for V_l and at 30°C for V_a. Overall, minimum temperatures are similar between species densities, there is a one-degree difference between density peaks, and 4 degrees for maximum temperature between species for V_l and one degree for V_a.

Figure 3.7 B shows R_0 densities for *A. aegypti* and *A. albopictus* and Figure 3.8 – 3.9 shows the distribution around the minimum, peak and maximum temperatures of all $R_0 s$. The temperatures at which the basic reproductive ratio is above zero are suitable for dengue transmission. We note that the transmission range differs with 2 °C between species and within species when comparing density forms.

3.3.3 Dengue outbreak time lag

Figure 3.10 shows the collected dengue cases and temperature data for Iquitos, Peru and San Juan, Puerto Rico. Iquitos dengue cases shows several dengue outbreaks between 2000 and 2009 with varying peaks of the number of cases. The biggest outbreak occurred between 2004 and 2005. For San

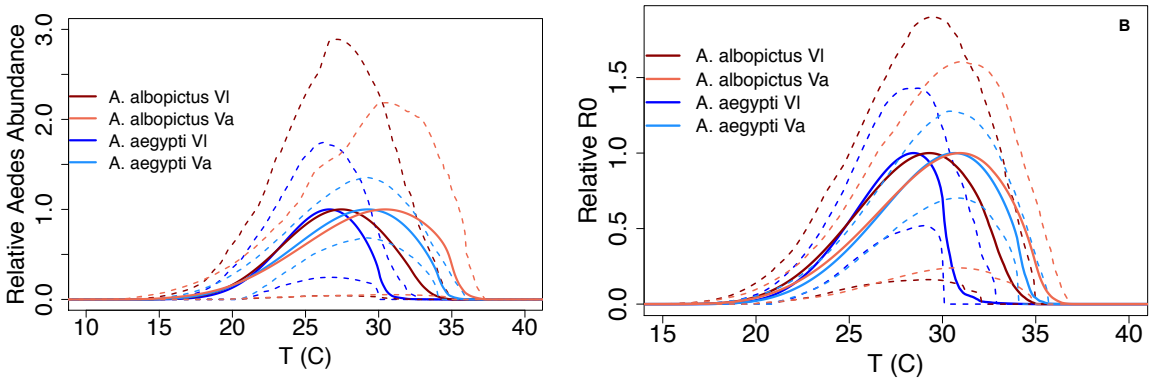

Figure 3.7: Figure A shows the mosquito density for both *Aedes aegypti* and *Aedes albopictus* using the life stages traits density (V_l) and the adult traits density (V_a). Figure B shows the basic reproductive ratio as it varies with temperature. The solid lines are the means of the posterior distributions of the thermal response curves. The dashed lines are the corresponding HPD intervals.

Juan, there are several outbreaks between 1990 and 2010, with the highest number of cases shortly after 1994, and a second highest outbreak in 1998.

We use weekly temperature data from Iquitos, Peru and San Juan, Puerto Rico to evaluate mosquito traits and calculate the posterior mean curve of the basic reproductive ratio $R_0(T)$. Since *A. aegypti* is the dengue vector present at these locations we only used *A. aegypti* mosquito traits.

Dengue cases show a variation in peak magnitude and timing, a higher number of cases correspond to the time following suitable temperatures. Although there are differences between the density forms when implemented in R_0, we found similar patterns in R_0 when evaluated at the temperature data (Figure 3.11). The only exception is that the life stages traits density V_l reaches higher peaks than the adult traits density V_a.

We calculate the cross-correlation between R_0 and dengue case data to determine whether the change in R_0 can potentially indicate a change in dengue cases. We are interested in the time lag at which the correlation between R_0 and dengue case data is strongest. The statistical significance of this lag is indicated by the dashed blue lines in the cross-correlation plot, bars that are outside the dashed lines range are statistically significant.

For Iquitos, at $x = -5 \cdots -18$ and $-51, -52$, R_0 at week $t+x$ is significantly positively correlated with dengue cases at week t. At $x = -46 \cdots -26$,

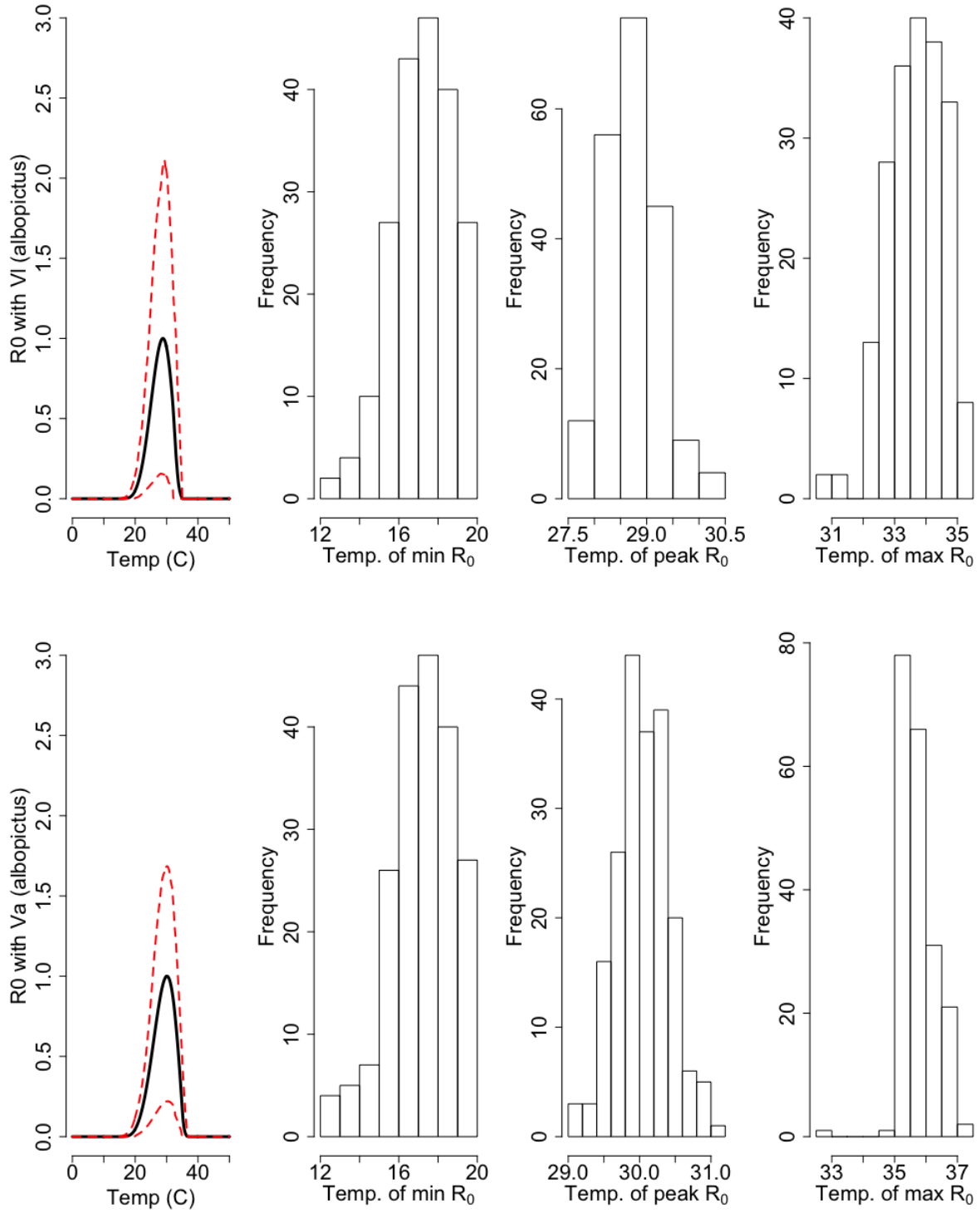

Figure 3.8: Histograms of the posterior distributions of the (left) lower temperature limit of *Aedes albopictus* R_0, (middle) peak temperature of *Aedes albopictus* R_0, (right) upper temperature limit of *Aedes albopictus* R_0 (Top) with V_l and (Bottom) with V_a.

R_0 at week $t + x$ is significantly negatively correlated with dengue cases at week t. Overall, the strongest correlation is negative ($= -0.25$) and occurs

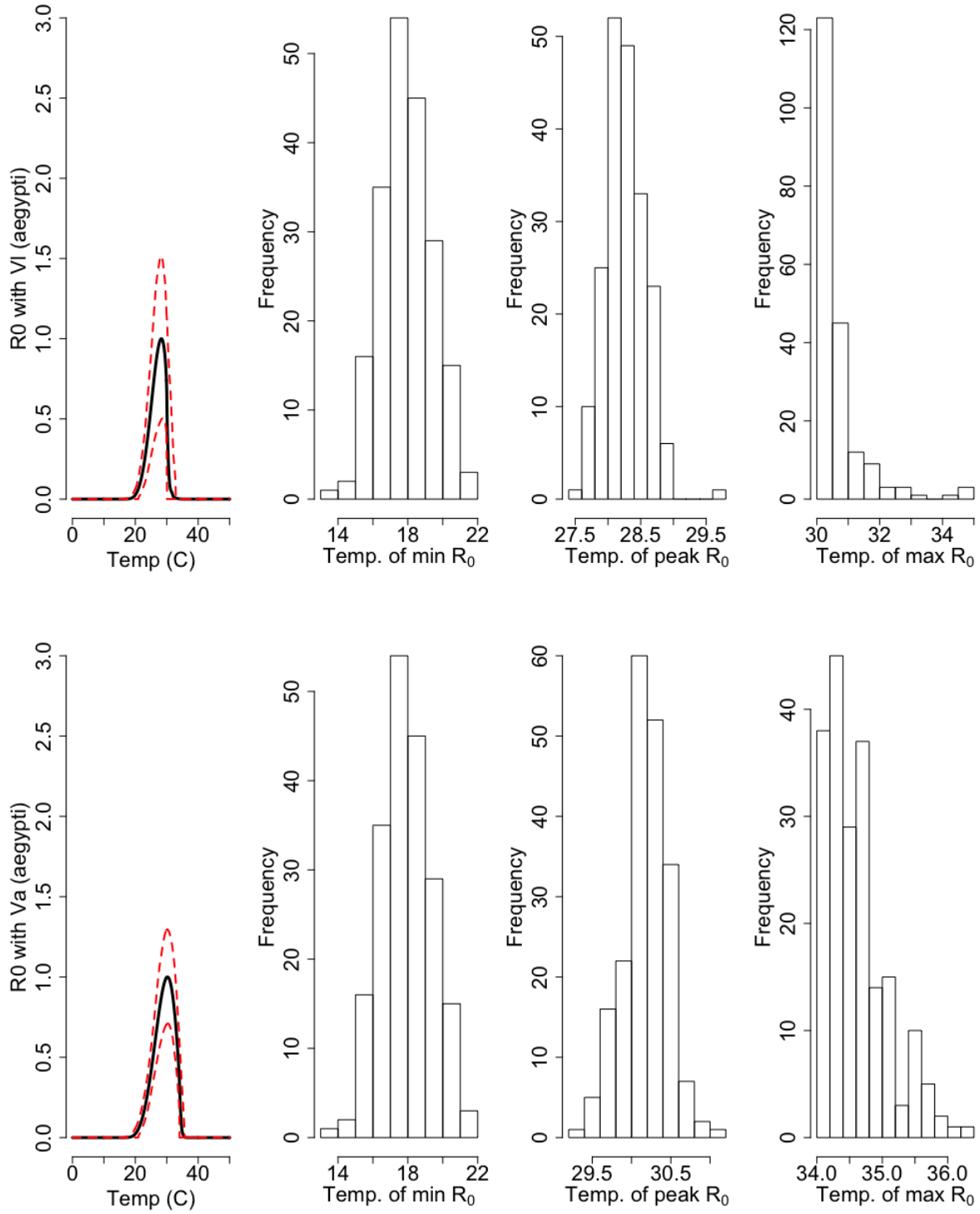

Figure 3.9: Histograms of the posterior distributions of the (left) lower temperature limit of *Aedes aegypti* R_0, (middle) peak temperature of *Aedes aegypti* R_0, (right) upper temperature limit of *Aedes aegypti* R_0 (Top) with V_l and (Bottom) withV_a .

at a time $(t - 37)$ meaning that a high value of R_0 37 weeks ago may indicate that the current dengue cases are most likely low. The highest positive

correlation ($= 0.23$) is at week -6, meaning that if R_0 was high 6 weeks ago, the current dengue cases are most likely high as well.

Similarly, for San Juan, at $x = -16 \cdots 0$ and $-47 \cdots -52$, R_0 at week $t + x$ is significantly positively correlated with dengue cases at week t. At $x = -20 \cdots -41$, R_0 at week $t + x$ is significantly negatively correlated with dengue cases at week t. Overall, the strongest correlation is negative ($= -0.347$) and occurs at a time $(t - 31)$ meaning that a high value of R_0 31 weeks ago may indicate that the current dengue cases are most likely low. The highest positive correlation ($= -0.18$) is at week -13, meaning that if R_0 was high 13 weeks ago, the current dengue cases are most likely high as well.

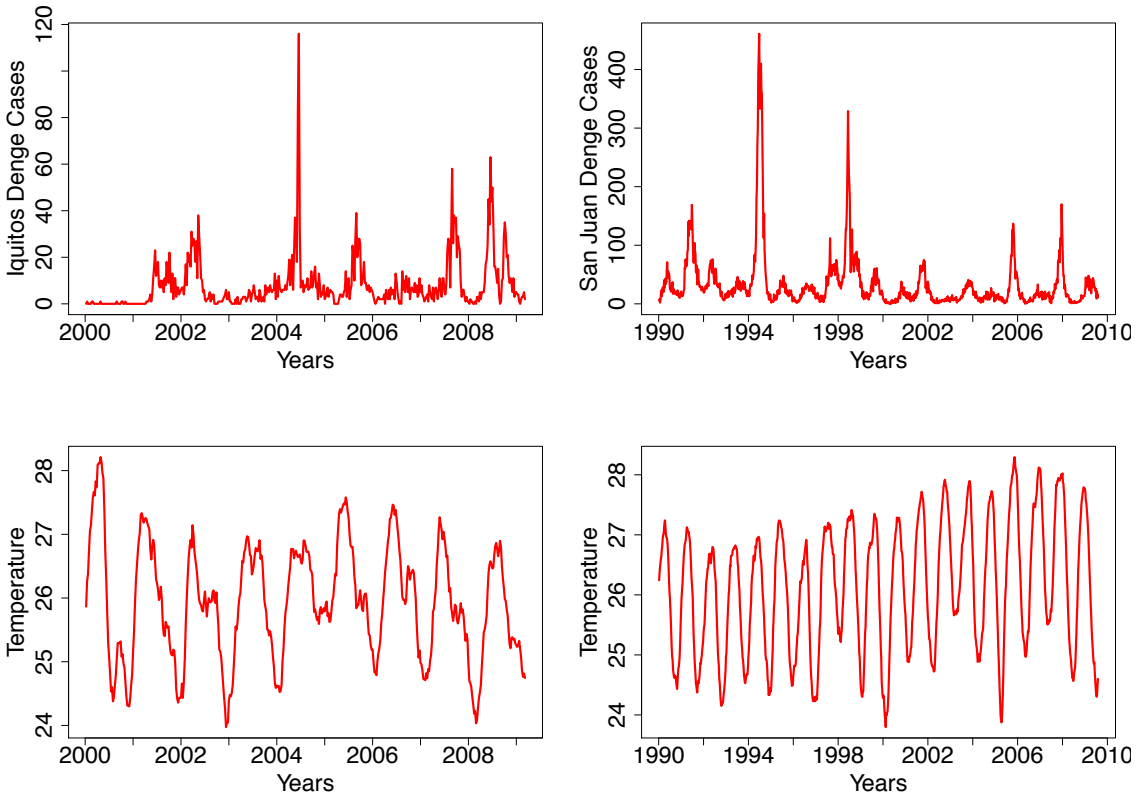

Figure 3.10: The top plots are the weekly dengue cases for Iquitos, Peru and San Juan, Puerto Rico. The bottom plots are the average weekly temperatures at the two locations.

3.4 Discussion

Temperature has important effects on adult mosquito traits that are directly linked to the VBD transmission, such as the biting rate, vector com-

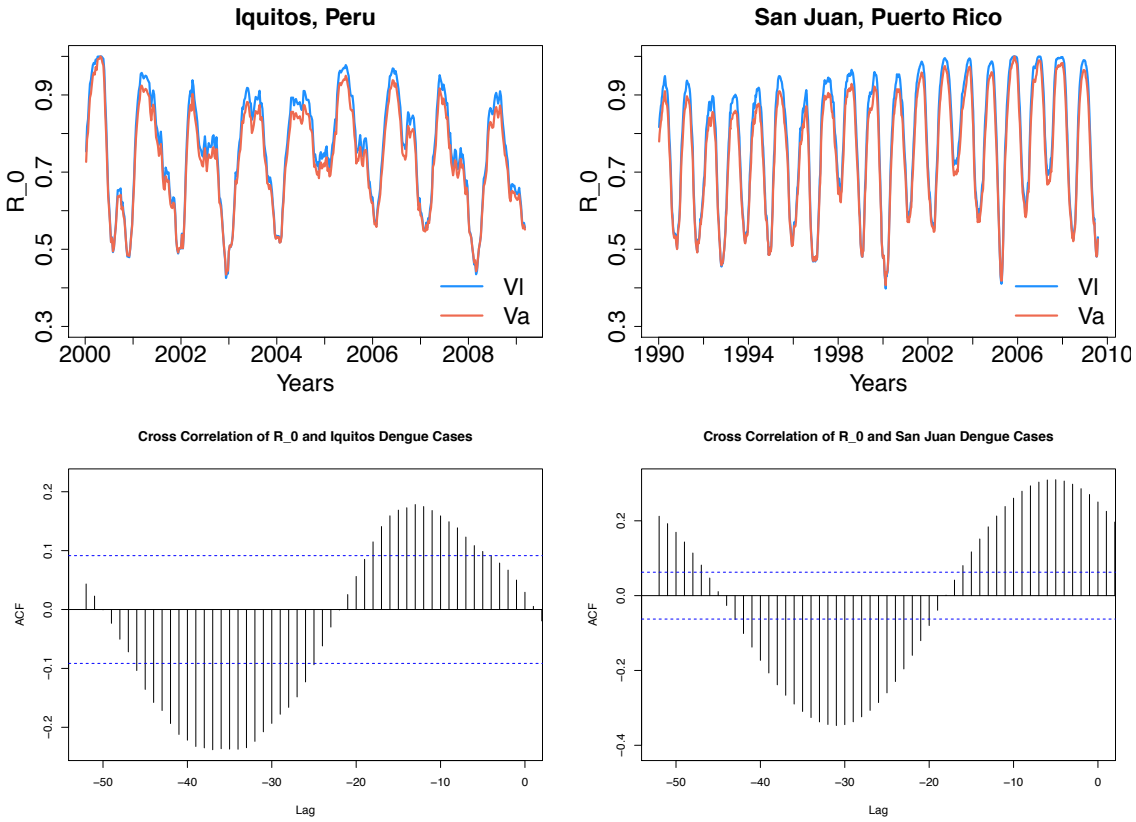

Figure 3.11: The to plots are the scaled basic reproductive ratios R_0 for Iquitos, Peru and San Juan, Puerto Rico. The bottom plots are the cross-correlations between the basic reproductive ratio R_0 and weekly dengue cases in Iquitos, Peru and San Juan, Puerto Rico.

petence, and adult mortality. Incorporating these effects in models has been shown to shift transmission predictions for systems such as malaria [50]. On the other hand, incorporating the effect of temperature on juvenile mosquito traits is still being investigated. A recent study with mosquito life stages data shows that the juvenile development time varies with temperature as an exponential decay curve, which translates to the development time getting smaller as the temperature increases [52]. However, that is not always the case, as mosquitoes, even in their juvenile stages, cannot survive beyond a certain high-temperature [131]. We incorporate this information into our Bayesian model by choosing a hump-shaped curve to fit our data, which allows traits to reach their peak at the optimal suitable temperature.

Moreover, we use our fitted curves in the total mosquito density using two different functional forms and both primary vectors of dengue, *A. albopictus* and *A. aegypti*. The two different forms are the adult traits form V_a and the

life stages traits form V_l. Overall, our model results show that *A. albopictus* adult density temperature growth range (7-37.3°C) is higher than *A. aegypti* (8-37.1°C). Previous studies that compared *A. albopictus* and *A. aegypti* showed that *A. albopictus* abundance and vector competence is higher than *A. aegypti* [132, 45]. This result indicates that *A. albopictus* has a wider temperature range suitable for growth than *A. aegypti*. We note the HPD intervals of all densities are overlapping which means that their differences are not necessarily statistically significant.

We also evaluated the basic reproductive ratio R_0 formula, derived from a mosquito-borne disease SIR type model, incorporating the thermal curves. The goal here is to find the suitable temperature for dengue transmission. Our results show that the suitable temperature range for a dengue outbreak is 17.24–33.74°C (R_0 with V_l) and 17.22–35.75°C (R_0 with V_a) when *A. albopictus* is the primary vector. Similarly, when *A. aegypti* is transmitting dengue virus the suitable temperature for transmission is 17.95–30.66°C (R_0 with V_l) and 17.95–34.65°C (R_0 with V_a). The suitability measure is based on whether the scaled basic reproductive ratio, R_0, is above zero at a given temperature. Our transmission suitability results are close to previous findings. Mordecai *et. al.* showed that the temperature range where *A. aegypti* and *A. albopictus* can transmit mosquito-borne diseases is between 18 and 34°C.

The weekly dengue cases and temperature data in Iquitos and San Juan allowed us to investigate cross-correlation between weekly dengue cases and R_0. We show that the lag at which the positive correlation is strongest for Iquitos is 6 weeks and for San Juan is 13 weeks. The basic reproductive ration at this lag could be potentially used as a strong predictor to detect future dengue risk area and temperature ranges. A previous study on dengue cases in Ecuador estimated the lag at which the correlation between minimum temperature and log dengue cases is 8 weeks which is relatively close to our estimate [133].

The trait data used in our model is imperfect and consists of small samples sizes. For example, our infection probability and parasite development

rate have a sample size of four data points. Thus, our thermal curves have a huge variation that carries to a high uncertainty in our R_0 estimates. Not only there is lack of laboratory trait data useful for our analysis but there is also a high variability in the methods implemented in the lab which makes it hard to combine trait data coming from different studies.

Using a mechanistic approach to understand the relationship between the basic reproductive ratio and the actual disease case data is important when evaluating predictive tools. Evaluating different density forms helps us identify the right form to use and when. For example, if the location we are interested in has a wide temperature range we can use the adult traits density form instead of the life stages density form. In other cases, the life stages density might be a better fit.

Chapter 4

Modeling Temperature Effect on Bluetongue Disease Spread

Abstract

The transmission of vector-borne diseases is governed by complex factors including pathogen characteristics, vector-host interactions, and environmental conditions. For instance, temperature is a major driver for many vector-borne diseases including Bluetongue viral (BTV) disease, which is a midge-borne disease threatening animal agriculture and the economy of affected countries. Using modeling tools, we seek to predict where transmission can occur based on suitable temperatures for BTV. We fit thermal performance curves to midge life history traits that are sensitive to temperature using a Bayesian approach. Then, we incorporate those into a new basic reproductive number, R_0, formula that includes midge traits' response to temperature variations. Our results show that outbreaks of BTV are more likely between 15°C and 33°C with predicted peak transmission at 26°C. The greatest uncertainty in R_0 is associated with the uncertainty in: mortality and fecundity of midges near optimal temperature for transmission; midges' probability of becoming infectious post infection at the lower edge of the thermal range; and the biting rate together with vector competence at the higher edge of the thermal range. We compare our R_0 to two other R_0 formulations and show that incorporating thermal curves in all three leads to similar BTV risk predictions. We base our analysis on thermal traits associated with two midge species, namely, *Culicoides sonorensis* and *Culicoides variipennis*. We use our results to create suitability maps indicating the areas at high and long-term risk of BTV transmission should these two species and the disease be present in these locations.

Keywords— Bluetongue disease, vector-borne diseases, Transmission, Bayesian Analysis

4.1 Introduction

With ongoing climate change, it is critical that we understand how temperature influences the dynamics of emerging diseases. Vector-borne diseases in particular are highly sensitive to climate factors, especially, temperature [50, 59, 6]. Bluetongue virus is not an exception; the biting midges of the *Culicoides* family responsible for transmitting BTV and multiple other species of arbovirus [134, 135], are highly sensitive to changes in temperature, and so is BTV transmission [136, 137]. There are more than 1,400 species of *Culicoides* around the world, but fewer than 30 of those species have been identified as competent vectors for BTV transmission [138].

BTV was first detected among merino wool sheep in South Africa in 1905. Since then, the disease has been found on every continent but Antarctica [139]. In recent years, outbreaks have occurred in North and Central Europe, regions of Asia, and Western North Africa [140]. Though the cause of the recent introduction of BTV to some of these regions (especially Northern Europe) is still unknown, it is believed that climate change is the main contributing factor, as the change in temperature of certain locations makes it suitable for midges to survive, and therefore transmit diseases [141].

BTV can infect most species of domestic and wild ruminants, including sheep, goats, and cattle [142]. Sheep are the most susceptible to the disease and show the highest morbidity and mortality [7, 141]. Across most strains of BTV's 27 serotypes, infected animals rarely show any clinical signs [143]. The severity of infection and whether or not clinical signs are shown depend on the particular serotype that is transmitted to the animal. The severity of infection can range from rapid fatality to quick recovery. Common signs include a blue tongue, fever, and excessive salivation [141]. Since clinical signs are rarely exhibited by animals infected with BTV, in many cases the disease goes without detection.

Undetected cases of BTV can result in mortality and BTV vaccine de-

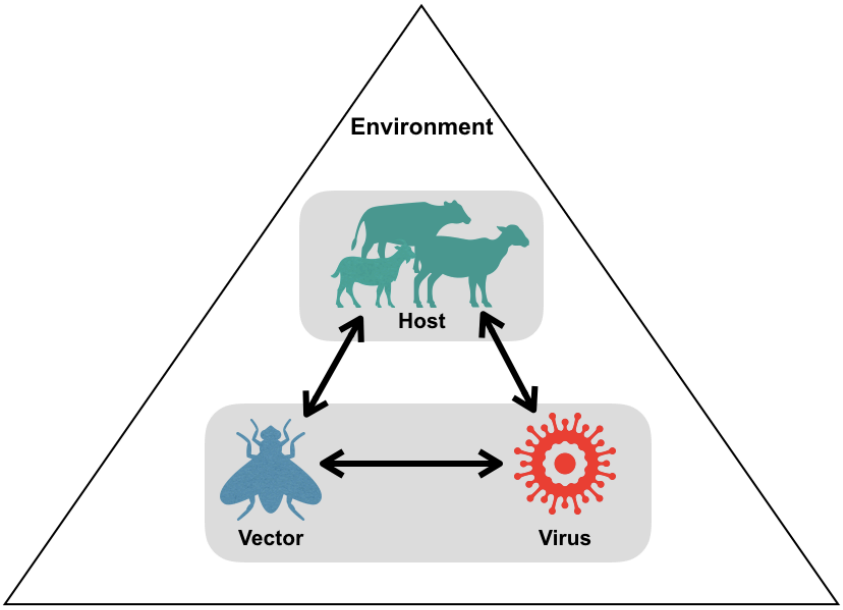

Figure 4.1: Bluetongue virus transmission diagram: the mechanisms underlying the transmission of bluetongue virus include, host-vector interactions, host-pathogen interactions, vector-pathogen interactions as well as the environmental effect on all interactions.

velopment still in its early stages [144]. An effective polyvalent vaccine that immunizes against more than one strain of BTV has yet to have been developed. Additionally, the use of attenuated vaccines poses significant health risks such as reduced milk production in lactating sheep, abortion, early embryonic death, and teratogenesis when used in pregnant females [145]. With the absence of an effective polyvalent vaccine for BTV and the associated risk with the vaccines available for certain strains of BTV, the effect of BTV on the U.S. beef industry, which was valued at $95 billion dollars in 2014, is costly [146]. The mandatory testing of animals and losses in foreign markets also contribute to the economic impact of BTV on the U.S. livestock industry.

The impact of BTV extends far beyond the United States; the spread of the disease to areas previously believed to not be at risk, such as North and Central Europe, regions of Asia, and Western North America, is concerning [7]. Though it is widely believed that climate change is behind this unprecedented spread of BTV to new areas, more research is needed to verify this hypothesis. Some of the cases of BTV-8 in Europe, specifically in France, have exceeded expectations and survived cold winters [147]. The cause of

these anomalies has yet to be determined. With such crucial components such as geographic spread and virus survival still unexplained, it is important that BTV is studied further in order to uncover the intricacies that dictate its impact.

BTV cannot survive on its own in the environment. As shown in Figure 4.1, BTV transmission involve host-vector interactions, host-virus interactions, vector-virus interactions, as well as, the effect of the environment. Once BTV is transmitted to a vector or a host, its survival is most notably dependent on temperature; while BTV can survive for years at certain temperatures, it can be inactivated in a matter of hours within a host at other temperatures [7].

Because of the complexity determining BTV and other VBD transmission, scientists often use mathematical modeling to understand the transmission process [148, 149, 68]. The classical Ross-MacDonald model of VBDs and similar models allowq us to calculate the corresponding basic reproductive ratio R_0 associated with the disease [128, 129]. This summary quantity is widely used to estimate how contagious the disease is and whether we will encounter an outbreak. When $R_0 > 1$, the disease is likely to spread leading to an outbreak, while $R_0 < 1$, indicates that the disease is likely to die out.

Here we are interested in answering the following questions: (1) How does R_0, and thus risk of transmission of BTV vary with temperature? (2) Do different model assumptions lead to different values of R_0s? and (3) Which traits cause the highest variation in R_0? To answer these questions, we take the following three step approach that has been used previously for other diseases such as malaria [50, 59]. First, we derive a new version of R_0 for BTV and we use Bayesian inference to fit lab data for midge temperature-sensitive traits and estimate the thermal responses of these traits. Next, we compare our R_0 to two previously derived forms when the midge density, V, is constant to see if there are major differences in the outbreak prediction. Then, we use a temperature-sensitive midge density, $V(T)$, expressed in terms of midge traits.

We compare the new results for all three forms of R_0, and perform an

uncertainty analysis to identify which parameters lead to high variation in R_0. This can indicate that further data collection is needed or that particular parameters have a higher impact on BTV disease transmission at different temperatures. Furthermore, estimating which temperature range results in having $R_0 > 1$, for given levels of other fixed parameters in our model, can inform future prevention and control strategies.

4.2 Methods

4.2.1 Derivation of R_0

To predict the outbreak potential of BTV, several forms of the basic reproductive number R_0 have been developed [149, 148, 68]. The classical reproductive ratio for a generic VBD [130, 50] is given by

$$R_0 = \left(\frac{V\ bc\ a^2}{d\ H\ \mu} e^{-\mu/\nu} \right)^{1/2} \quad \text{(from Dietz 1993 [130])} \tag{4.1}$$

where V is midge population density; bc is vector competence (the product of the probability that a midge can transmit the infection to an uninfected host, b, and the probability that a midge gets infected when biting an infected host, c); a is the per-midge biting rate; μ is the adult midge mortality rate; ν is the pathogen development rate ($\nu = 1/EIP$ with EIP the extrinsic incubation period); H is host density; and d is infected host recovery rate. The model used to derive this version of R_0 is a system of delay differential equations that assumes no exposed class and that susceptible midges move to the infected class shortly after contact with an infected host. A similar scenario can be described using a system of ordinary differential equations while expressing the delay between the contact with infected host and midges becoming infectious in terms of an exposed class. In this case, the reproductive number for the midge-borne viral disease (BTV) can be expressed as,

$$R_0 = \left(\frac{V\ bc\ a^2}{d\ H\ \mu} \frac{\nu}{\nu + \mu} \right)^{1/2} \quad \text{(from Gubbins et. al. 2008 [148])} \tag{4.2}$$

This version of R_0 is a reduced version from a model that uses multiple types of host and multiple types of midge species as in [149, 148].

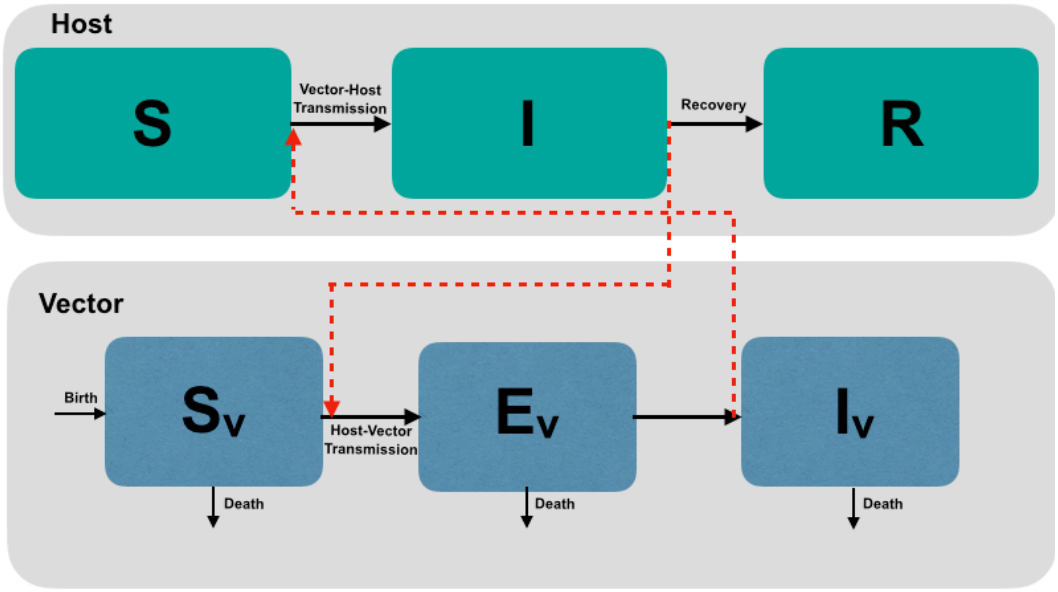

Figure 4.2: A schematic illustration of BTV transmission. The host population is composed of three classes: susceptible (S), infected (I), and recovered (R). The midge population is composed of a susceptible class (S_v), three exposed classes (E_v), and an infected class (I_v). Black arrows show movement between classes and red arrows indicate contact potentially leading to transmission.

Figure 4.2 shows a schematic representation of our BTV transmission model (Equations (C.1)-(C.8) in Appendix C) which considers a single host population split into susceptible individuals that are vulnerable to BTV disease (S), infected individuals that have acquired infection (I), and individuals who have recovered from the disease (R). In addition, we consider a vector population containing susceptible midges (S_v), three levels of exposed individuals (E_v), and an infected class of midges (I_v). The exposed classes in the model represent the extrinsic incubation period that midges undergo before becoming able to transmit infection. To calculate the basic reproductive number R_0, we use a next generation matrix method described in [150, 151], which leads to the following R_0 equation:

$$R_0 = \left(\frac{V\ bc\ a^2}{d\ H\ \mu} \left(\frac{3\ \nu}{3\ \nu + \mu} \right)^3 \right)^{1/2} \tag{4.3}$$

all parameters in our R_0, except d and H, are assumed to be temperature

dependent. The term $\left(\frac{3\,\nu}{3\,\nu+\mu}\right)^3$ in our R_0 represents the number of midges that survive the extrinsic incubation period, leading to a slight difference between the three R_0 forms. We can represent all three formulas of R_0 with a simple equation given by:

$$R_0 = \left(\frac{V g f}{d\ H\ \mu}\right)^{1/2} \tag{4.4}$$

$$= \left(\frac{(midge\ density)\overbrace{(transmission\ potential)}^{g}\overbrace{(prob\ of\ becoming\ infectious)}^{f}}{(host\ recovery\ rate)\ (host\ density)\ (vector\ mortality)}\right)^{1/2} \tag{4.5}$$

where the expression for V and g are the same for all three versions and are given by:

$$V = \frac{F\ p_E\ p_L\ p_P}{\mu^2\ (\rho_E + \rho_L + \rho_P)} \tag{4.6}$$

$$g = a^2\ bc \tag{4.7}$$

where F is eggs per female per day, p_E, p_L, and p_P are survival probabilities for eggs, larvae, and pupae; ρ_E, ρ_L, and ρ_P are development times for eggs, larvae and pupae, respectively; μ is adult midge mortality; a is midge biting rate and bc is midge competence. The difference between the three R_0 formulas lies in the functional form, f, representing the probability of midges surviving to become infectious post infection. Table 4.1 summarizes the functional forms for each of the three models considered.

Figure 4.3 shows all three functional forms as we fix the parasite development rate ν and vary the midge mortality rate μ. We use all three forms in our analysis while comparing the constant vector density case V to temperature-sensitive density $V(T)$.

Ref	Formula	Traits Used
Dietz 1993	$f = e^{-\mu\,\nu}$	μ : adult mortality rate
Gubbins et. al. 2008	$f = \dfrac{\nu}{\nu + \mu}$	ν : pathogen development rate
new R_0	$f = \left(\dfrac{3\nu}{3\nu + \mu}\right)^3$	

Table 4.1: Functional forms used in R_0 formulas and the parameters involved.

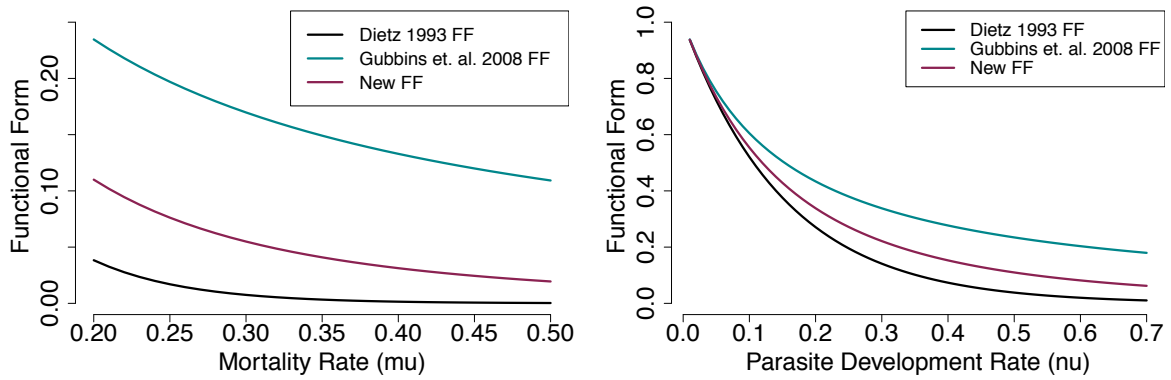

Figure 4.3: (Left) Functional forms f versus midge mortality rate μ with a fixed $\nu = \text{mean}(\nu(T))$. (Right) Functional forms f versus pathogen development rate ν with a fixed $\mu = \text{mean}(\mu(T))$

4.2.2 Bayesian fitting of temperature-sensitive traits

Midges are among ectotherms sensitive to temperature. The thermal performance for these temperature-dependent traits are generally hump-shaped start at zero and begin increasing at a minimum temperature to reach a peak value as temperature increases, then sharply drops to a lower value at a maximum temperature [123, 122].

Here, we collect trait data corresponding to two midge species from the family *Culicoides*, namely, *Culicoides sonorensis* and *Culicoides variipennis*, both found the US [152]. The data collection method consisted of assembling data from tables as well as digitizing data points from graphs in previously published papers; details on each trait data is provided in Appendix C.

We are particularly interested in laboratory experiments on midge traits' variation with constant temperatures, ideally with three or more data points. For the digitization, we used a free software named PlotDigitizer [113].

We use the temperature-dependent trait fits in all three R_0 formulas for comparison. Following a method first introduced by [50], we fit unimodal curves to temperature-sensitive traits that appear in R_0. For the unimodal curves, we chose between a Brière (Equation (4.8)) or a quadratic formula (Equation (4.9)) depending on the trend seen in data.

$$\text{Brière: } kT(T - T_{Min})\sqrt{T_{Max} - T} \tag{4.8}$$

$$\text{Quadratic: } inter - n.slope\ T + qd\ T^2 \tag{4.9}$$

where the constants k, T_{Min}, T_{Max}, $inter$, $n.slope$, and qd are the result of fitting trait data, and each trait requires specific values for the equation to fit the data. For more information on the values, see Appendix C.

Similar to [59], we use a Bayesian approach for our fitting method. For each continuous trait, we choose a normal distribution as our likelihood that represents the data. We truncated the likelihood distributions at zero to avoid negative values for all thermal curves, and we truncated at one when fitting probabilities. We chose priors for each of the fitting form parameters to assure parameters have the correct sign and range. When fitting probabilities, we often switched our likelihood to a binomial distribution.

We use a Markov Chain Monte Carlo (MCMC) sampling in JAGS/rjags to fit our models [153]. For each fit, we run five MCMC chains with 5000 step burn-in followed by 25000 samples, of which 5000 thinned samples were kept for subsequent analyses. We used these 5000 samples of each parameter to calculate the associated trait thermal curves, resulting in 5000 thermal fits of the trait data. Next, we use the mean of all 5000 posterior distributions as the thermal curve fitting the trait data.

After generating the 5000 posterior mean curves for each of trait, we derive the 5000 posterior curves for R_0 then calculate the mean to get the temperature-dependent R_0. For each posterior mean, we calculated the cor-

responding 95% highest posterior density (HPD) interval which is the smallest credible interval in which 95% of the distribution lies [126]. Our analysis was implemented in R [127]. More details on likelihoods and priors used can be found in Appendix C.

4.2.3 Uncertainty in R_0

The R_0 formulas (Equation 4.1, 4.2, **??**) depend on multiple temperature-sensitive traits and so does its posterior density. Hence, there are many sources of uncertainty in the mean posterior density that can be identified through uncertainty analysis. We calculate the uncertainty associated with f, g, and V by varying one while keeping the rest constant.

Next, we calculate the 95% credible interval around the mean posterior curve and measure the relative width of the interval, i.e. the difference between the upper and lower quantiles. We repeat this process for each individual component, f, g, and V then plot all the curves together against temperature. In this plot, we can identify which model component creates the most uncertainty in R_0 by identifying the curve with the highest value at a given temperature.

4.2.4 Mapping suitability

To demonstrate an application of understanding the thermal suitability of BTV, we mapped both suitability and risk, at global scales. First, we present the geography of suitability across the globe by mapping the number of months of suitable temperatures for transmission - i.e. where $R_0 > 0$, using monthly average temperatures from the WorldClim dataset [154].

Second, we map livestock at risk of transmission, using the latest FAO Gridded Livestock of the World (GLW3) data for 2010, which details global distributions of sheep, goats, cows, and others, at a 5 minute scale [155]. To create a visually accessible risk map, suitability was scaled 0-1, and this was multiplied by 1+log(livestock). Thus we create a scaled risk map, balancing the season length and livestock density, to emphasize areas of coincidence,

rather than simple suitability. In this case we used the GLW3 sheep distribution [156], as the primary host at risk. All map calculations and manipulations were run in R using packages raster [157, 158], maptools [159] and Rgdal [160], following methods described in [161].

4.3 Results

Midge thermal traits

Midge density V: Recall the midge density formula given by

$$V(T) = \frac{F(T)\, p_E(T)\, p_L(T)\, p_P(T)}{\mu(T)^2\, (\rho_E(T) + \rho_L(T) + \rho_P(T))} \tag{4.10}$$

To estimate midge density V, we use survival probabilities $p_E,\ p_L,\ p_P$, for egg, larvae and pupae; and development times $\rho_E,\ \rho_L,\ \rho_P$ corresponding to the egg, larvae, and pupae life stages; the fecundity measure represented by the number of eggs per female per day F; and adult mortality rate μ. Figure 4.4 A shows the development time in days for eggs, larvae, and pupae. The data are fitted using a quadratic function, under the assumption that juvenile midges at a given stage will need more time to develop at very low ($<$20°C) and very high ($>$35°C) temperatures. For eggs, the development time ranges from 60 to 70 days; for larvae, from 15 to 35 days; and for pupae between 40 and 80 days. We fit the survival probabilities using a Brière curve (Figure 4.4 B). The survival probability is relatively high for eggs ($0.2 < p_E < 0.8$), very low for larvae ($p_L < 0.2$), but almost always 100% for the pupae stage ($p_P \sim 1$).

Given all the traits contributing to the midge density formula we can evaluate $V(T)$ to visualize how midge density varies with temperature. Figure 4.6 shows that midge density V is highest between 20 °C and 28 °C; it increases at temperatures higher that 10 °C and decreases when temperature exceeds 28 °C.

Transmission potential, g, is estimated by calculating the product of midge biting rate a and vector competence bc. We were not able to find data for the probability of a vector getting infected after a bite, so we assumed

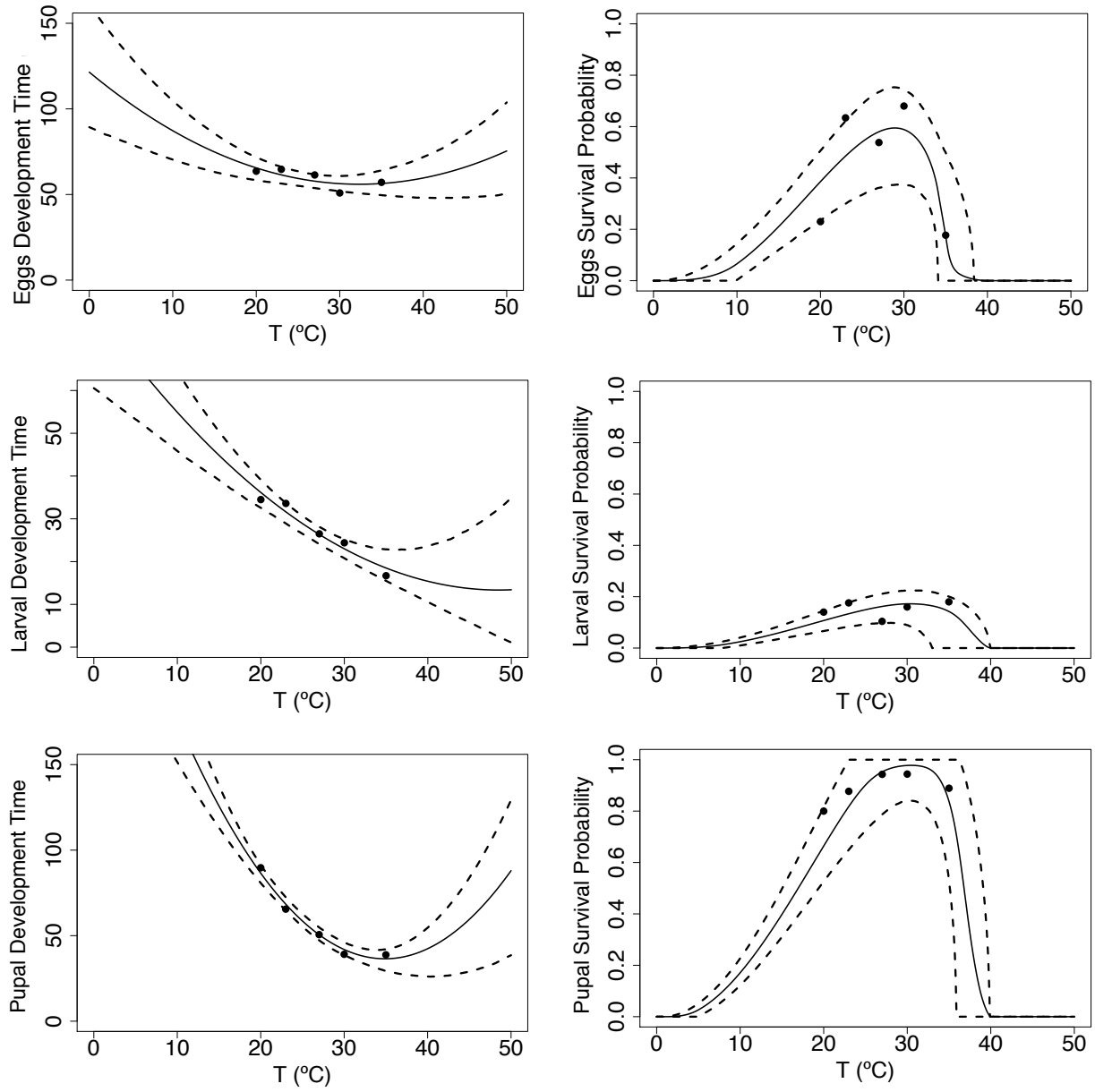

Figure 4.4: Figures in Column A show development time in days for midge juvenile stages, eggs ρ_E, larvae ρ_L, and pupae ρ_P. Figures in Column B show survival probabilities for midge juvenile stages, eggs p_E, larvae p_L, and pupae p_P. The solid line is the mean of the posterior distributions of the thermal response curves while the dashed lines represent the HPD intervals

that there will be a 50% chance for midges to become infected after biting an infected host $c = 0.5$. The biting rate a and the probability of transmitting infection b are fitted using a Brière curve (see Figure 4.7).

$$g(T) = b(T)c\, a^2(T); \tag{4.11}$$

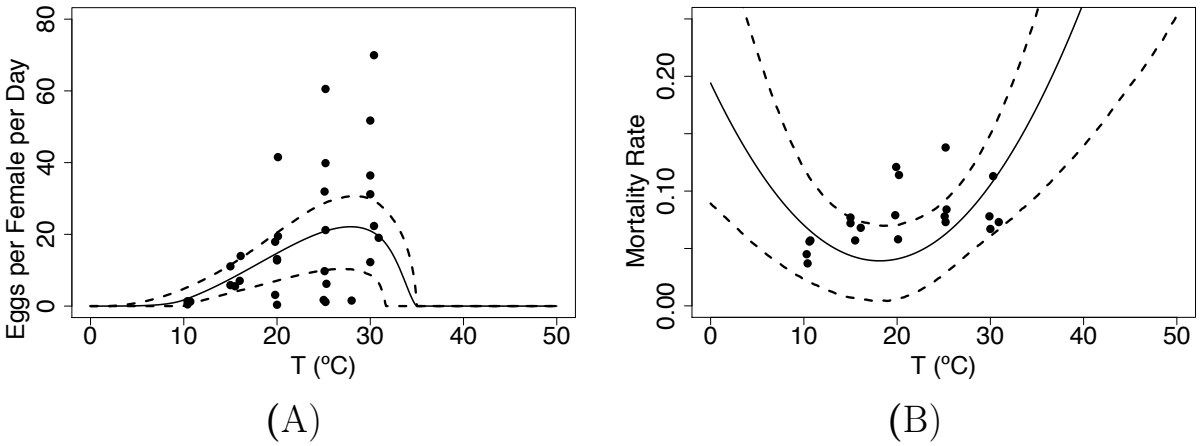

Figure 4.5: (A) Eggs per female per day F and (B) adult mortality rate μ traits as they vary with temperature. The solid line is the mean of the posterior distributions of the thermal response curves while the dashed lines represent the HPD intervals

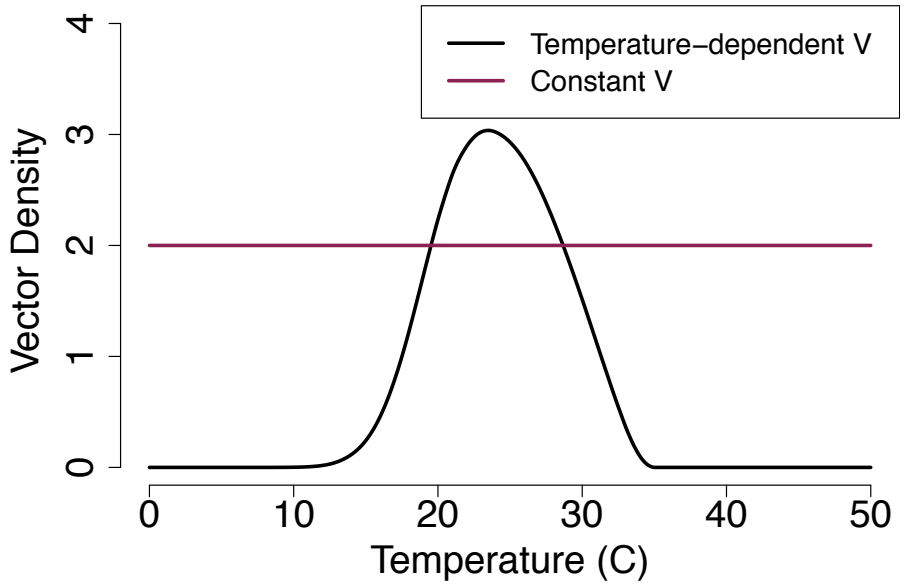

Figure 4.6: Modeled midge density as it varies with temperature. To obtain the temperature-dependent midge density, we evaluate Equation 4.10 at all temperature-dependent traits using the fitted curves. A constant value $V = 2$ shown for comparison for subsequent modeling.

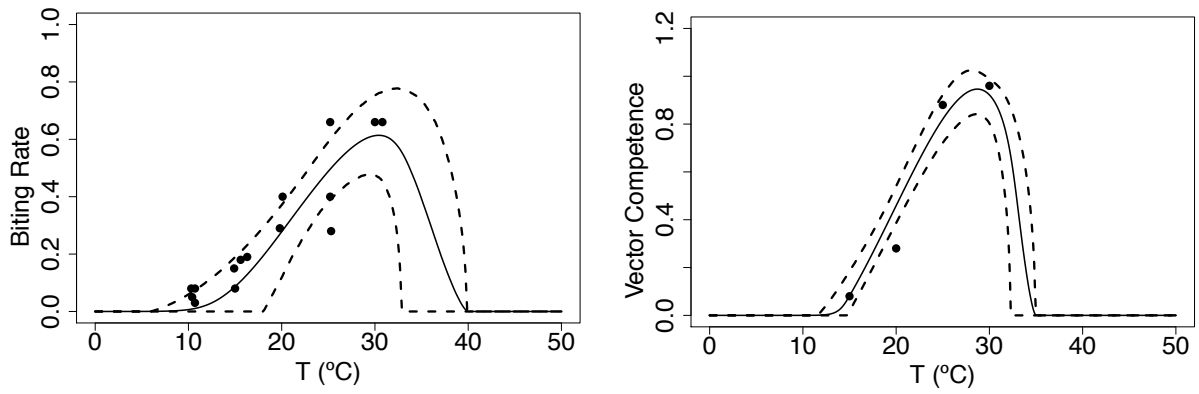

(A) (B)

Figure 4.7: (A) Biting rate a and (B) probability that midges transmit infection when biting an uninfected host b. The solid line is the mean of the posterior distributions of the thermal response curves while the dashed lines represent the HPD intervals

$$f(\nu(T), \mu(T)) = \begin{cases} e^{-\mu(T)/\nu(T)} & \text{Dietz 1993 [130]} \\ \dfrac{\nu(T)}{\nu(T) + \mu(T)} & \text{Gubbins et. al. 2008 [148]} \\ \left(\dfrac{3\nu(T)}{3\nu(T) + \mu(T)}\right)^3 & \text{new } R_0 \end{cases} \quad (4.12)$$

Functional form, f, is given by three different formulas depending on the model we use. All three formulas use the mortality rate μ given in Figure 4.5 (B), and the parasite development rate ν fitted using a Brière curve in Figure 4.8.

Equation 4.12 shows all the different formulas used in the models we present in this paper. Recall, each of these formulas is the probability that a midge becomes infectious post infection. Figure 4.9 shows the variation of the functional form with temperature based on the two temperature-dependent traits μ and ν. Although there are differences between the magnitude of these curves, we can see that their peak occurs at the same temperature (25 °C), which is due to the traits' thermal curves used in the formula.

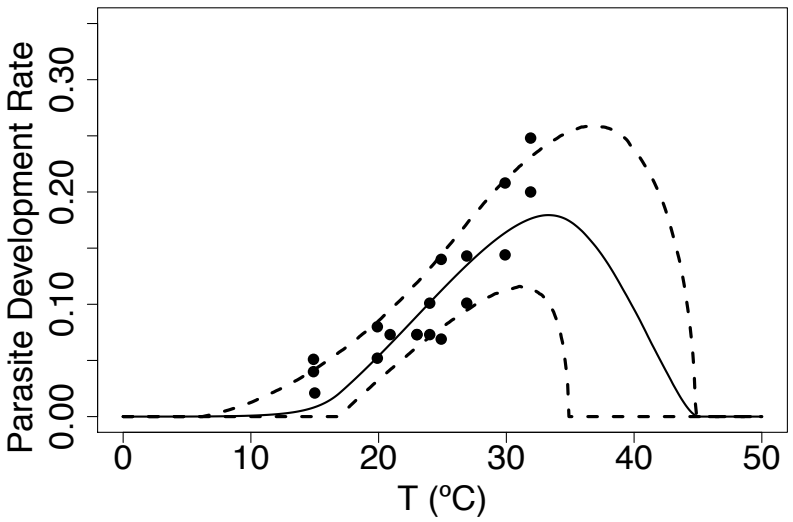

Figure 4.8: Parasite development rate (ν) is the inverse of extrinsic incubation period ($\nu = 1/EIP$). The solid line is the mean of the posterior distributions of the thermal response curves while the dashed lines represent the HPD intervals

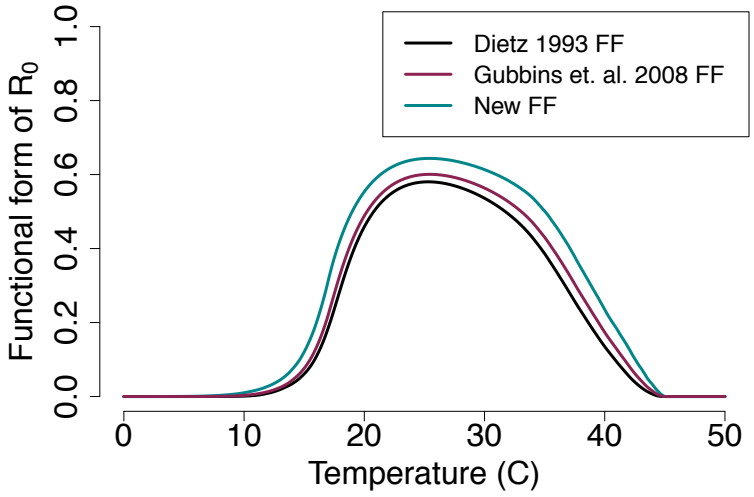

Figure 4.9: Functional forms used in R_0 versus temperature, where each solid line represents a different model.

Thermal response of R_0

We use thermal traits to evaluate R_0 given by Equation 4.4 with constant midge density V (Figure 4.10 A) and with temperature-dependent midge density $V(T)$ (Figure 4.10 B). The three models are slightly different when constant midge density is used but become agree when temperature-dependent midge density is used. This is due to all the temperature-sensitive traits used to calculate $V(T)$; however, this also leads to a higher uncertainty

shown in the range of HPD interval in Figure 4.10 (B). The lower thermal bound of the three posterior means are different by a magnitude of 1°C. However, the peak temperature and upper thermal limits are in agreement for all three models. With these results, we predict that $R_0 > 1$ occurs at temperature greater than 15°C and less than 33°C, meaning that BTV is likely to cause an outbreak within this temperature range. We note that this prediction is based on assuming $c = 0.5$ which may not be always true in reality.

Source of uncertainty in R_0

In Figure 4.10 (B), a high variation around R_0 posterior density is shown in the large HPD interval. To determine the source of this uncertainty, we plot the calculated relative widths for each R_0 component, see Figure 4.11. The results show that at a low temperature range ($14°C < T < 18°C$) uncertainty in R_0 is mainly due to the uncertainty in the functional form$f$. At intermediate temperatures ($18°C < T < 33°C$), the uncertainty is caused by the midge density $V(T)$. At very high temperatures ($33°C < T < 35°C$), the transmission potential g is the component producing the most variability in R_0.

Spatial BTV risk maps

Figure 4.12 illustrates the number of months each area is at risk of bluetongue disease transmission under the assumption that *Culicoides sonorensis* and *Culicoides variipennis* are the main vectors. The results show that, with the current average temperature, much of central Africa, south Asia, central and the northern part of South America, and northern Australia are suitable for bluetongue transmission year-round. These areas are also the warmest parts of the world, and as we move away from these parts the temperature is lower and the number of suitability months is reduced gradually.

Next, we use sheep worldwide distribution to determine areas where sheep are at risk of acquiring BTV. The choice of sheep was mainly because of data

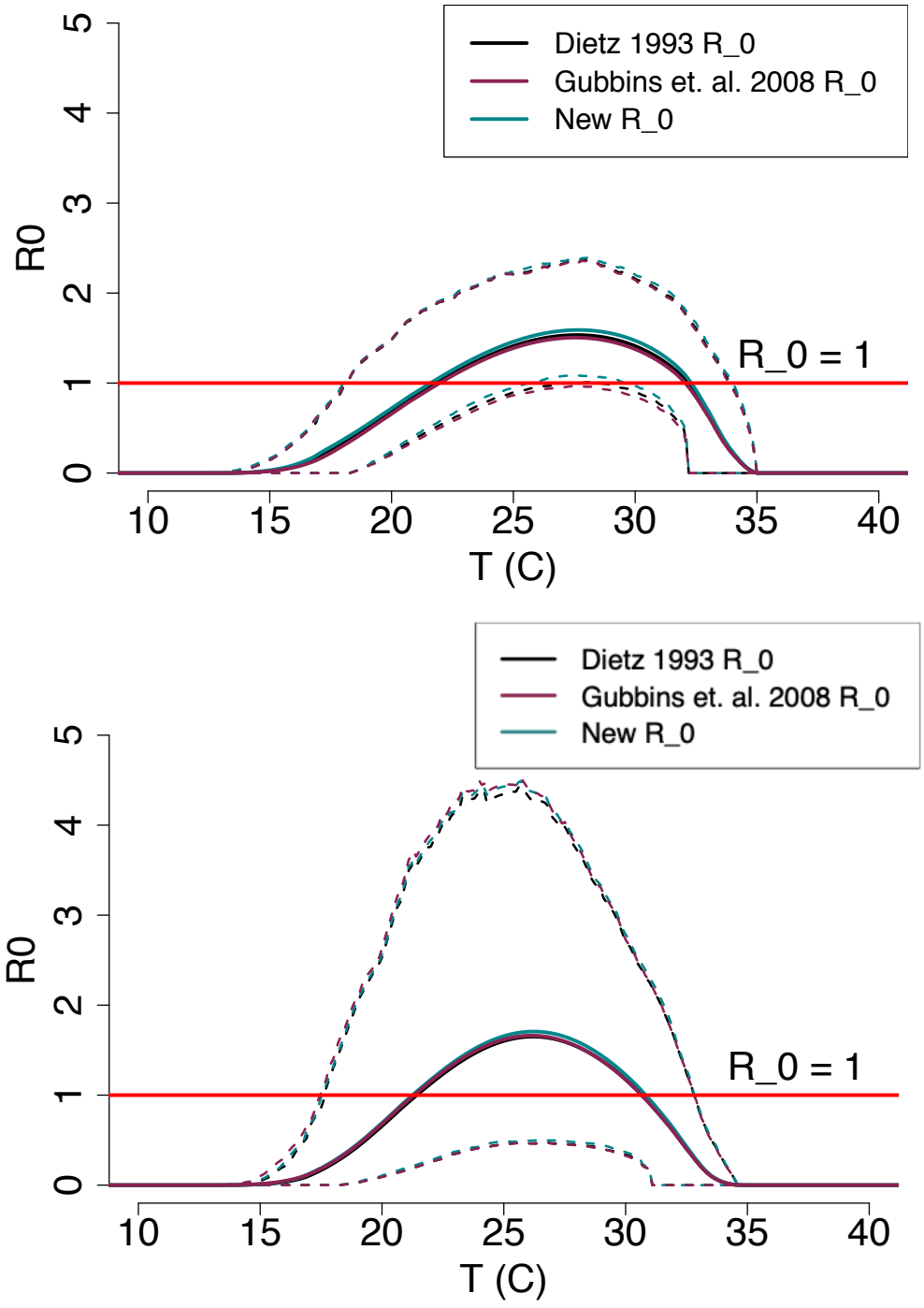

Figure 4.10: (Top) R_0 with constant midge density V and (Bottom) R_0 with temperature-dependent midge density $V(T)$. The plots shows the magnitude of R_0 changing as temperature increases. Each solid line represent the mean of the posterior distributions of R_0 while the dashed lines are the HPD intervals.

availability, but sheep are also the BTV host with highest mortality and morbidity. The results show that the areas where sheep are at the highest

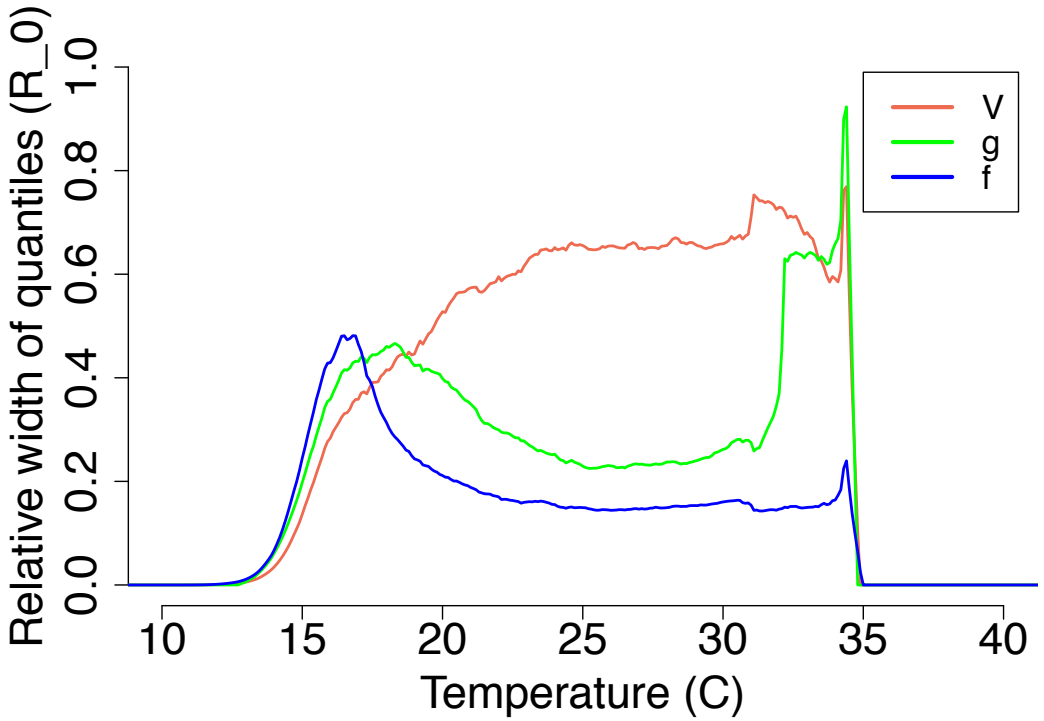

Figure 4.11: The source of uncertainty in $R_0(T)$ is measured by calculating the relative width of quantiles with each component varying with temperature while the remaining components are kept constants.

risk (scale>3) are located around the equator. The next highest risk regions (1<scale<3) include areas with the high livestock industry, such as central and south America and Europe.

4.4 Discussion

Here we are intersted in the effect of temperature on BTV spread. As highlighted in [162], BTV has been studied through different modeling approaches. This systematic review summarizes BTV models used post-1998 [162], most of which relied more on strong modeling assumptions rather than data. The results have been used to inform animal health decision-making by identifying at-risk areas and the risk of spread in case of introduction [163]. Although a few cited models have used the R_0 approach to study BTV, our model is different in the sense that it incorporates temperature across a wide range leading to an R_0 that is also temperature dependent. Linking R_0 to temperature can help identify BTV outbreak risk based on

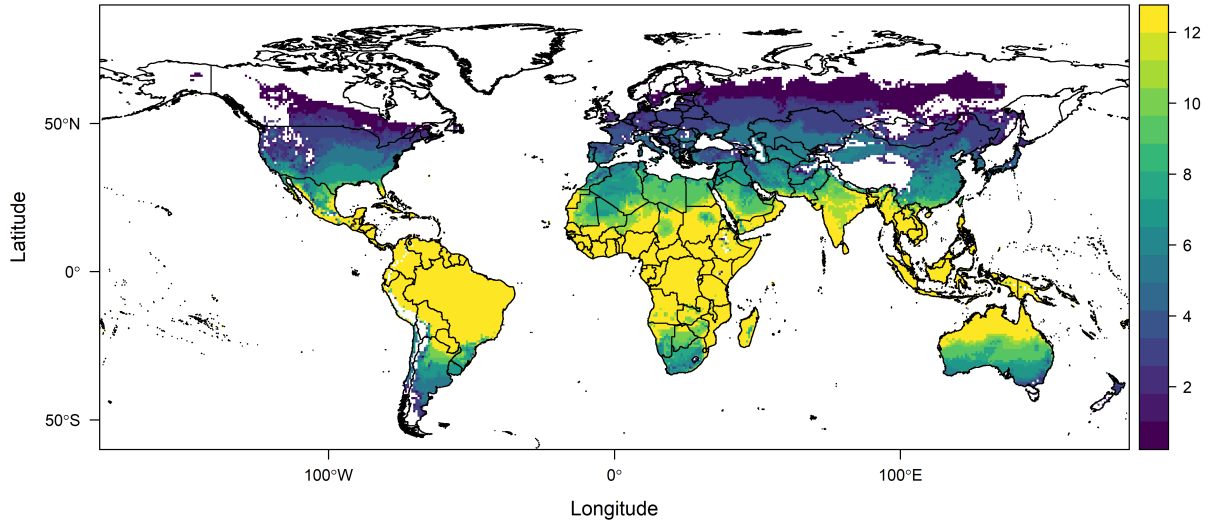

Figure 4.12: Map of the number of months (1-12) areas are at risk of bluetongue virus transmission according to our temperature-dependent R_0. This map based on the current mean monthly temperatures and is restricted to bluetongue disease caused by the two midge species *Culicoides sonorensis* and *Culicoides variipennis*.

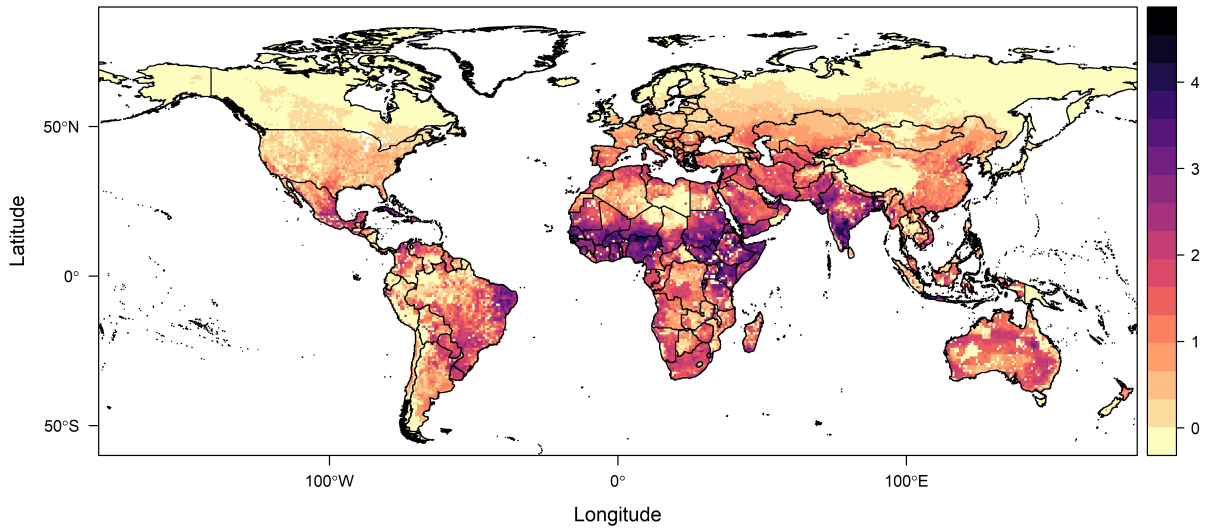

Figure 4.13: Scaled transmission risk suitability of bluetongue virus for sheep, as the primary host at risk, worldwide. the scale ranges from a low risk, 0, to a high risk, 5.

temperature at particular locations, which can inform management policies and control strategies.

We use a Ross-Macdonald type modeling approach to describe BTV transmission [128, 129]. We also adopt two previously used BTV models, [130] and [148], to compare their resulting $R_0 s$ to ours. This mechanistic

approach allowed us to derive the basic reproduction ratio's posterior distribution as a function of temperature. We were able to both determine the suitable temperature for possible BTV outbreaks when $R_0 > 1$ and the temperatures at which BTV outbreaks are likely to die out when $R_0 < 1$. We note that the thermal response of R_0 here is dependent on our model assumptions, for example setting the infection probability to be $c = 0.5$ and choosing the host density H and recovery rate d such that $Hd = 1$.

Based on the available traits' laboratory data we used in our model, we predict that BTV outbreaks, at least from the examined midge species, can occur within the temperature range of 15°C and 33°C, with outbreak peak at about 26°C. This result was obtained regardless of which R_0 formula used, i.e., all three different models lead to the same predictions. Similarly, investigating the lower thermal limit, peak, and upper thermal limit of R_0 led to no difference between peaks and upper thermal limits for all three forms and a difference between the lower thermal limits of 1 °C. This indicates that the uncertainty of the temperature effects swamp the effects due to the differences in modeling assumptions for these particular models.

Previous studies also investigated temperatures suitable for other vector-borne diseases. For example, a study on three mosquito-borne diseases, Zika, dengue, and chickungunya transmitted by *Aedes aegypti* and *Aedes albopictus* showed that the transmission is likely to occur between 18-34°C with peak transmission between 26-29°C [17]. Moreover, the temperatures suitable for the transmission of the plant-borne disease, citrus greening, between 16°C and 33°C with peak transmission at 25°C [164]. Together with our findings, this shows that there are similarities between ectotherm vectors in the way they respond to temperature. For example, their traits follow humped shaped thermal performance curves. But there are differences in the temperatures ranges they tolerate, and the temperatures at which their performance is maximal.

Incorporating different temperature-dependent traits into the model resulted in high uncertainty in the R_0 posterior density. Our uncertainty analysis allowed us to determine the traits responsible for causing uncertainty

in R_0 at each part of the temperature range. For instance, at a low temperature range ($14°C < T < 18°C$) more data are needed for the parasite development rate, ν, and mortality rate, μ, to reduce this uncertainty in the functional form f. At medium temperatures ($18°C < T < 33°C$) the uncertainty in R_0 is caused by V, meaning that more data are needed in traits contributing to estimating the midge density. Overall, the biting midge density $V(T)$ appears to be the main source of uncertainty at a wide temperature range. While at very high temperatures ($33°C < T < 35°C$) we need more data on vector competence bc and biting rate a. Reducing the uncertainty in R_0 will improve our predictions and our control and prevention suggestions.

Furthermore, we created spatial risk maps showing the number of months per year each worldwide location is suitable for BTV disease transmission given the presence of two midge species, namely, *Culicoides sonorensis* and *Culicoides variipennis*. The results show that warmer areas are at risk year-round while colder ares are at risk during fewer months. However, these results are based on current temperatures and with climate change and the continuous rising of global temperatures, the area at risk of BTV may expand to include places with a previously lower risk [165].

Chapter 5

Discussion

Vector-borne diseases form 17% of infectious diseases and put 80% of the world population at risk [112, 166]. Most of these diseases do not have cures or vaccines, and thus prevention and control remain the best options to deal with outbreaks when they occur [167]. While other researchers are working on advancing the knowledge on cures and vaccines for VBDs [168], modelers feel the responsibility of advancing the knowledge on understanding the mechanisms and dynamics of such diseases to inform control and prevention. In this work, I focus on a mosquito-borne disease, dengue, and a midge-borne disease, bluetongue, as case studies.

Current and future changes in climate, especially temperature, have a huge impact on VBD transmission [169, 170, 171, 96]. Thus, understanding the temperature effect on VBDs will allow us to improve our current strategies. For instance, temperature is a critical determinant of ectotherms abundance. Hence, understanding the temperature-density relationship will guide the timing and the amount of spraying needed to reduce vector abundance, and therefore decrease the transmission risk should an outbreak start.

When estimating mosquito abundance, previous models focus on the adult mosquito traits since adult females are the ones responsible for spreading the pathogen [6, 50, 27]. In Chapter 2, I argue that juvenile stage traits are also important in shaping the adult population. As a result, I propose a system of ordinary differential equations modeling *Aedes aegypti* at each of the four juvenile stages, namely, eggs, larvae, pupae, and adults. I restrict

the adult stage to females while the other stages include both sexes. I derive the total female mosquito density V_d and compare it to three models previously used; a life stage trait-dependent density V_l [74]; an adult trait-dependent density V_a [26]; and a sine wave density V_s [75]. I use the mean squared error (MSE) between our estimates and *Aedes aegypti* abundance data as a measure of estimate goodness.

The results show that a simple non-linear regression fit of the data using the sine wave density V_s lead to a lower MSE, i.e. a closer estimate of the data. While the life stage trait-dependent density V_l and the dynamical density V_d are the next closest estimates, with the adult trait-dependent density V_a being the farthest estimate. This result means that when *Aedes aegypti* abundance data are available, a simple forecasting method using V_s can be better. However, that is not always the case, and when abundance data are not available and there is a need to estimate *Aedes aegypti* abundance at a certain location, it is best to use V_l or V_d. These densities only require the temperature at the particular location and traits related to the ecology of the mosquito to give a close estimate of *Aedes aegypti* abundance. One study highlighted the importance of incorporating life stage temperature-dependent traits to investigate the potential for dengue in six US cities[52]. Our proposed model comparison could test other temperature and abundance scenarios, and thus inform future models on which model version is better to implement.

Infectious diseases differ in the way they spread between direct and indirect transmission [172, 173, 174]. Directly transmitted infectious diseases include the flu and sexually transmitted disease, while indirect transmission includes water-borne (hepatitis A), air-borne (chickenpox) and vector-borne (malaria) diseases. Generally, studying the spread of infectious diseases relies on understanding the interactions between the host, the pathogen (and the vector when applicable) as well as the role of the environment.In particular, the basic reproductive ratio R_0 is used to detect outbreak risk [175, 176, 177]. Similarly, I use the basic reproductive ratio R_0 to determine VBDs' outbreak suitability, and because VBDs are sensitive to temperature, I am interested

in the temperature-dependent R_0.

I investigate the effect of temperature on juvenile and adult stages of these VBD vectors and highlight differences in modeling approaches. The methods I implement are all based on using Bayesian models to fit thermal curves to vector traits' data and evaluate model parameters at these curves. Incorporating these thermal curves leads to a temperature-dependent R_0 which allows us to determine the temperature range suitable for disease transmission. For instance, I found that the suitable temperature for a dengue outbreak is between 17°C and 35°C for *Aedes albopictus*, and between 17°C and 34°C for *Aedes aegypti*.

For bluetongue, we investigate the effect of temperature on the biting midges. The results show that, similar to mosquitoes, temperature affects midge traits including the juvenile stages traits. We fit temperature-sensitive midge traits and derive a thermal response for the basic reproductive ratio R_0. Our analysis show that the transmission suitability is between 16°C and 33°C. These temperature ranges indicate where surveillance should take place to prevent large outbreaks according to our model.

The limitations associated with our approach lie in the high variation among the Bayesian fitting of thermal curves leading to uncertainty in our predictions. This issue can be solved if more data are generated, especially at extremely low and high temperatures. Therefore, more laboratory and field experiments investigating the effect of temperature variation, in particular, and other climate factors, in general, on vector traits are encouraged for all vectors. Not only ectotherms are sensitive to local temperature changes, but they are also able to adapt to global temperature changes. For example, acclimating vector eggs at higher constant temperatures leads to a higher thermal tolerance for adults [178, 179]. Our mechanistic methods can easily be adjusted to make predictions under new temperature scenarios and adapted to fit other vector-borne diseases.

Appendix A

Appendix for Chapter 2

A.1 Thermal Traits

We evaluate the thermal functions described in Table 2.1 at temperature varying from 0°C to 50°C to look at *A*edes aegypti adult and juvenile trait responses to temperature. Then, we these thermal curves we look at the total mosquito densities V_a and V_l variation with temperature.

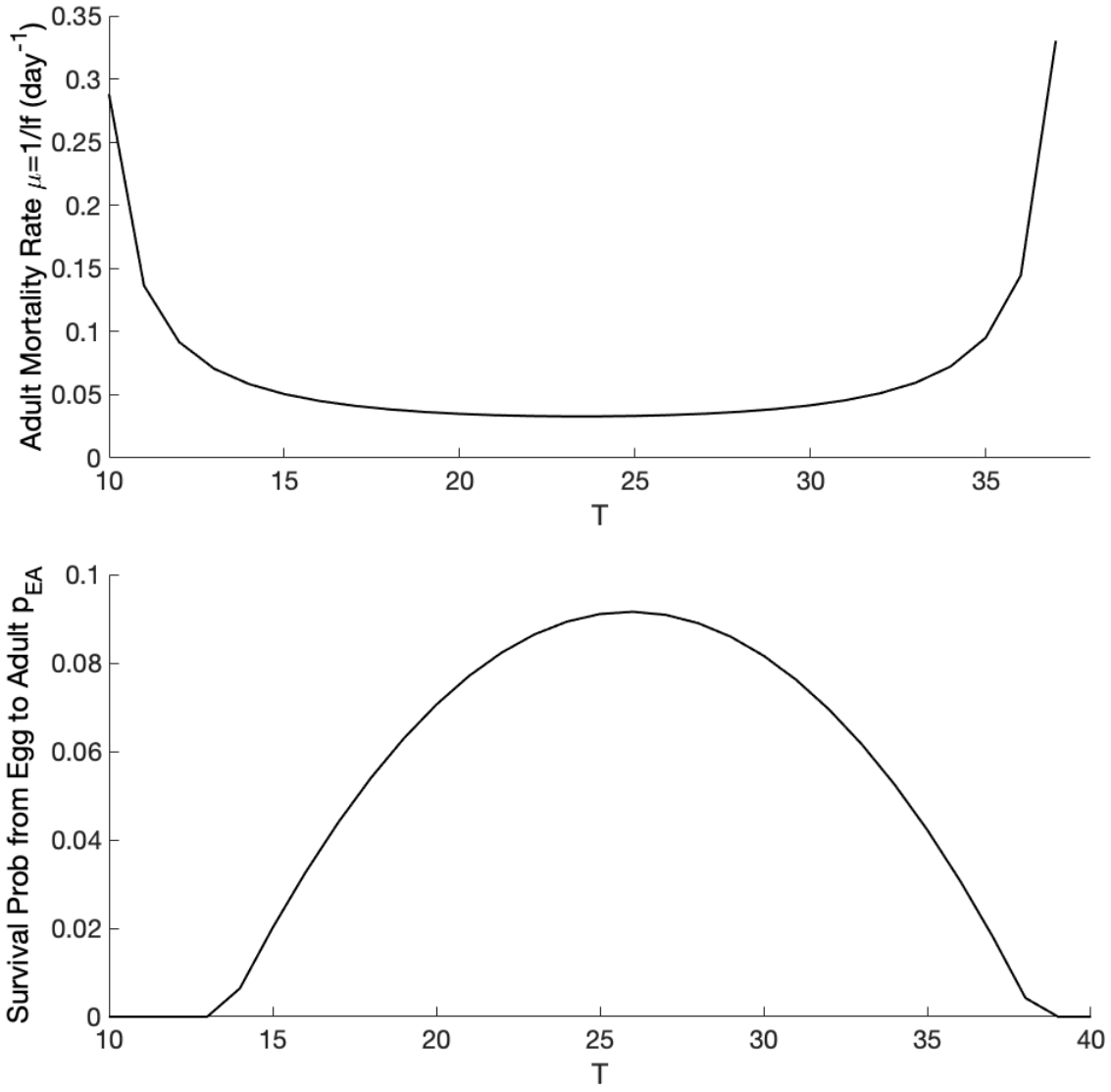

Figure A.1: Adult mosquito mortality rate μ and the survival probability from eggs to adult p_{EA} as they vary with the temperature range of 0°C to 50°C [17, 86].

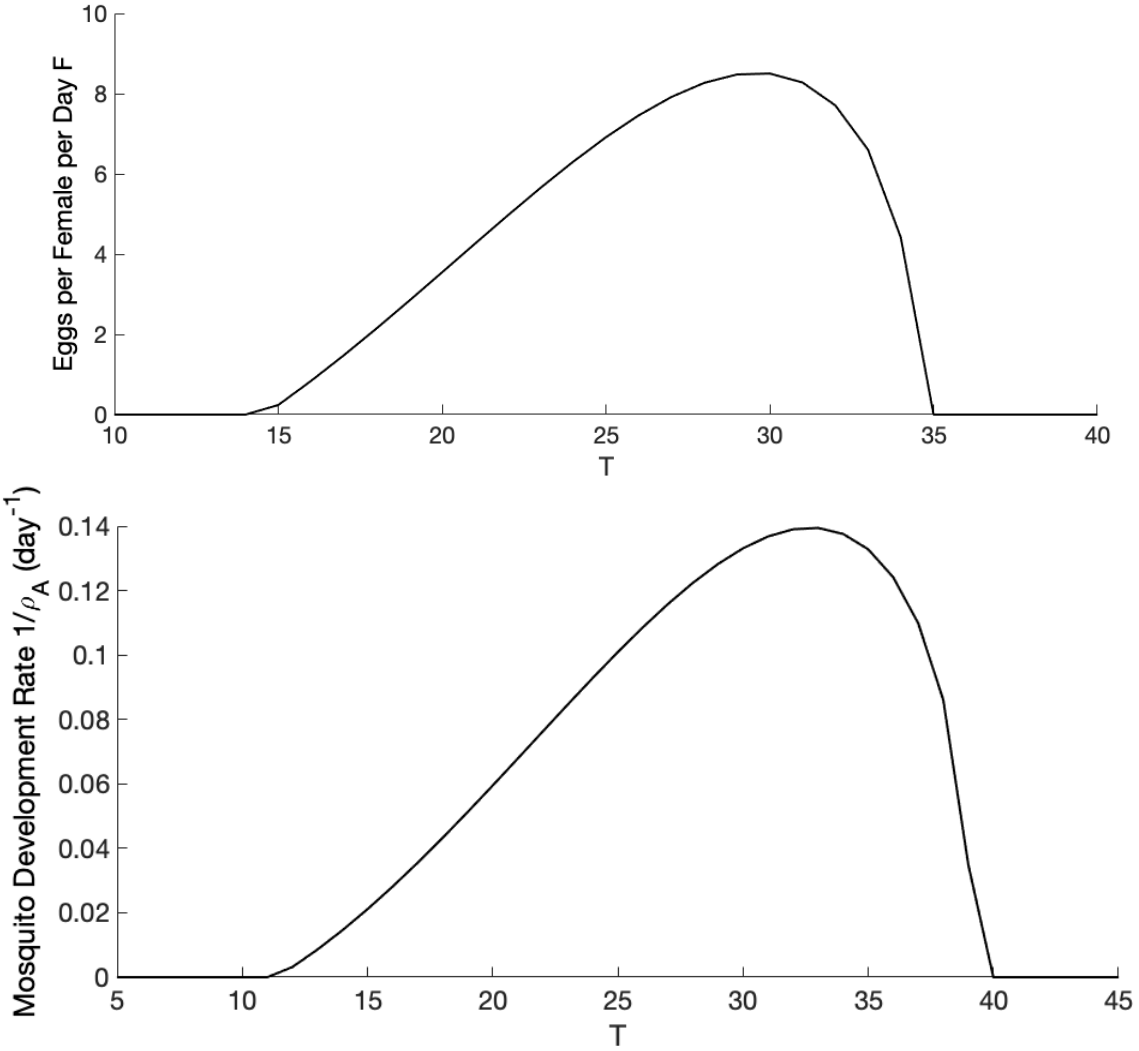

Figure A.2: Adult mosquito fecundity F [87, 52] and the adult mosquito development rate $1/\rho_A$[17, 86] as they vary with the temperature range of 0°C to 50°C .

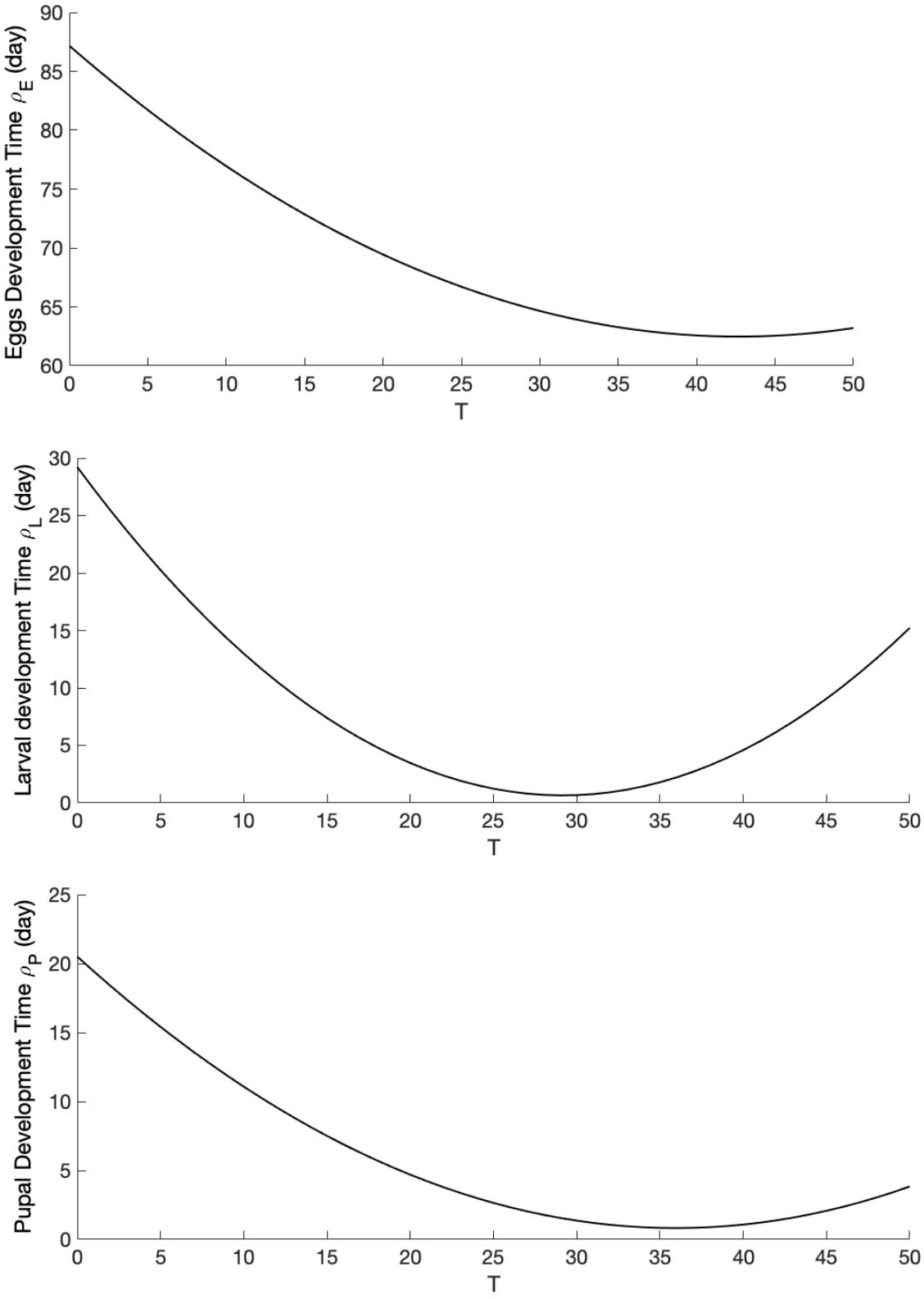

Figure A.3: Juvenile stages development time, eggs ρ_E, larvae ρ_L, and pupae ρ_P as they vary with the temperature range of 0°C to 50°C [87, 52].

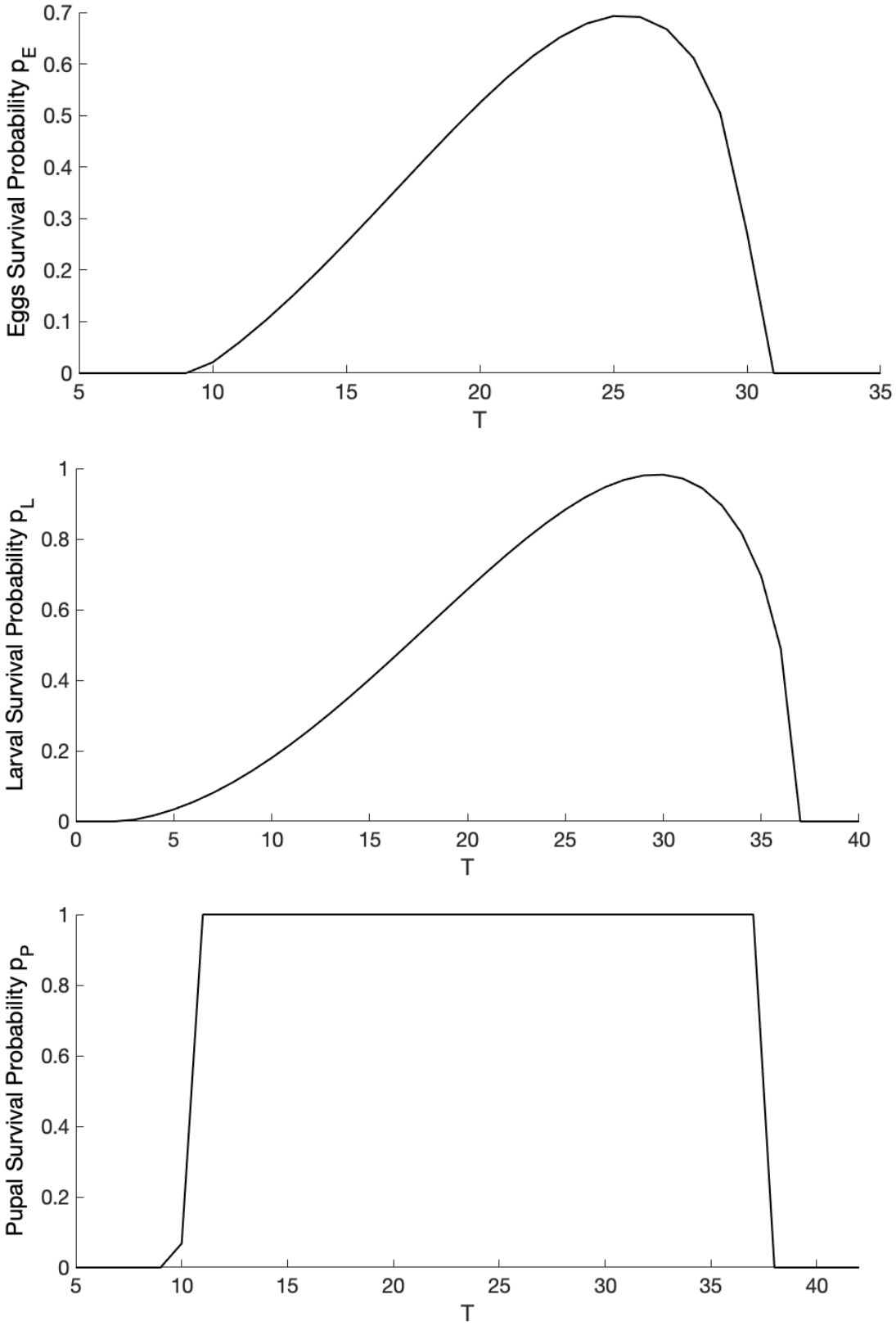

Figure A.4: Juvenile stages survival probability, eggs p_E, larvae p_L, and pupae p_P as they vary with the temperature range of 0°C to 50°C [88].

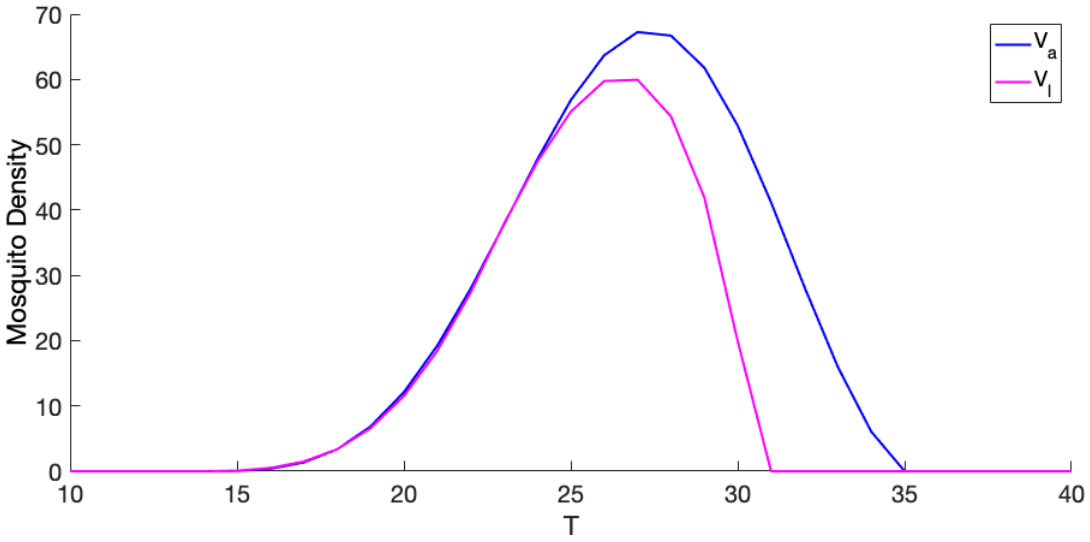

Figure A.5: Adult trait dependent mosquito density V_a and life stage trait dependent mosquito density V_l as they vary with the temperature range of 0°C to 50°C.

Appendix B

Appendix for Chapter 3

B.1 Bayesian Fitting of Traits Thermal Curves

To fit each trait, we chose a unimodal functional form as the mean function. To model the observed data we use normal distributions for all thermal traits. We used priors appropriate for the biological description of the data, taking into account the positivity of their values as well as their range. The values in the priors are decided as we go until the appropriate fitting curve is obtained. We collected juvenile and adult data for *A. albopictus* and for *A. aegypti* we collected juvenile data and used already published data for adults [17], however we were unable to find eggs development rate and larval survival probability for *A. aegypti* and used these two curves from *A. albopictus*. Below are plots of individual thermal trait fits and the table containing all information about likelihood distributions and priors. The tables summarize all values used in our Bayesian model.

Model Parameter	Mean Function	Parameters	Prior	Likelihood
Biting Rate		T_0	dunif(0, 24)	dnorm
a	Brière	T_m	dunif(25,45)	
		c	dgamma(1,10)	
		τ	dgamma(0.00001, 0.001)	
Transmission Prob.		T_0	dunif(0,24)	dnorm
b	Brière	T_m	dunif(25,45)	
		c	dgamma(7,10000)	
		τ	dgamma(100, 1)	
Infection Prob.		T_0	dunif(0,24)	dnorm
c	Brière	T_m	dunif(25,45)	
		c	dgamma(7,10000)	
		τ	dgamma(100, 1)	
Egg-to-adult Prob.		T_0	dunif(0,24)	dnorm
p_{EA}	Quadratic	T_m	dunif(25,45)	
		qd	dgamma(1,1)	
		τ	dgamma(0.0001, 0.0001)	
Eggs per Female per Day		T_0	dunif(0, 20)	dnorm
F	Brière	T_m	dunif(35, 45)	
		c	dgamma(1,.1)	
		τ	dgamma(0.001, 0.001)	
Parasite Development Rate		T_0	dunif(0, 20)	dnorm
ν	Brière	T_m	dunif(30,45)	
		c	dgamma(1,10)	
		τ	dgamma(0.0001, 0.0001)	
Adult Lifespan		T_0	dunif(0,15)	dnorm
$lf = 1/\mu$	Quadratic	T_m	dunif(35,45)	
		qd	dgamma(4,1)	
		τ	dgamma(0.001, 0.001)	
Adult Development Rate		T_0	dunif(0, 26)	dnorm
$1/\rho_A$	Brière	T_m	dunif(25,45)	
		c	dgamma(1,10)	
		τ	dgamma(0.00001, 0.001)	

Table B.1: *Aedes albopictus*: Bayesian model values used. For each thermal trait, we specify the likelihood distribution and the priors used for each parameter.

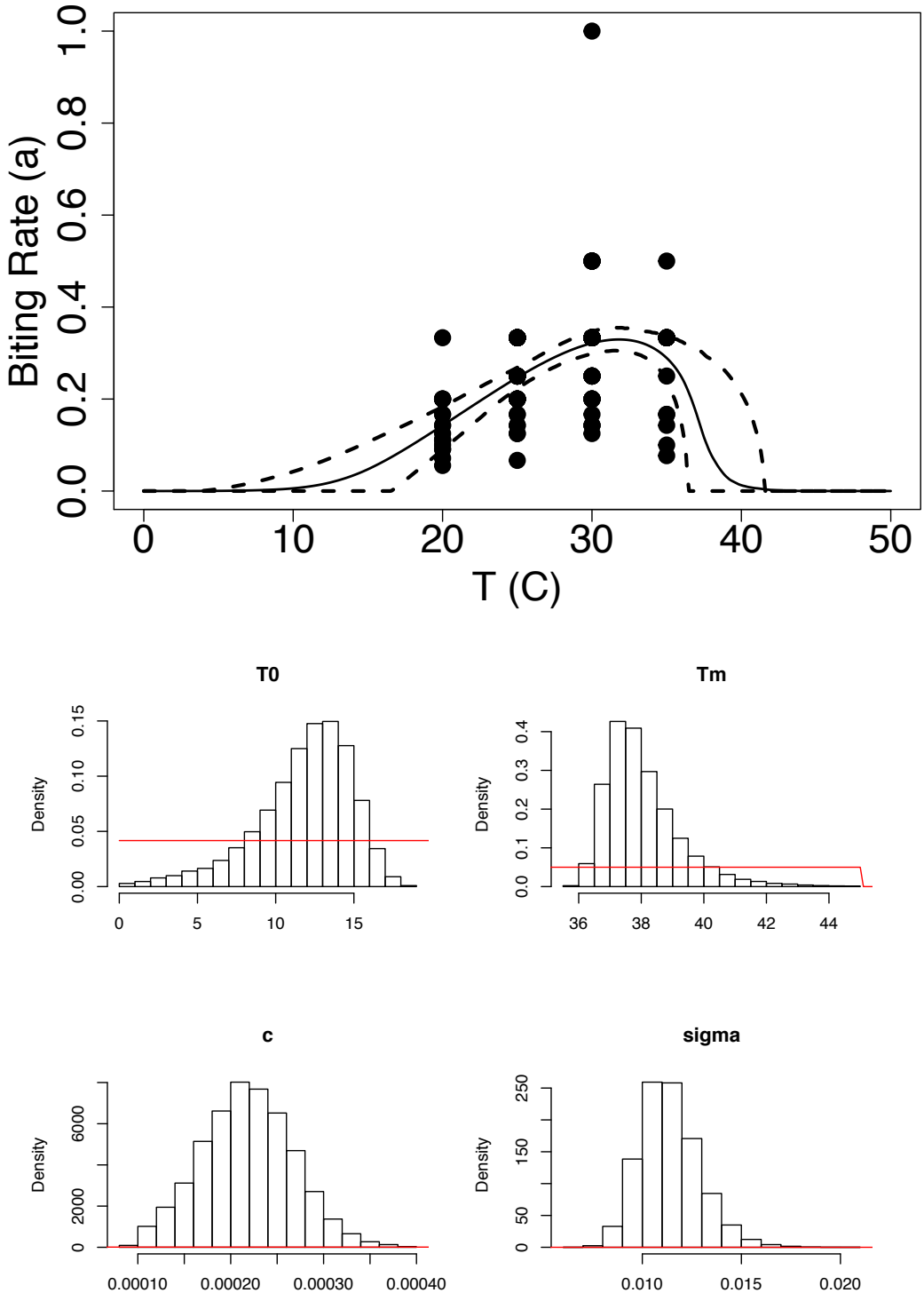

Figure B.1: *Aedes albopictus*: Mean of the posterior distributions of the thermal response curves for the biting rate a in solid line and HPD interval in dashed black. Histograms of the posterior distribution for each parameter of the Brière fit for the biting rate a. The prior distribution for each parameter is plotted in red. The Brière fit is determined by the equation $cT(T - T_{Min})\sqrt{T_{Max} - T}$ using a normal distribution with standard deviation σ.

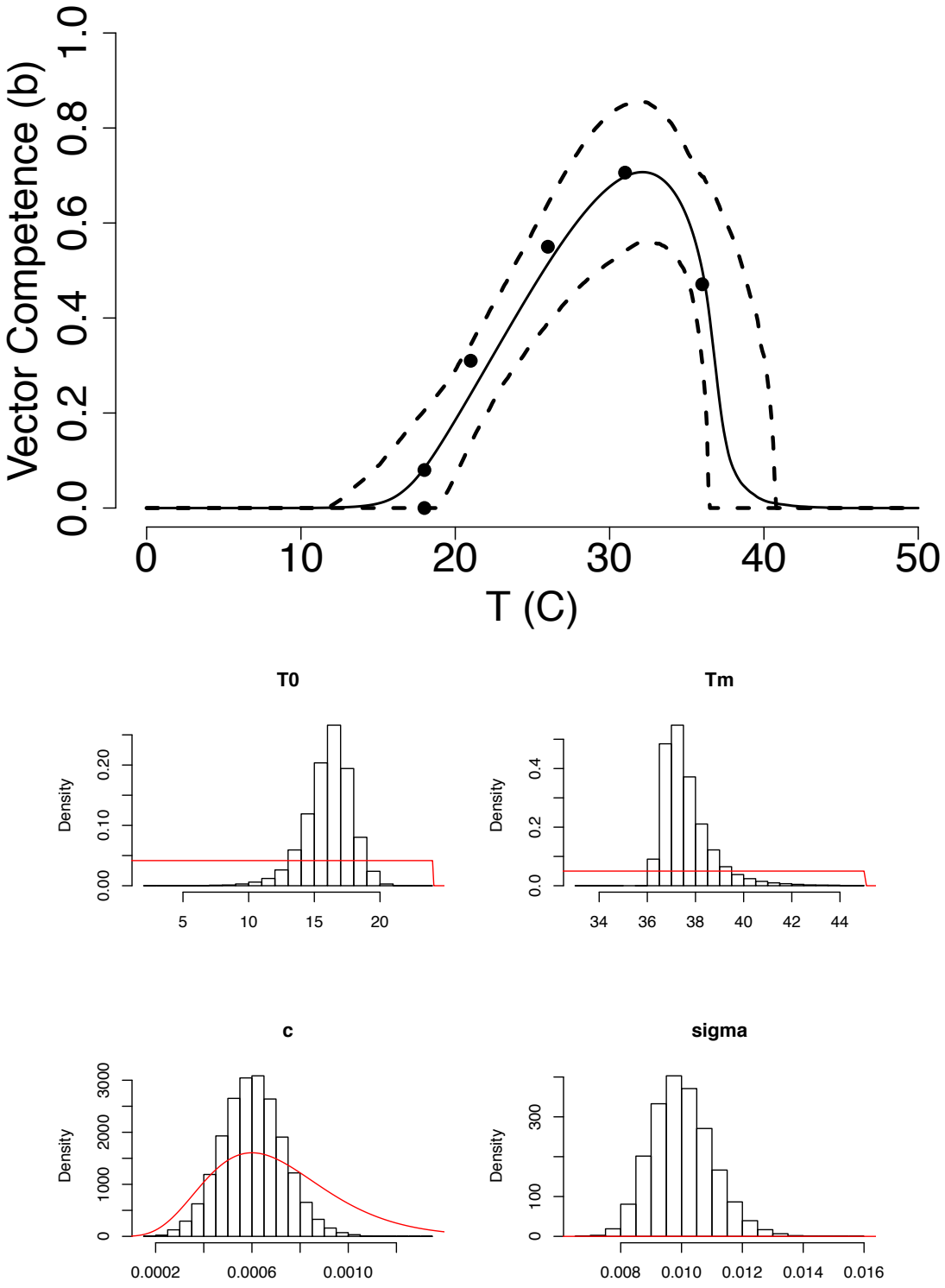

Figure B.2: *Aedes albopictus*: Mean of the posterior distributions of the thermal response curves for the probability of a vector transmitting the virus when biting b and HPD interval in dashed black. Histograms of the posterior distribution for each parameter of the Brière fit for the probability b. The prior distribution for each parameter is plotted in red. The Brière fit is determined by the equation $cT(T - T_0)\sqrt{|T_m - T|}$ using a normal distribution. The vector competence (bc) is the product of b and c.

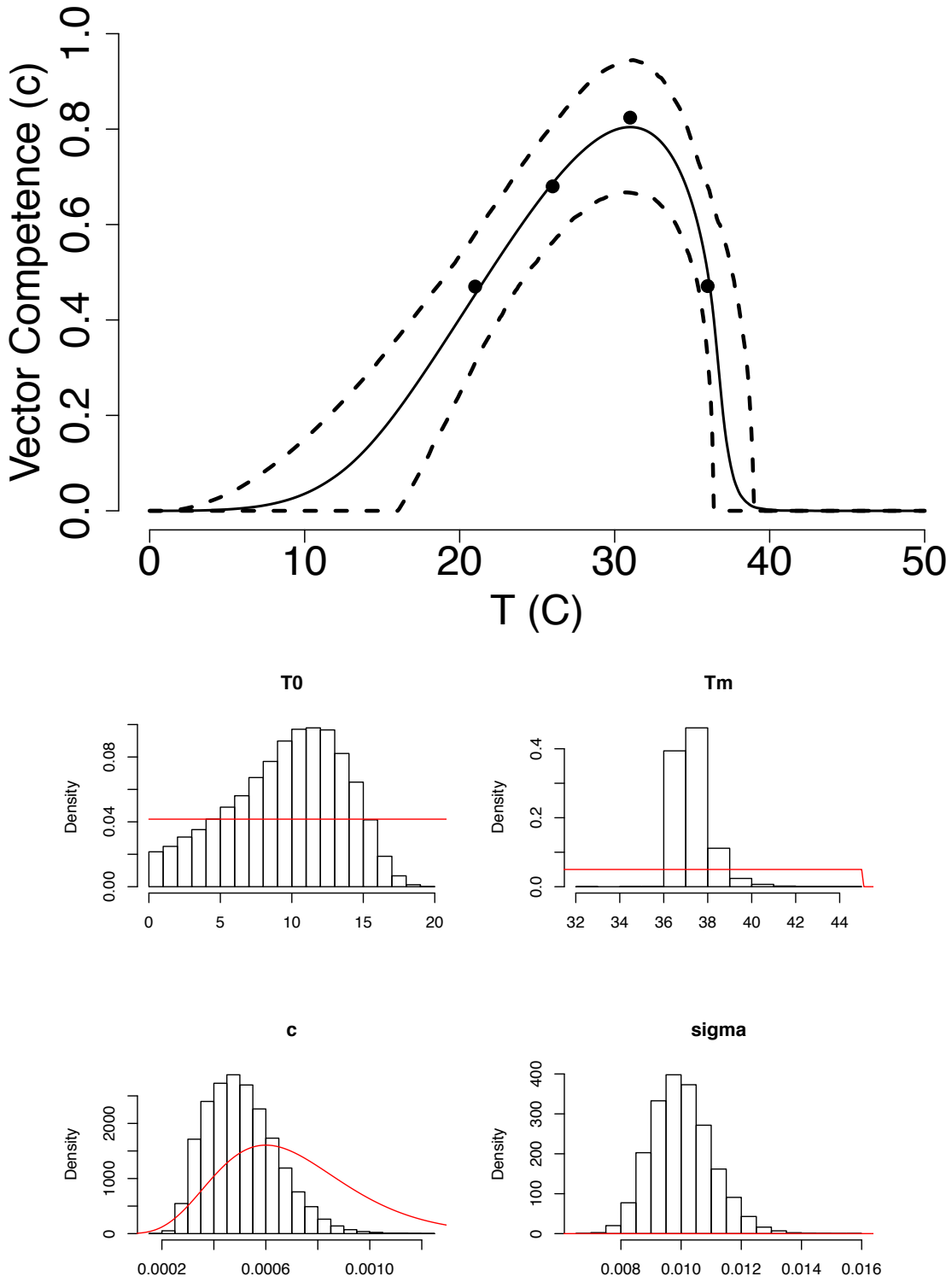

Figure B.3: *Aedes albopictus*: Mean of the posterior distributions of the thermal response curves for the probability of a vector getting infected after a blood meal containing a pathogen c in solid line and HPD interval in dashed black. Histograms of the posterior distribution for each parameter of the Brière fit for the probability c. The prior distribution for each parameter is plotted in red. The Brière fit is determined by the equation $cT(T - T_0)\sqrt{|T_m - T|}$ using a normal distribution. The vector competence (bc) is the product of b and c.

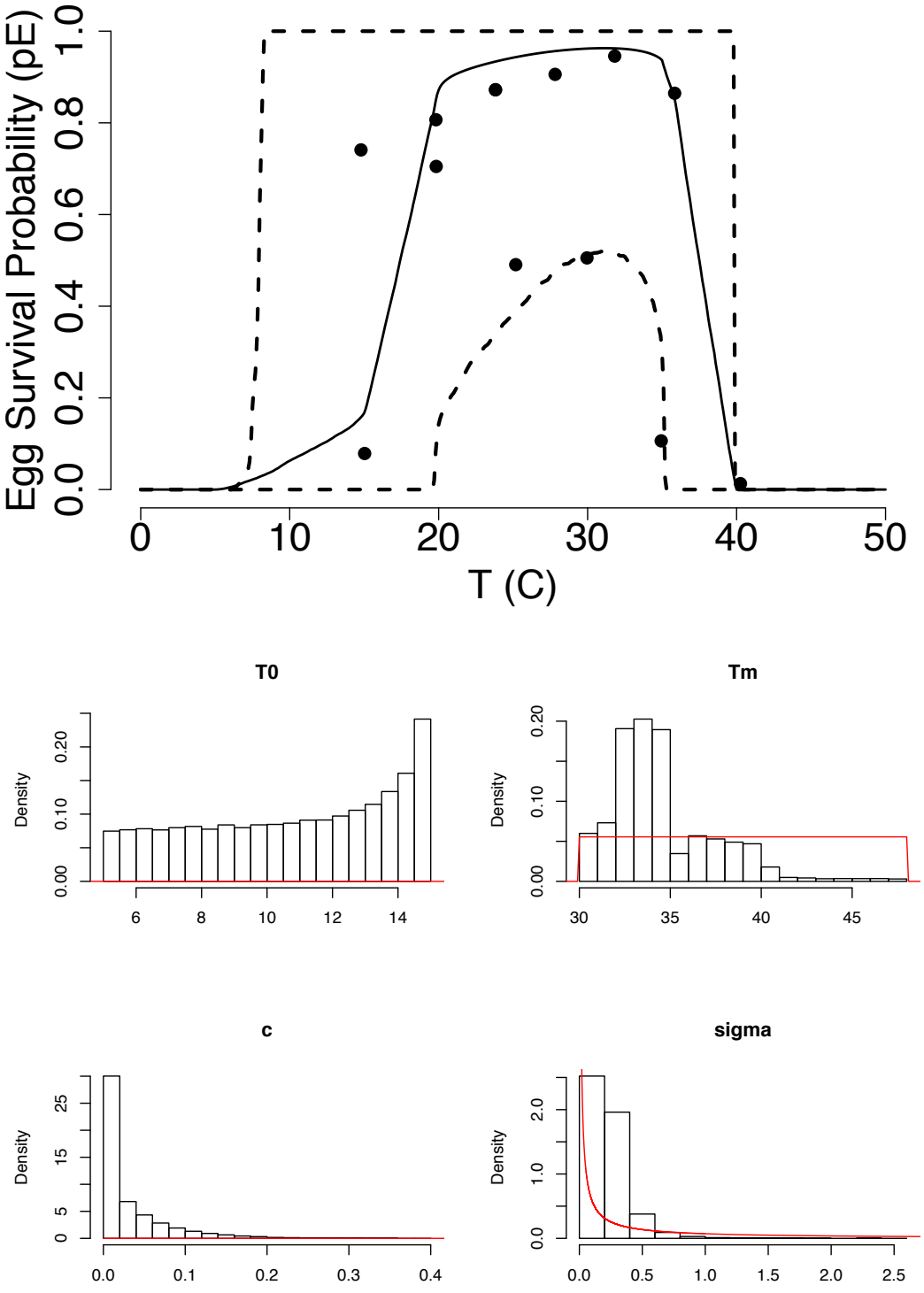

Figure B.4: *Aedes albopictus*: Mean of the posterior distributions of the thermal response curves for the survival probability for eggs p_E in solid line and HPD interval in dashed black. Histograms of the posterior distribution for each parameter of the quadratic fit for the probability p_E. The prior distribution for each parameter is plotted in red. The quadratic fit is determined by $-qd(T - T_0)(T_m - T)$ using a normal distribution with standard deviation σ.

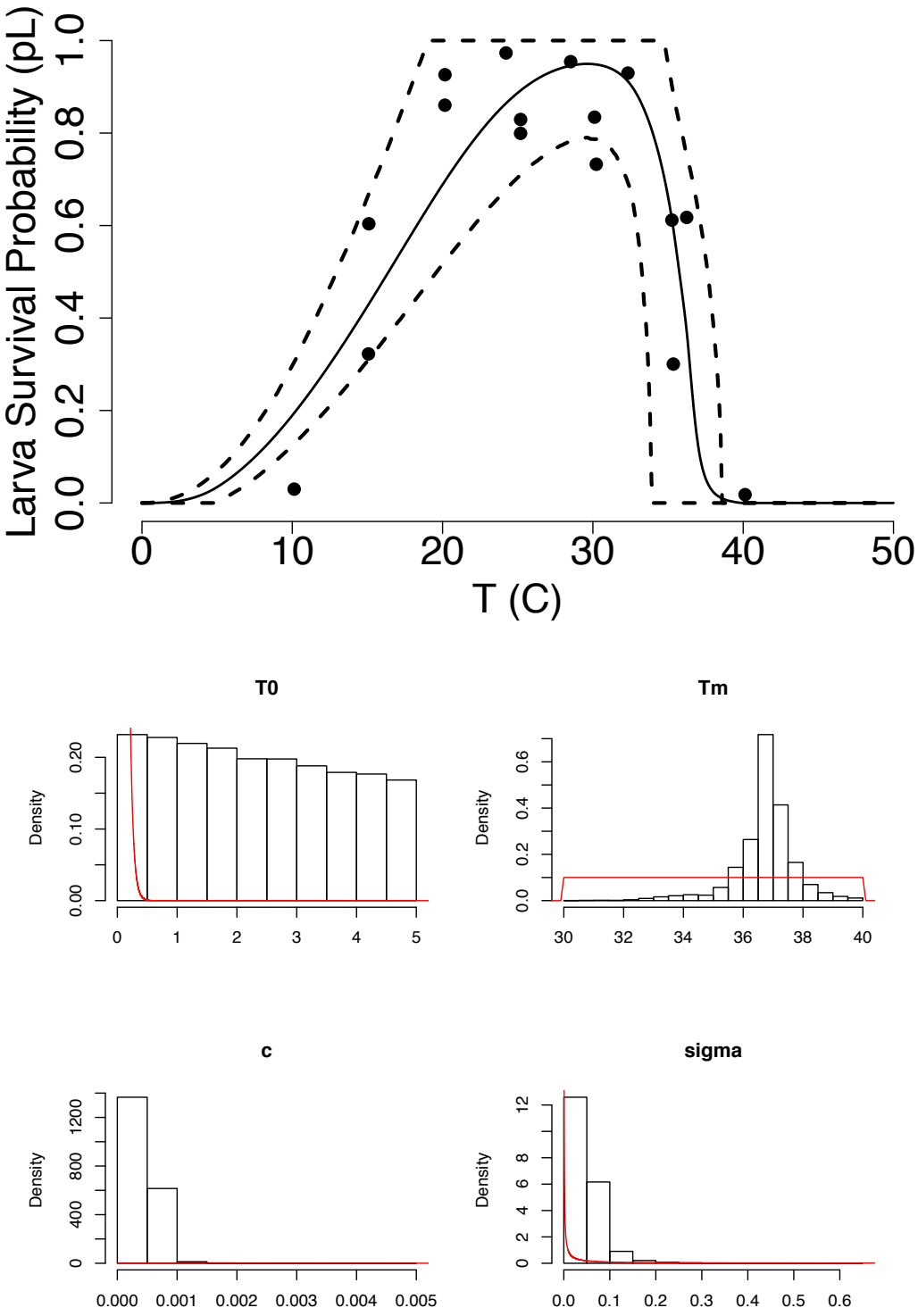

Figure B.5: *Aedes albopictus*: Mean of the posterior distributions of the thermal response curves for the survival probability for eggs p_L in solid line and HPD interval in dashed black. Histograms of the posterior distribution for each parameter of the Brière fit for the probability p_L. The prior distribution for each parameter is plotted in red. The Brière fit is determined by the equation $cT(T - T_0)\sqrt{|T_m - T|}$ using a normal distribution with standard deviation σ.

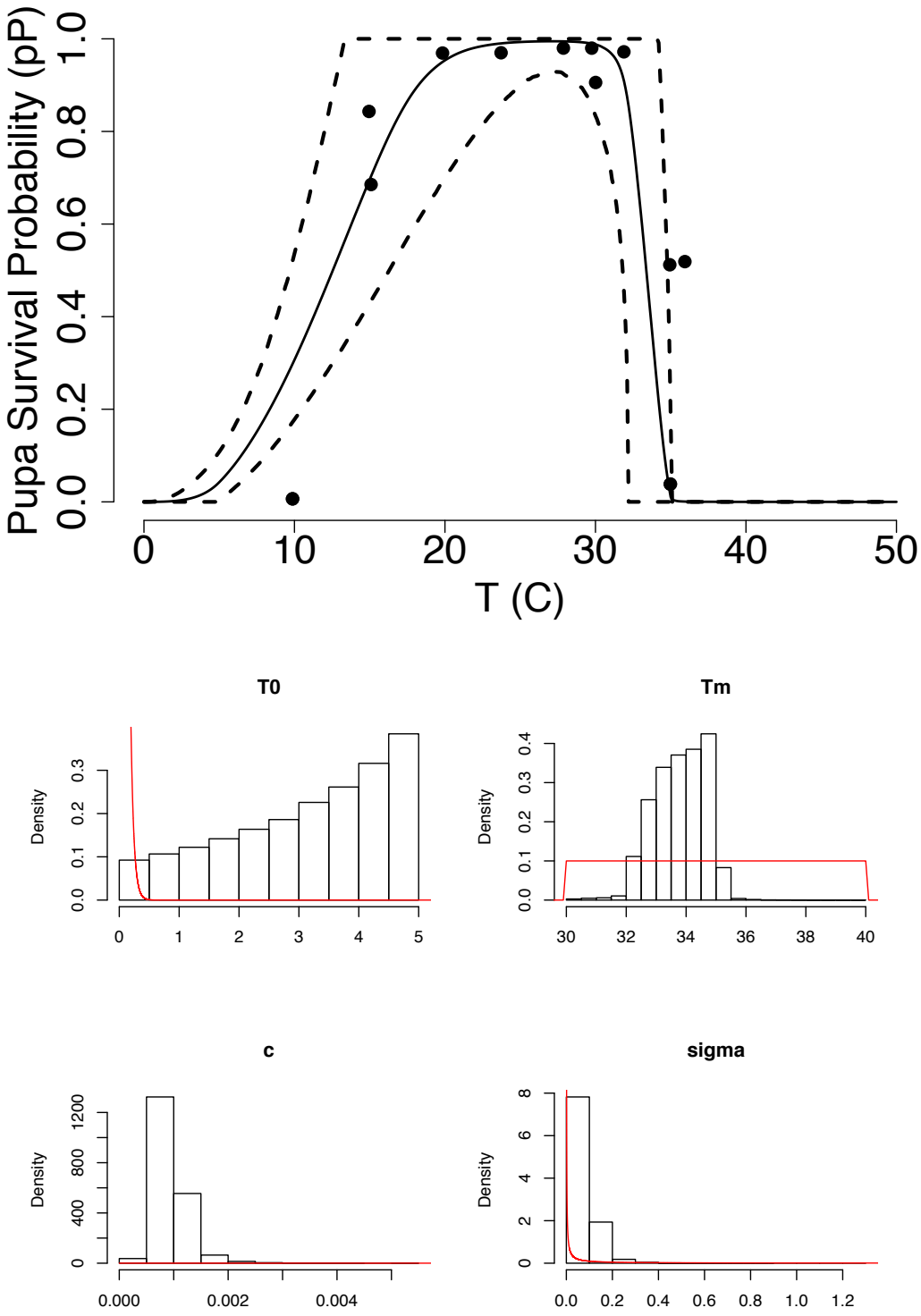

Figure B.6: *Aedes albopictus*: Mean of the posterior distributions of the thermal response curves for the survival probability for eggs p_P in solid line and HPD interval in dashed black. Histograms of the posterior distribution for each parameter of the Brière fit for the probability p_P. The prior distribution for each parameter is plotted in red. The Brière fit is determined by the equation $cT(T - T_0)\sqrt{|T_m - T|}$ using a normal distribution with standard deviation σ.

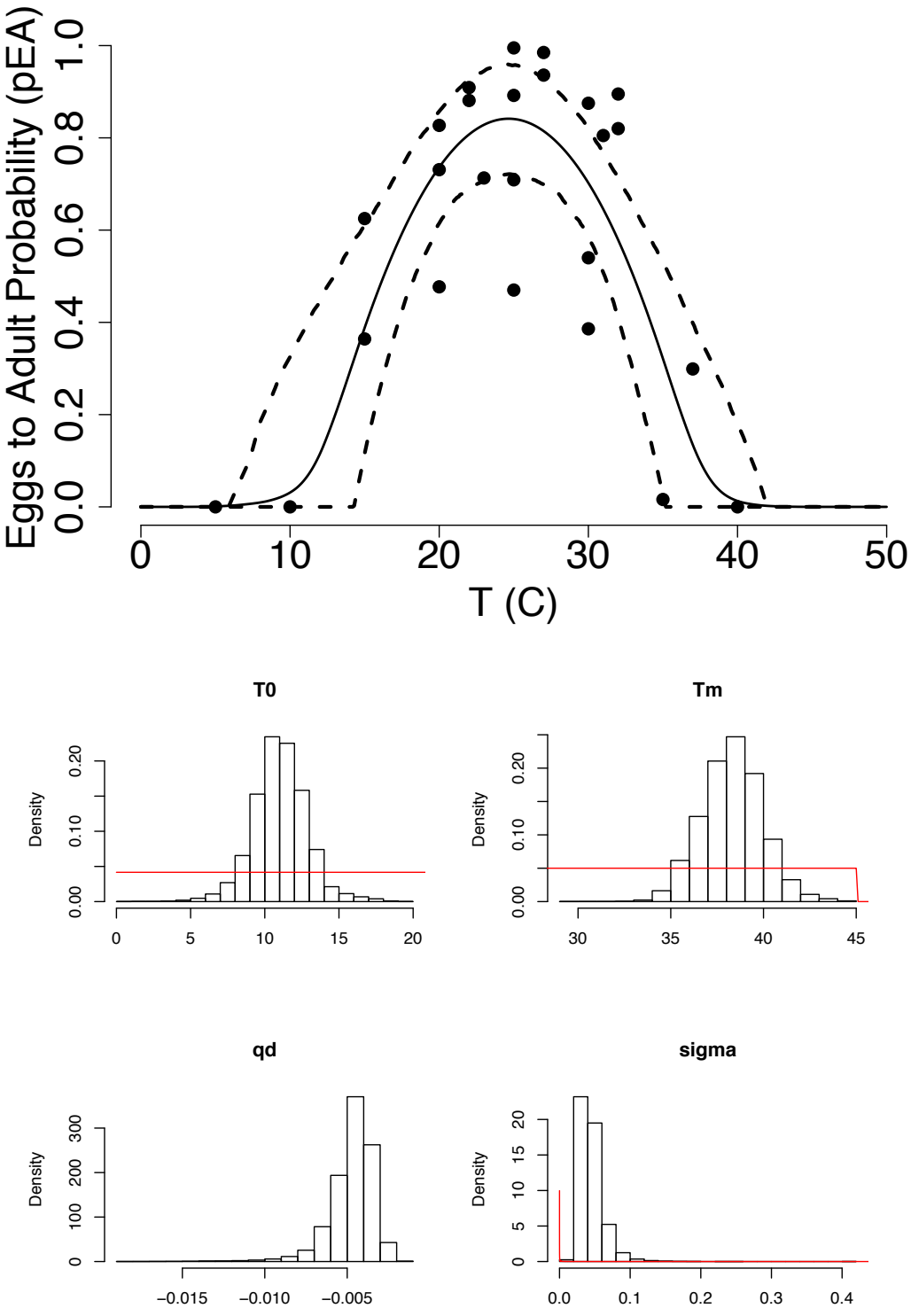

Figure B.7: *Aedes albopictus*: Mean of the posterior distributions of the thermal response curves for the survival probability from eggs to adults p_{EA} in solid line and HPD interval in dashed black. Histograms of the posterior distribution for each parameter of the Brière fit for the probability p_{EA}. The prior distribution for each parameter is plotted in red. The Brière fit is determined by the equation $cT(T - T_0)\sqrt{|T_m - T|}$ using a normal distribution with standard deviation σ.

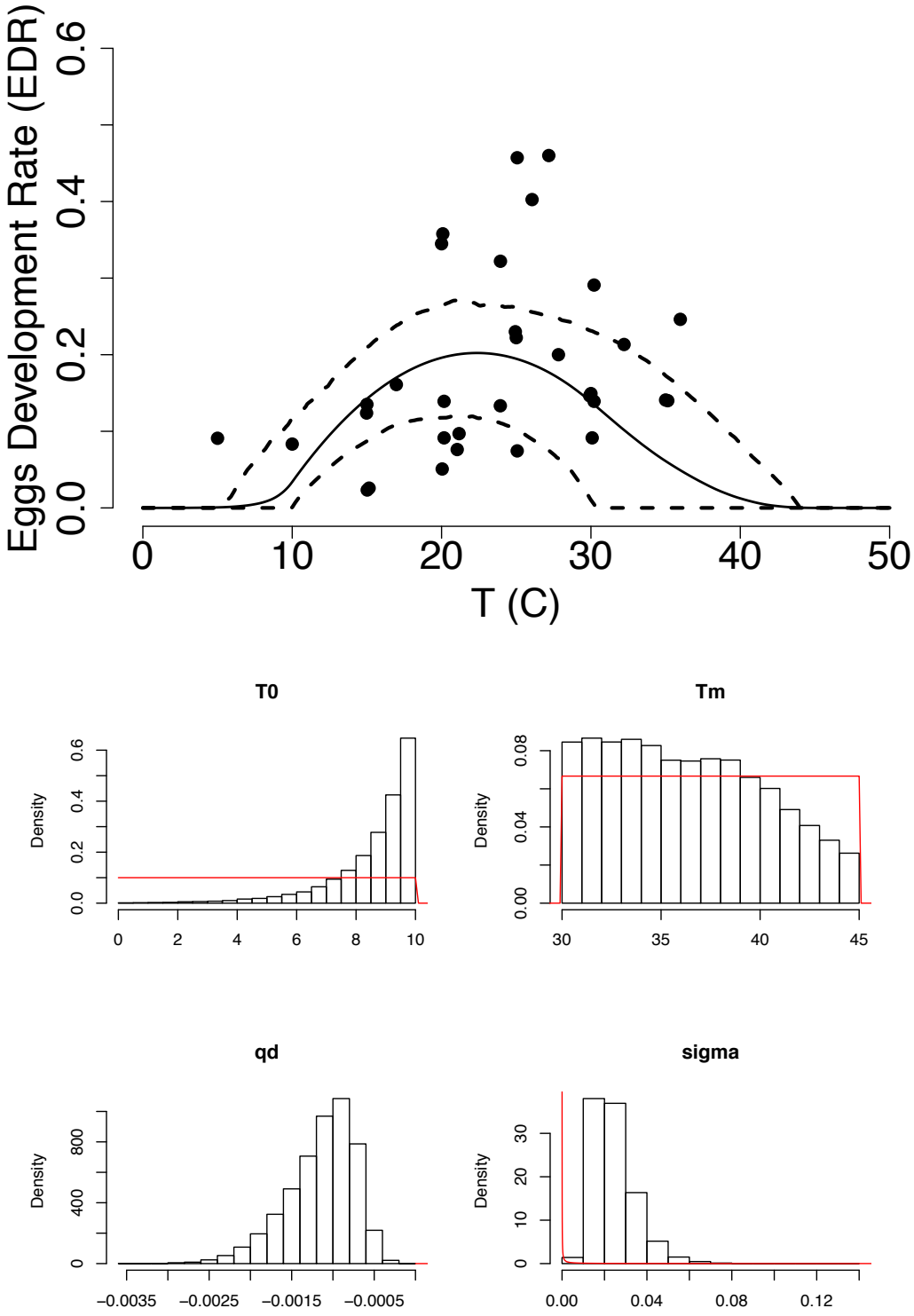

Figure B.8: *Aedes. albopictus*: Mean of the posterior distributions of the thermal response curves for eggs development rates (inverse of development times ρ_E) in solid lines and HPD interval in dashed black. Histograms of the posterior distribution for each parameter of the quadratic fit. The prior distribution for each parameter is plotted in red. the quadratic fit is determined by $-qd(T - T_0)(T_m - T)$ using a normal distribution with standard deviation σ.

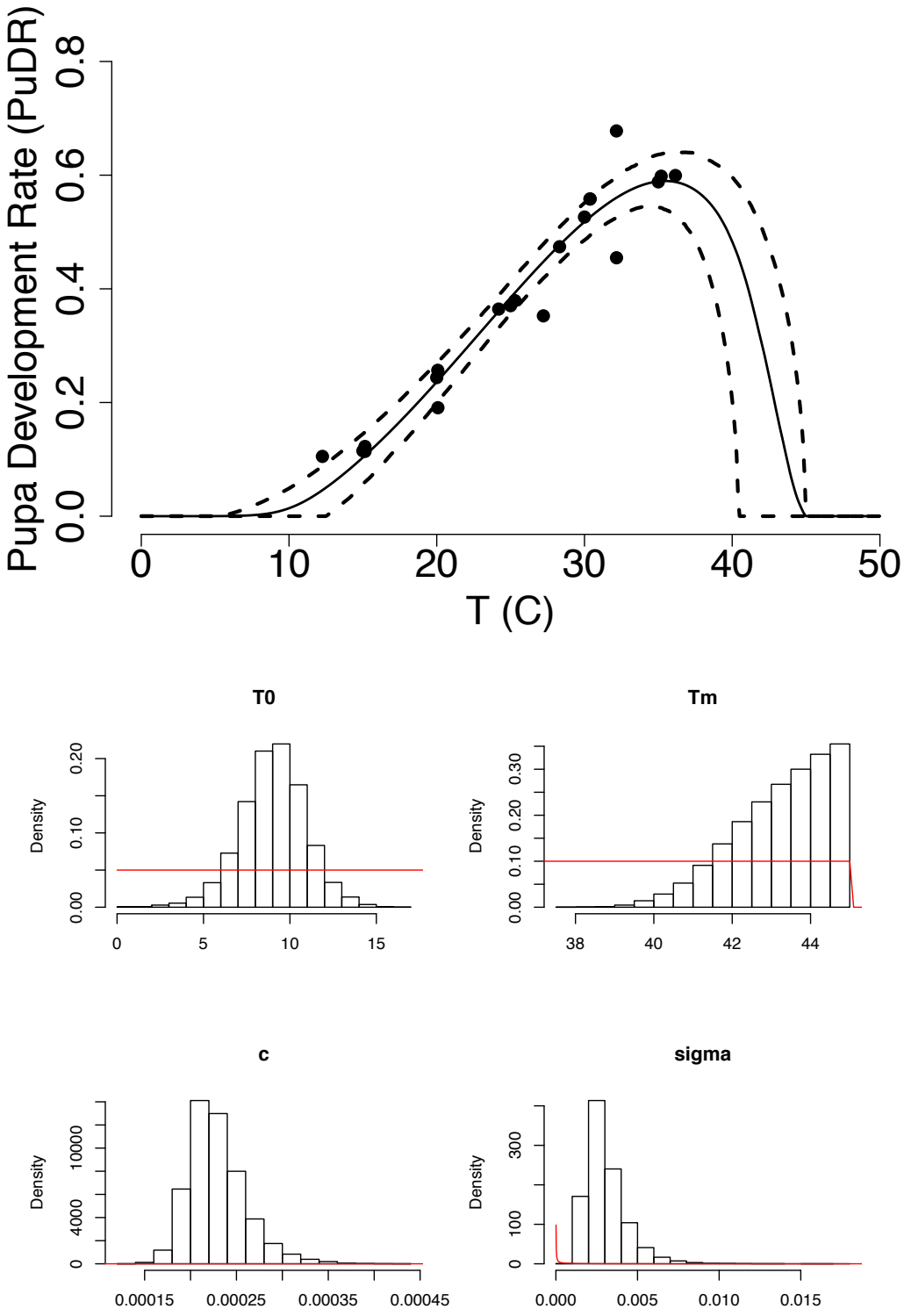

Figure B.9: *Aedes. albopictus*: Mean of the posterior distributions of the thermal response curves for pupal development rates (inverse of development times ρ_P) in solid lines and HPD interval in dashed black. Histograms of the posterior distribution for each parameter of the quadratic and Brière fits. The prior distribution for each parameter is plotted in red. The Brière fit is determined by the equation $cT(T - T_0)\sqrt{|T_m - T|}$ using a normal distribution with standard deviation σ.

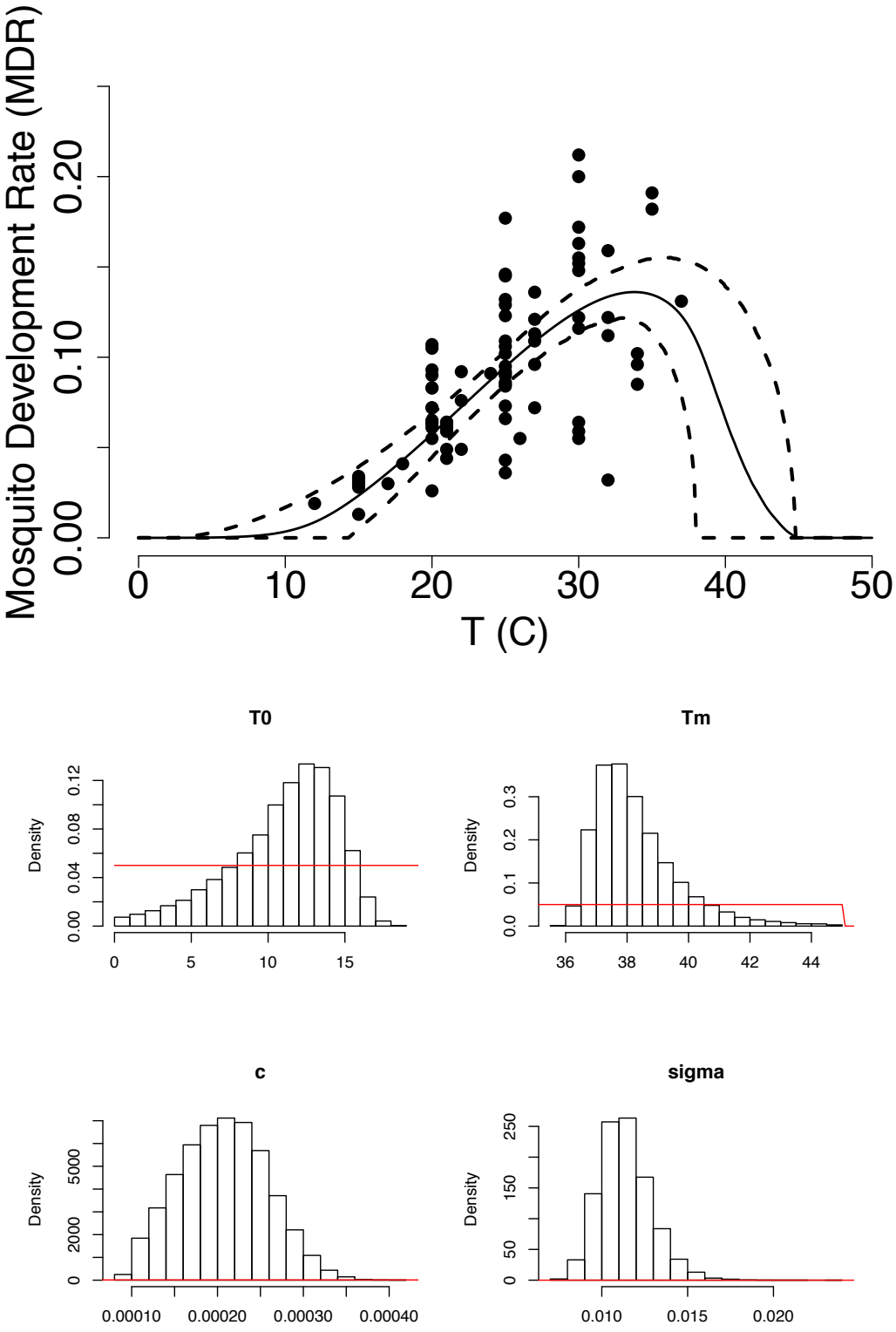

Figure B.10: *Aedes. albopictus*: Mean of the posterior distributions of the thermal response curves for adult development rates (inverse of development times ρ_A) in solid lines and HPD interval in dashed black. Histograms of the posterior distribution for each parameter of the quadratic and Brière fits. The prior distribution for each parameter is plotted in red. The Brière fit is determined by the equation $cT(T-T_0)\sqrt{|T_m-T|}$ using a normal distribution with standard deviation σ.

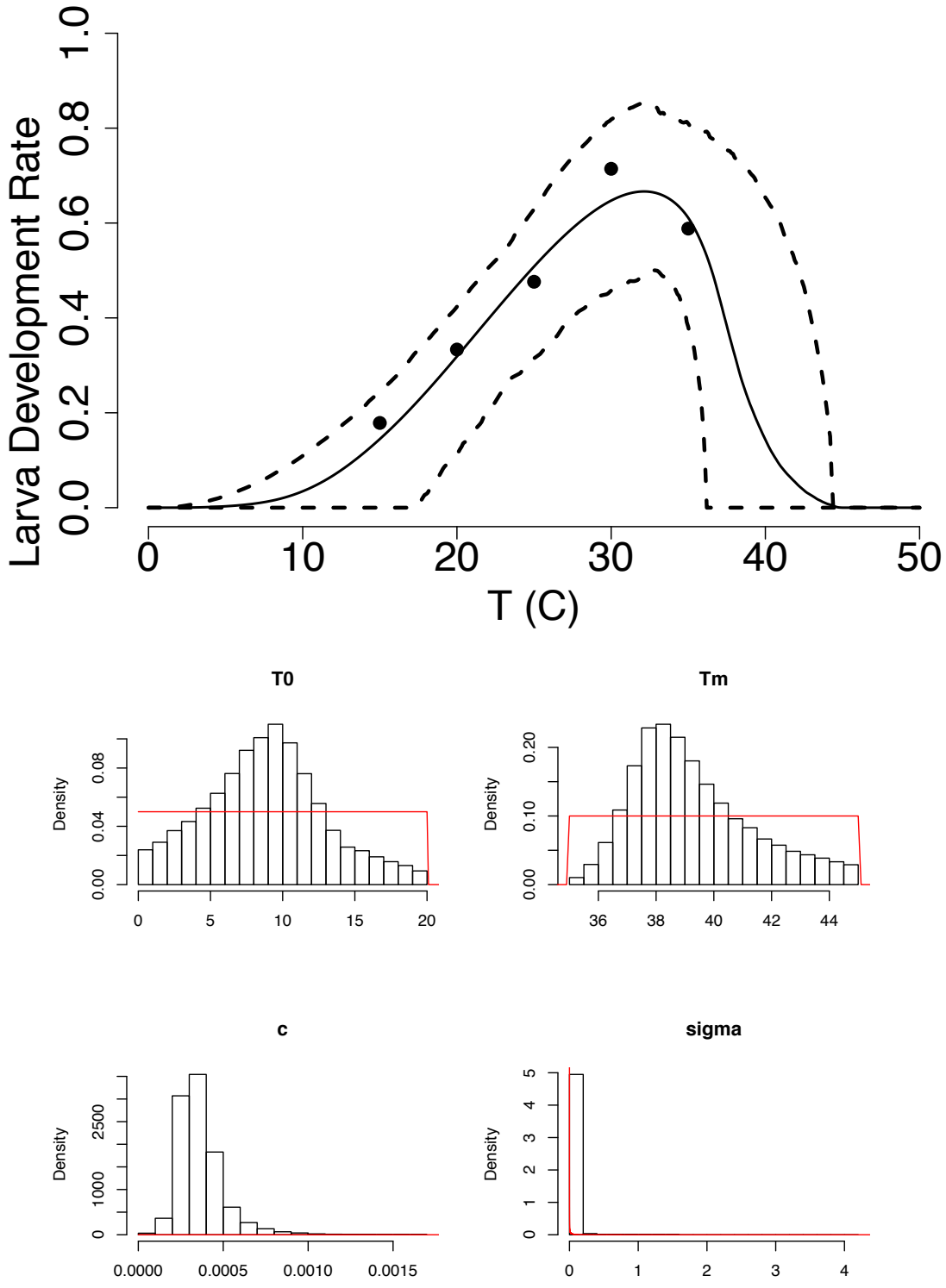

Figure B.11: *Aedes albopictus*: Mean of the posterior distributions of the thermal response curves for larval development rate (instar 1) in solid line and HPD interval in dashed black. Histograms of the mean posterior distribution for each parameter of the Brière fit. The prior distribution for each parameter is plotted in red. The Brière fit is determined by the equation $cT(T - T_0)\sqrt{|T_m - T|}$ using a normal distribution with standard deviation σ.

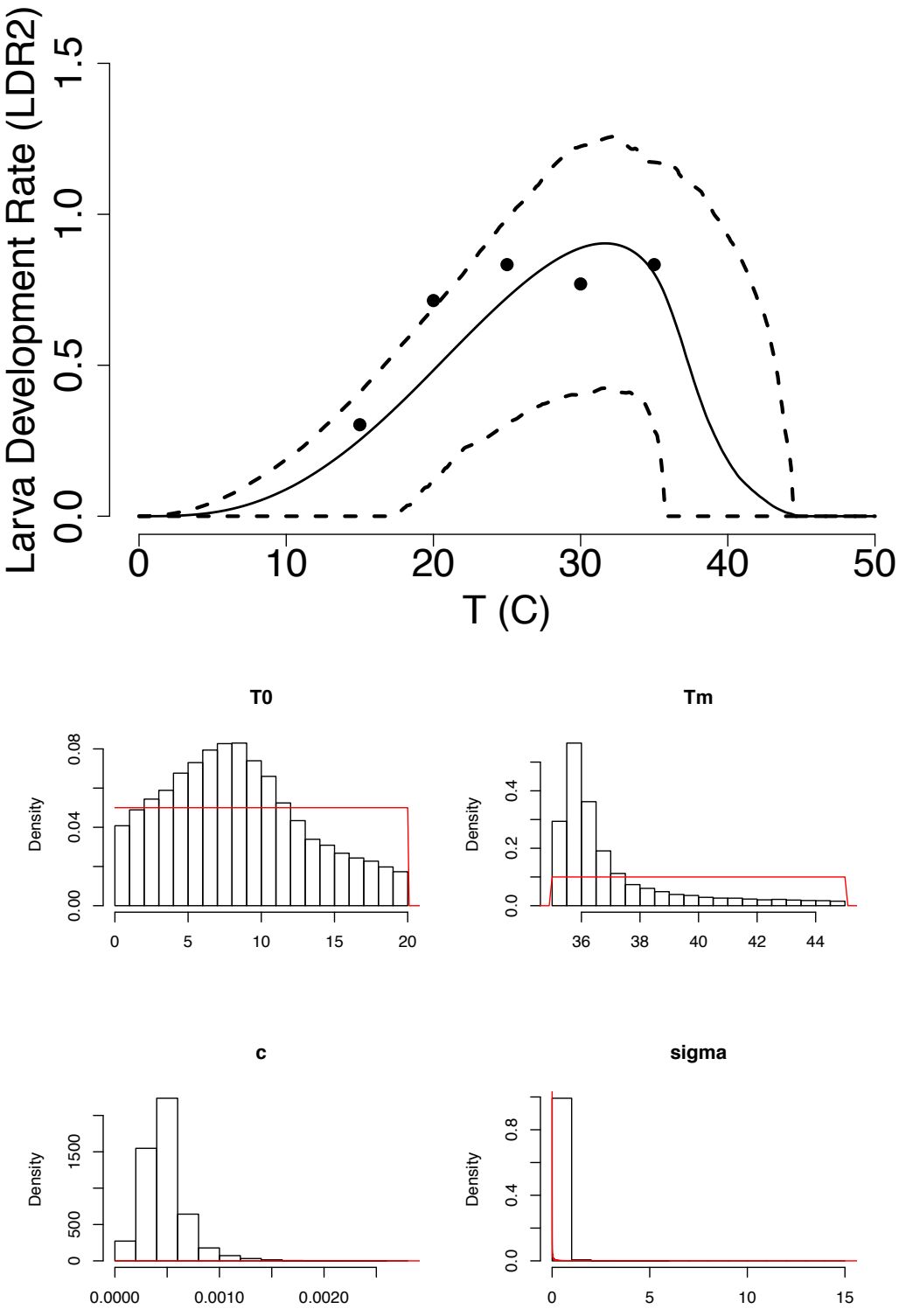

Figure B.12: *Aedes albopictus*: Mean of the posterior distributions of the thermal response curves for larval development rate (instar 2) in solid line and HPD interval in dashed black. Histograms of the mean posterior distribution for each parameter of the Brière fit. The prior distribution for each parameter is plotted in red. The Brière fit is determined by the equation $cT(T - T_0)\sqrt{|T_m - T|}$ using a normal distribution with standard deviation σ.

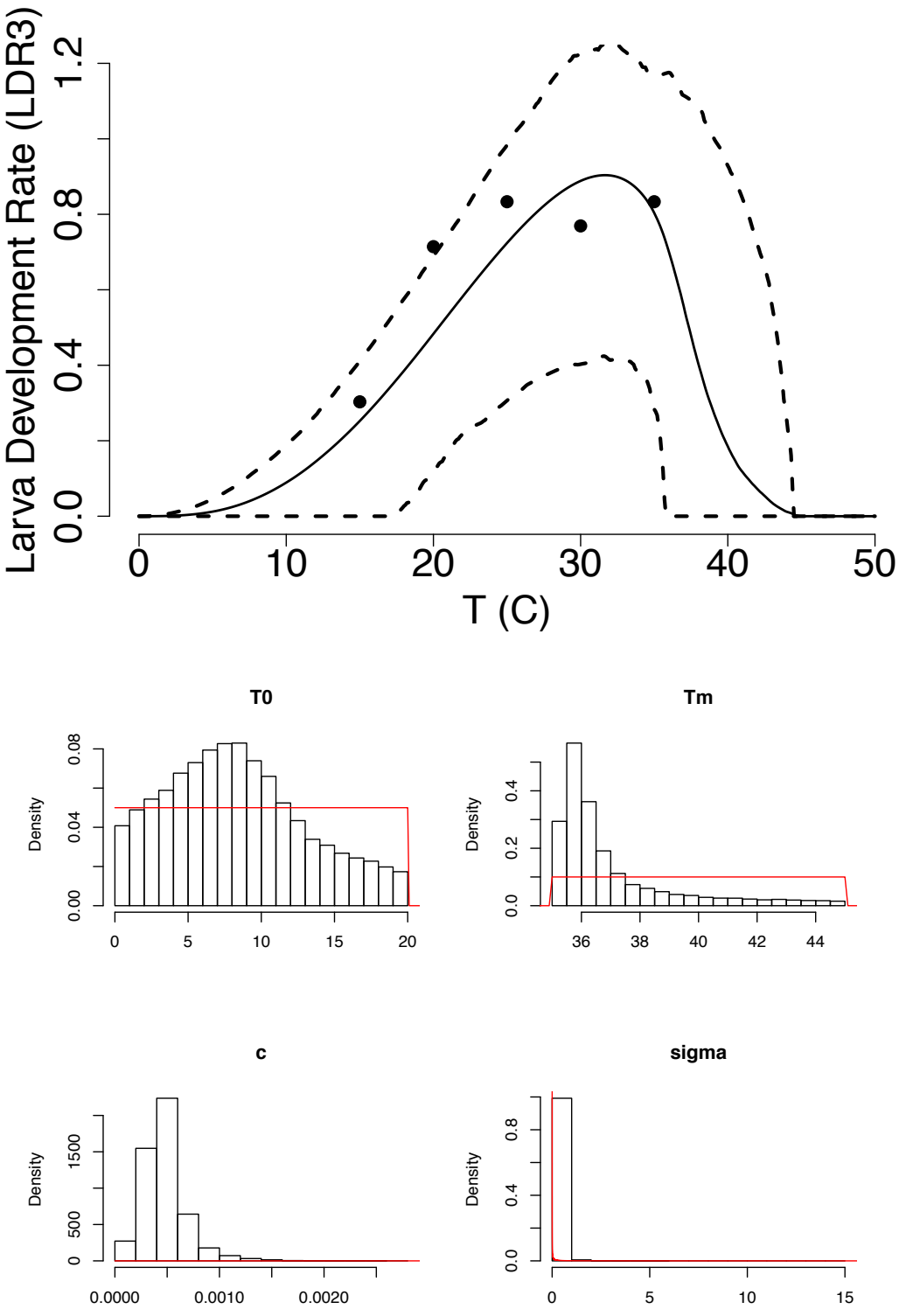

Figure B.13: *Aedes albopictus*: Mean of the posterior distributions of the thermal response curves for larval development rate (instar 3) in solid line and HPD interval in dashed black. Histograms of the mean posterior distribution for each parameter of the Brière fit. The prior distribution for each parameter is plotted in red. The Brière fit is determined by the equation $cT(T - T_0)\sqrt{|T_m - T|}$ using a normal distribution with standard deviation σ.

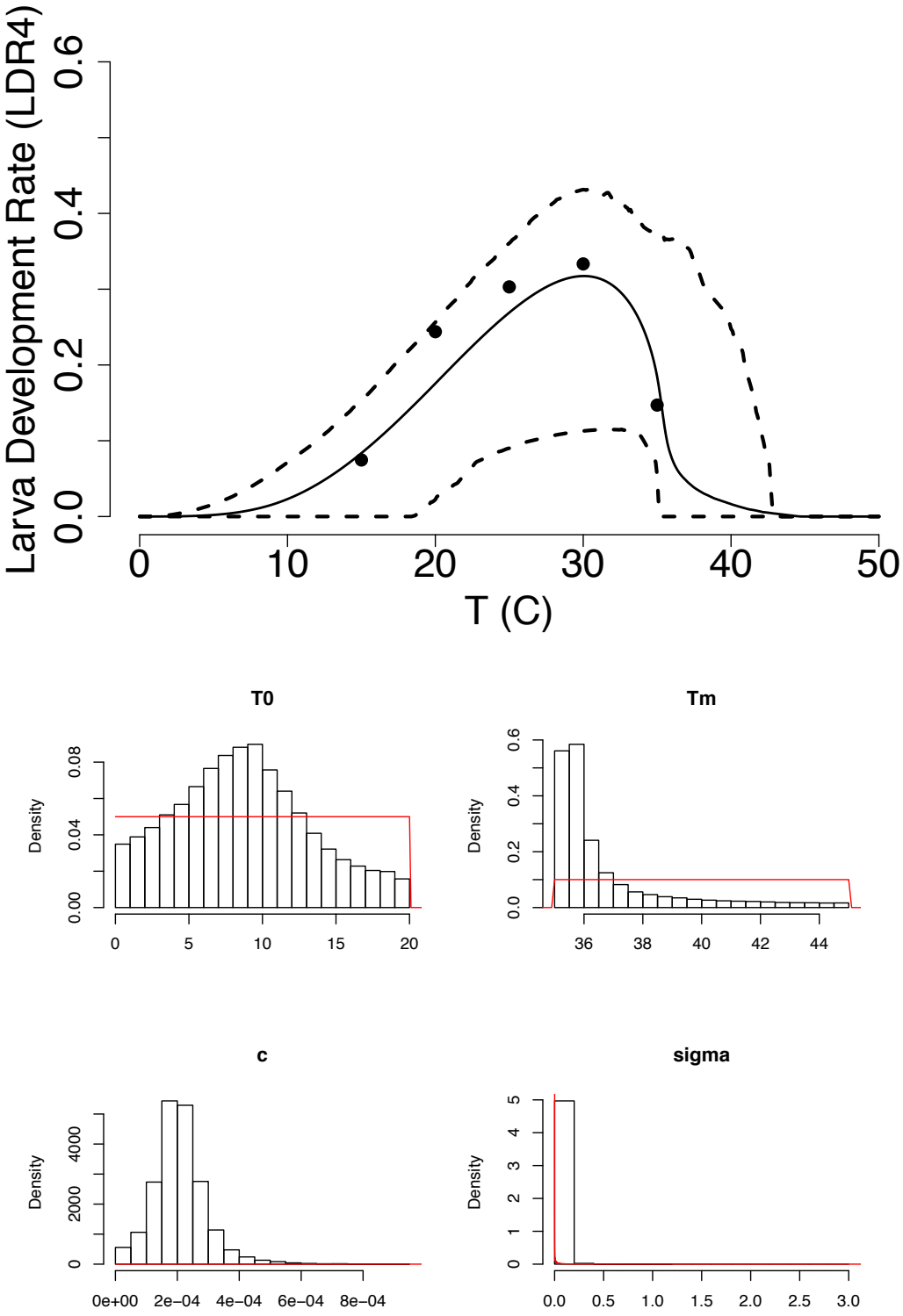

Figure B.14: *Aedes albopictus*: Mean of the posterior distributions of the thermal response curves for larval development rate (instar 4) in solid line and HPD interval in dashed black. Histograms of the mean posterior distribution for each parameter of the Brière fit. The prior distribution for each parameter is plotted in red. The Brière fit is determined by the equation $cT(T - T_0)\sqrt{|T_m - T|}$ using a normal distribution with standard deviation σ.

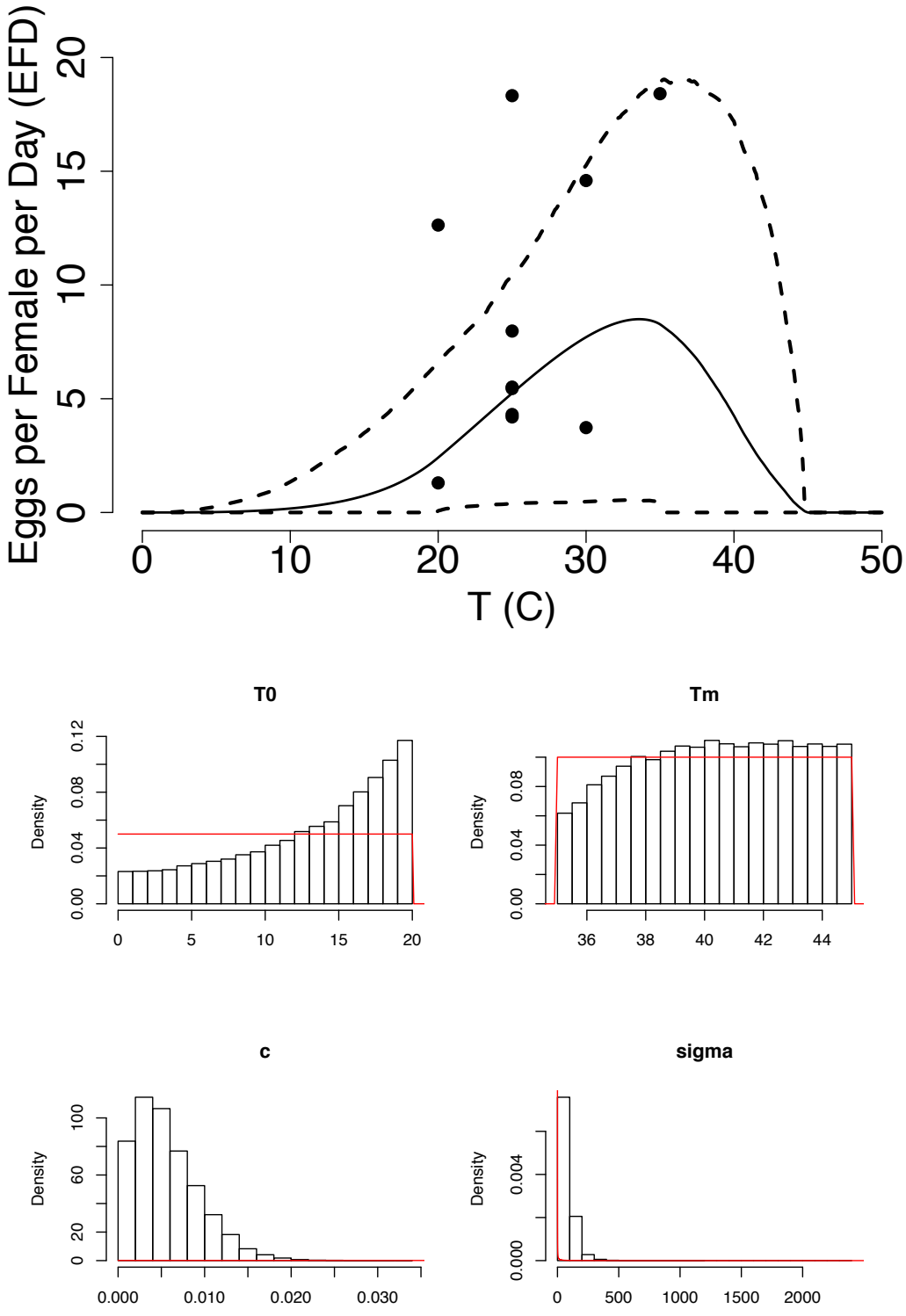

Figure B.15: *Aedes albopictus*: Mean of the posterior distributions of the thermal response curves for fecundity F in solid line and HPD interval in dashed black. Histograms of the posterior distribution for each parameter of the Brière fit for fecundity F. The prior distribution for each parameter is plotted in red. The Brière fit is determined by the equation $cT(T-T_0)\sqrt{|T_m-T|}$ using a normal distribution with standard deviation σ.

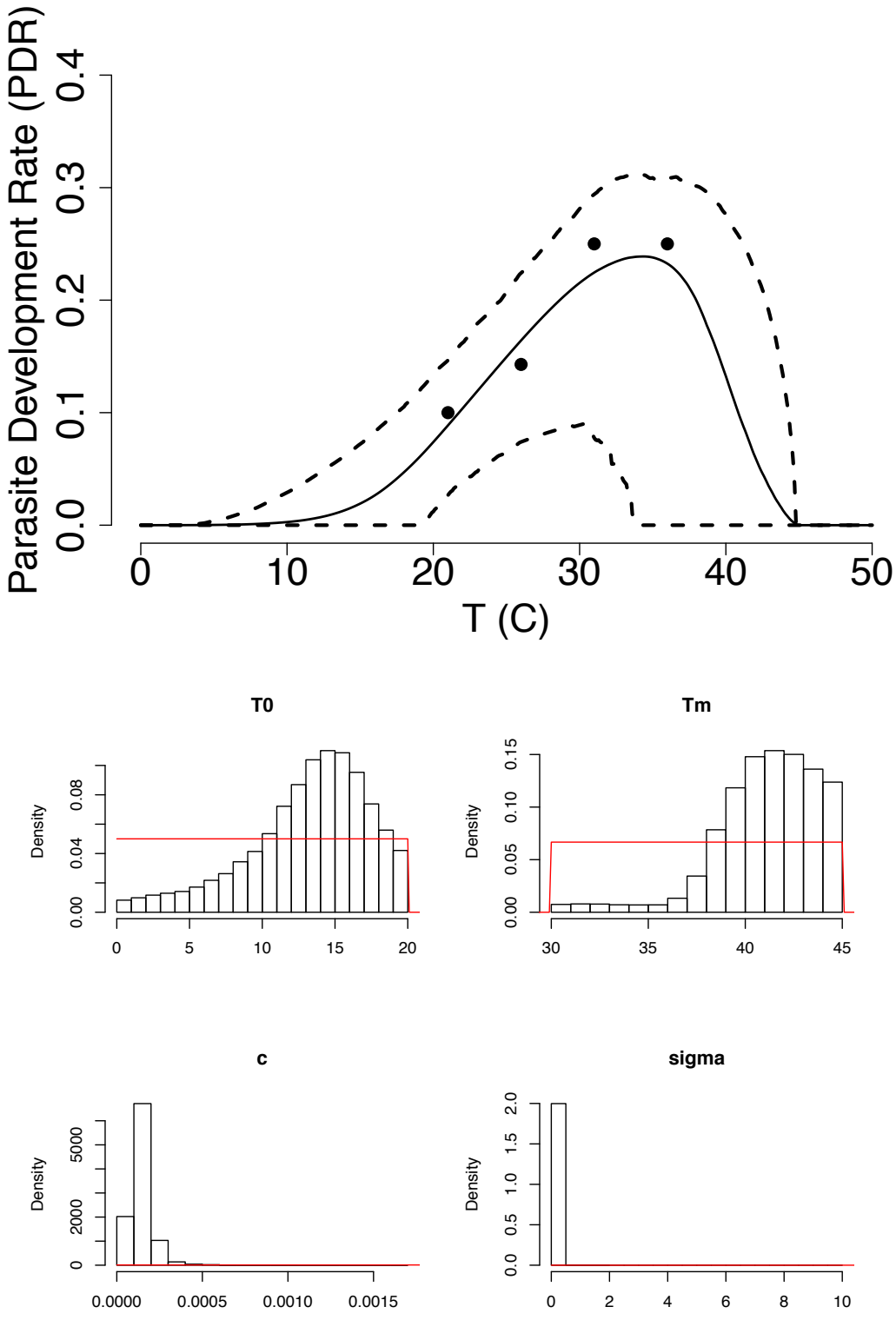

Figure B.16: *Aedes albopictus*: Mean of the posterior distributions of the thermal response curves for the parasite development rate ν in solid line and HPD interval in dashed black. Histograms of the posterior distribution for each parameter of the Brière fit for the parasite development rate ν. The prior distribution for each parameter is plotted in red. The Brière fit is determined by the equation $cT(T - T_0)\sqrt{|T_m - T|}$ using a normal distribution with standard deviation σ.

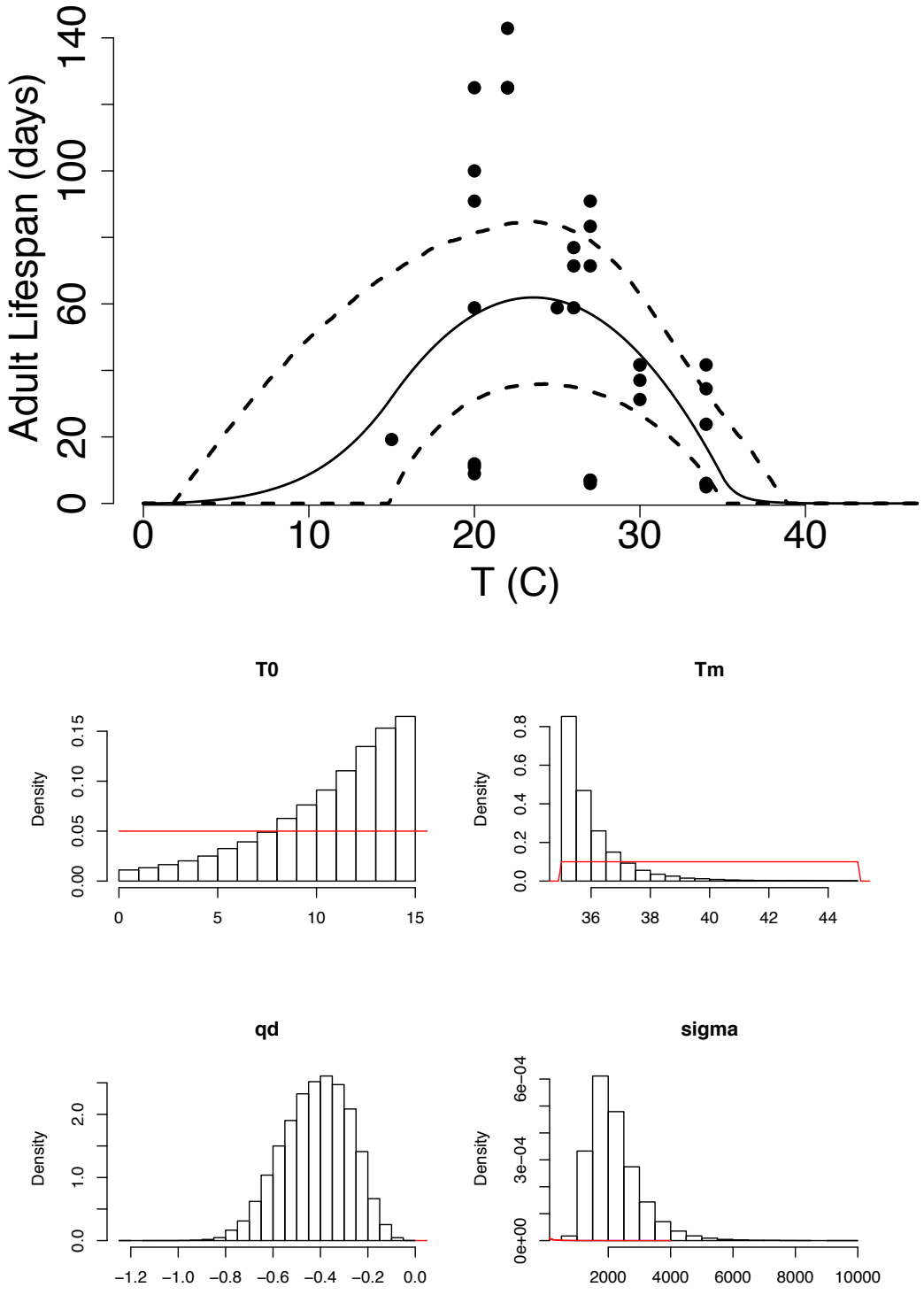

Figure B.17: *Aedes albopictus*: Mean of the posterior distributions of the thermal response curves for the adult lifespan (inverse mortality rate $lf = 1/\mu$) in solid line and HPD interval in dashed black. Histograms of the posterior distribution for each parameter of the quadratic fit for lifespan lf. The prior distribution for each parameter is plotted in red. The prior distribution for each parameter is plotted in red. The prior distribution for each parameter is plotted in red. The quadratic fit is determined by $-qd(T - T_0)(T_m - T)$ using a normal distribution with standard deviation σ.

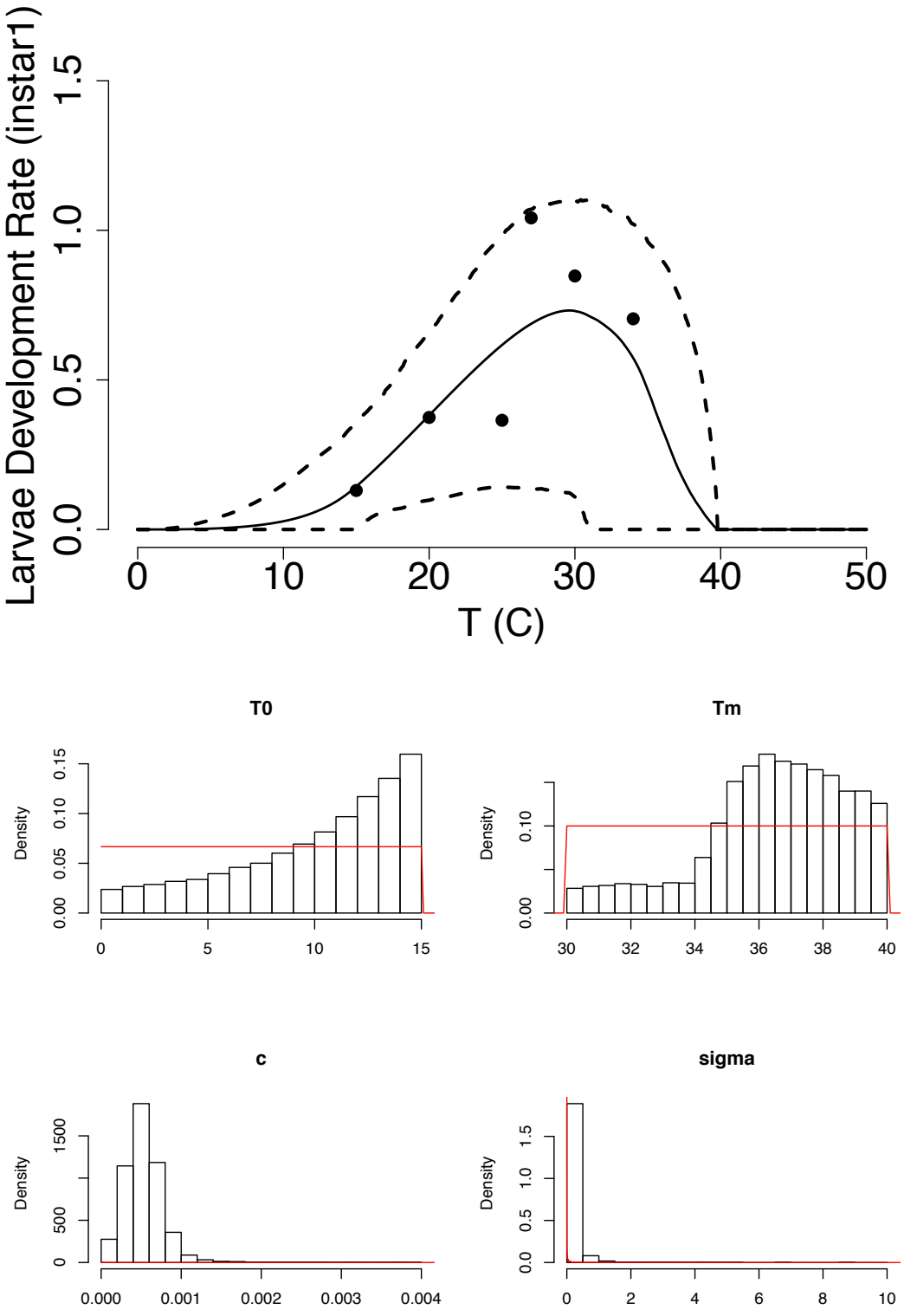

Figure B.18: *Aedes aegypti*: Mean of the posterior distributions of the thermal response curves for larval development rate (instar 1) in solid line and HPD interval in dashed black. Histograms of the posterior distribution for each parameter of the Brière fit. The prior distribution for each parameter is plotted in red. The Brière fit is determined by the equation $cT(T-T_0)\sqrt{|T_m-T|}$ using a normal distribution with standard deviation σ.

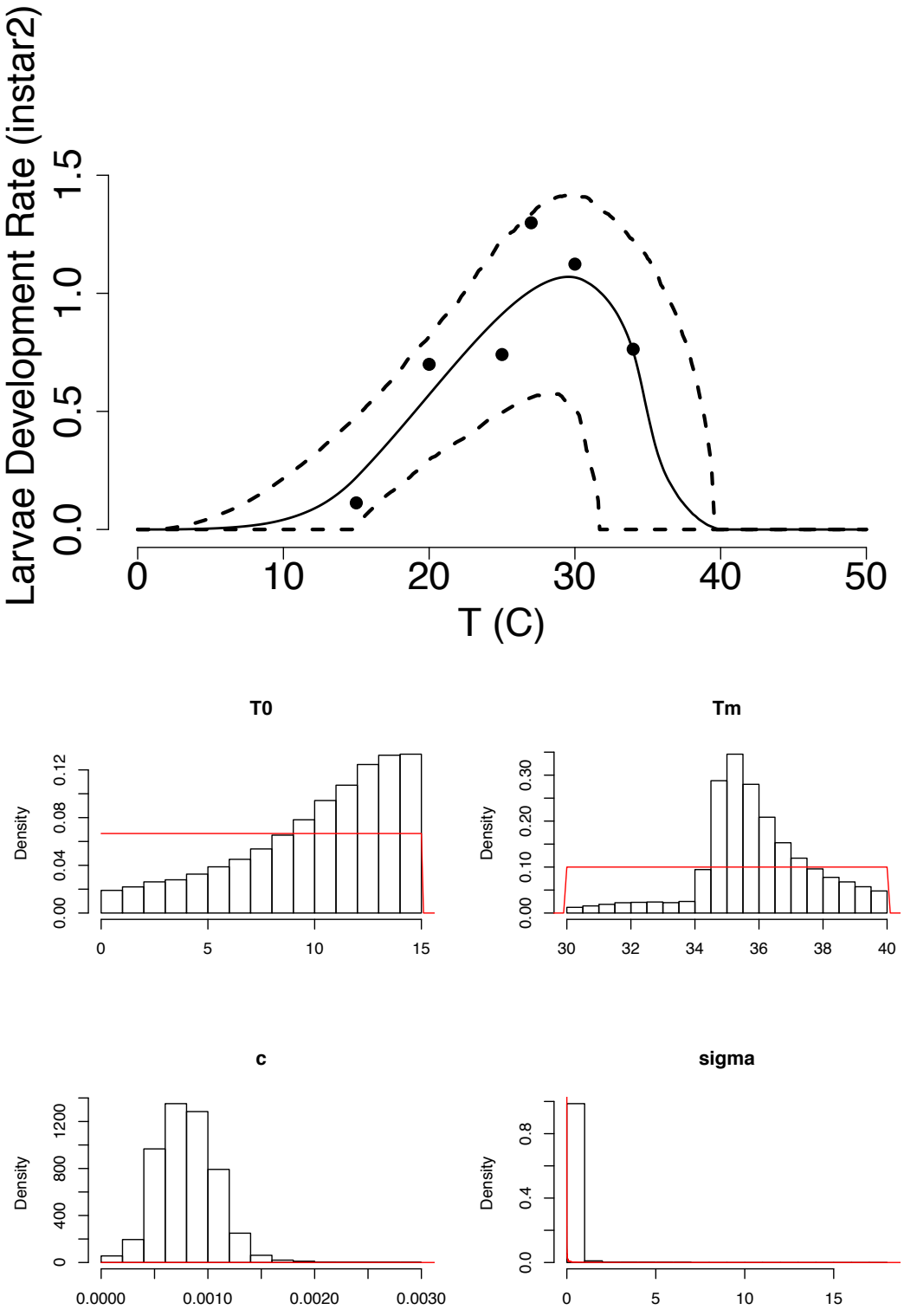

Figure B.19: *Aedes aegypti*: Mean of the posterior distributions of the thermal response curves for larval development rate (instar 2) in solid line and HPD interval in dashed black. Histograms of the posterior distribution for each parameter of the Brière fit. The prior distribution for each parameter is plotted in red. The Brière fit is determined by the equation $cT(T-T_0)\sqrt{|T_m-T|}$ using a normal distribution with standard deviation σ.

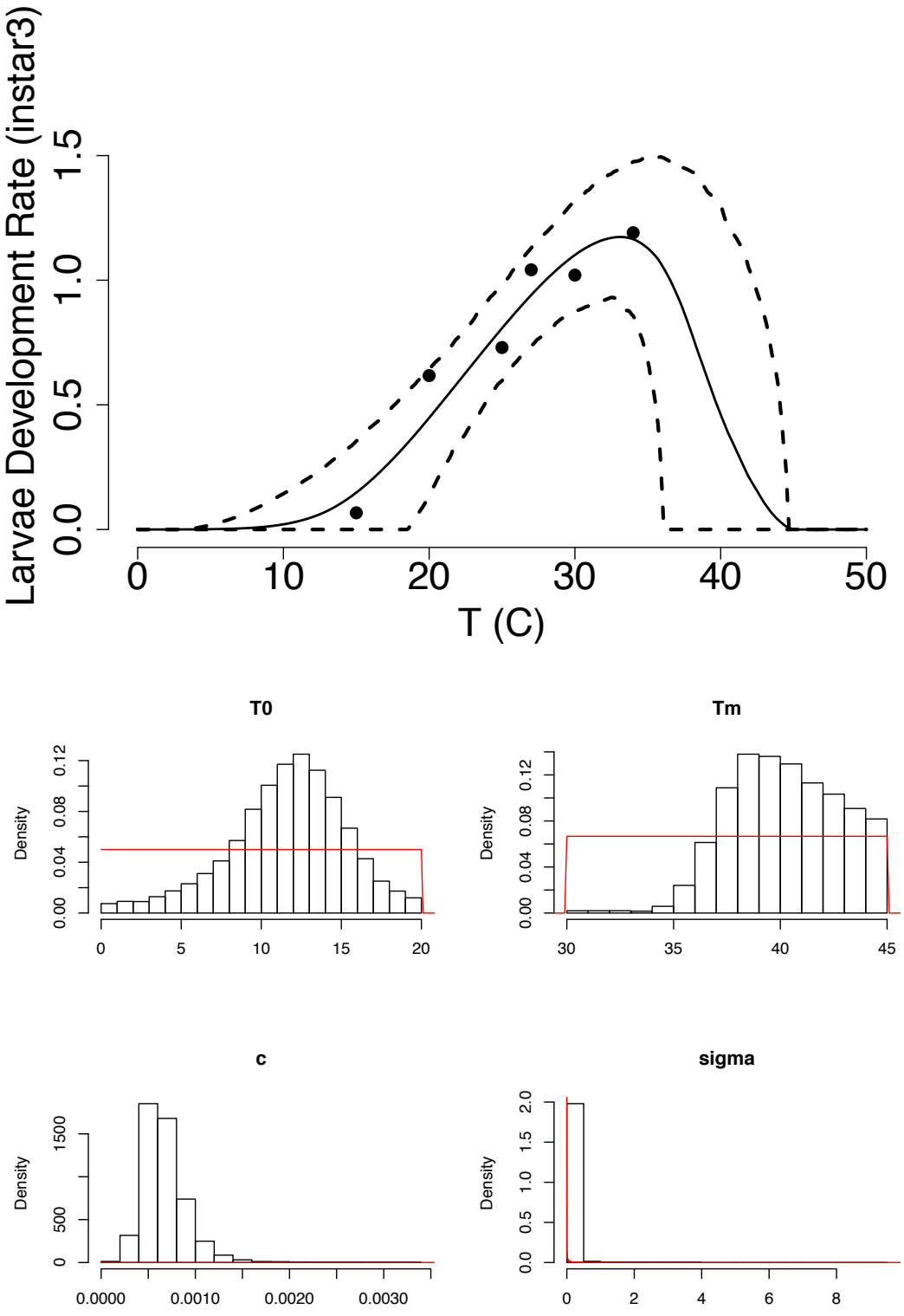

Figure B.20: *Aedes aegypti*: Mean of the posterior distributions of the thermal response curves for larval development rate (instar 3) in solid line and HPD interval in dashed black. Histograms of the posterior distribution for each parameter of the Brière fit. The prior distribution for each parameter is plotted in red. The Brière fit is determined by the equation $cT(T-T_0)\sqrt{|T_m-T|}$ using a normal distribution with standard deviation σ.

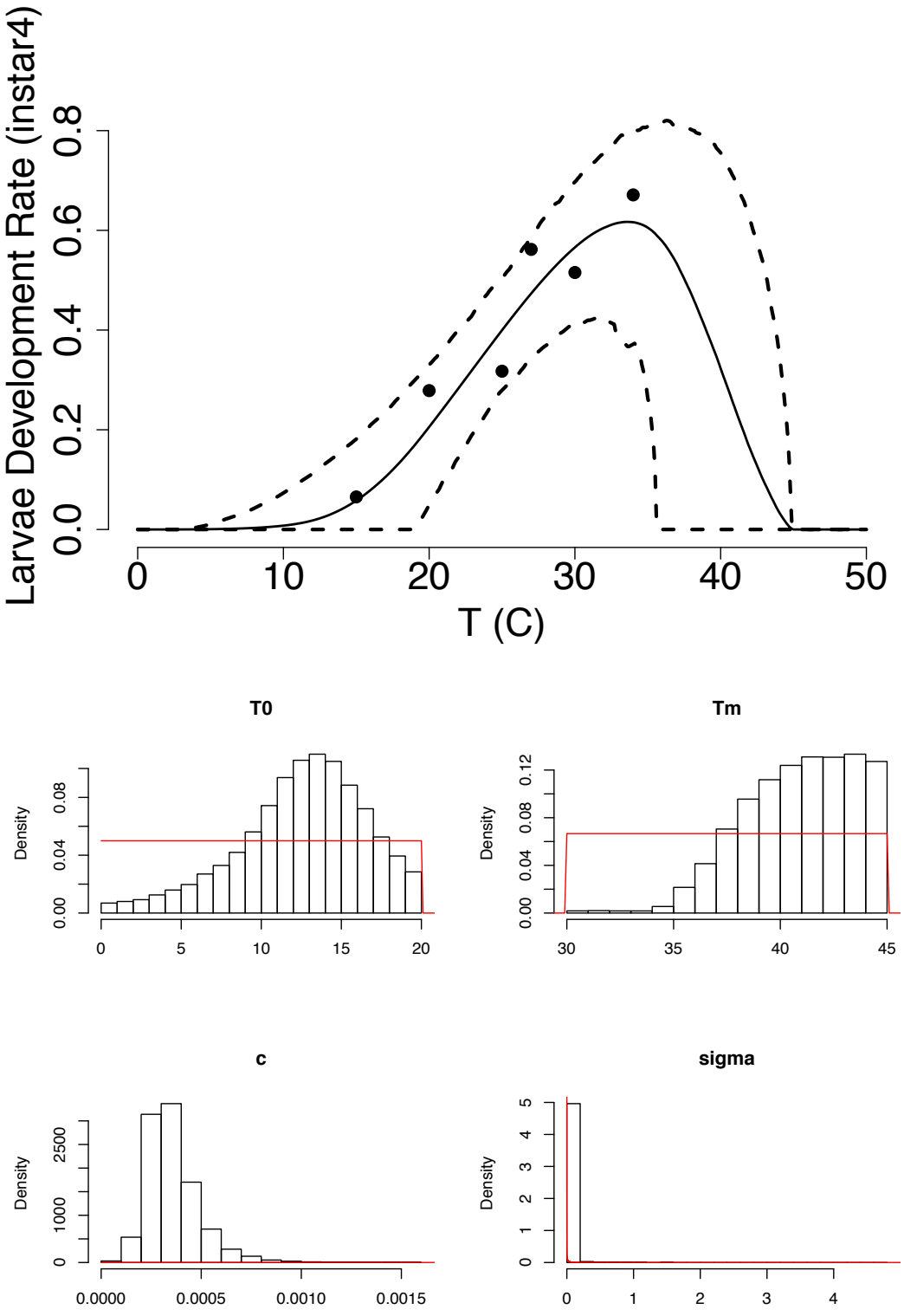

Figure B.21: *Aedes aegypti*: Mean of the posterior distributions of the thermal response curves for larval development rate (instar 4) in solid line and HPD interval in dashed black. Histograms of the posterior distribution for each parameter of the Brière fit. The prior distribution for each parameter is plotted in red. The Brière fit is determined by the equation $cT(T-T_0)\sqrt{|T_m-T|}$ using a normal distribution with standard deviation σ.

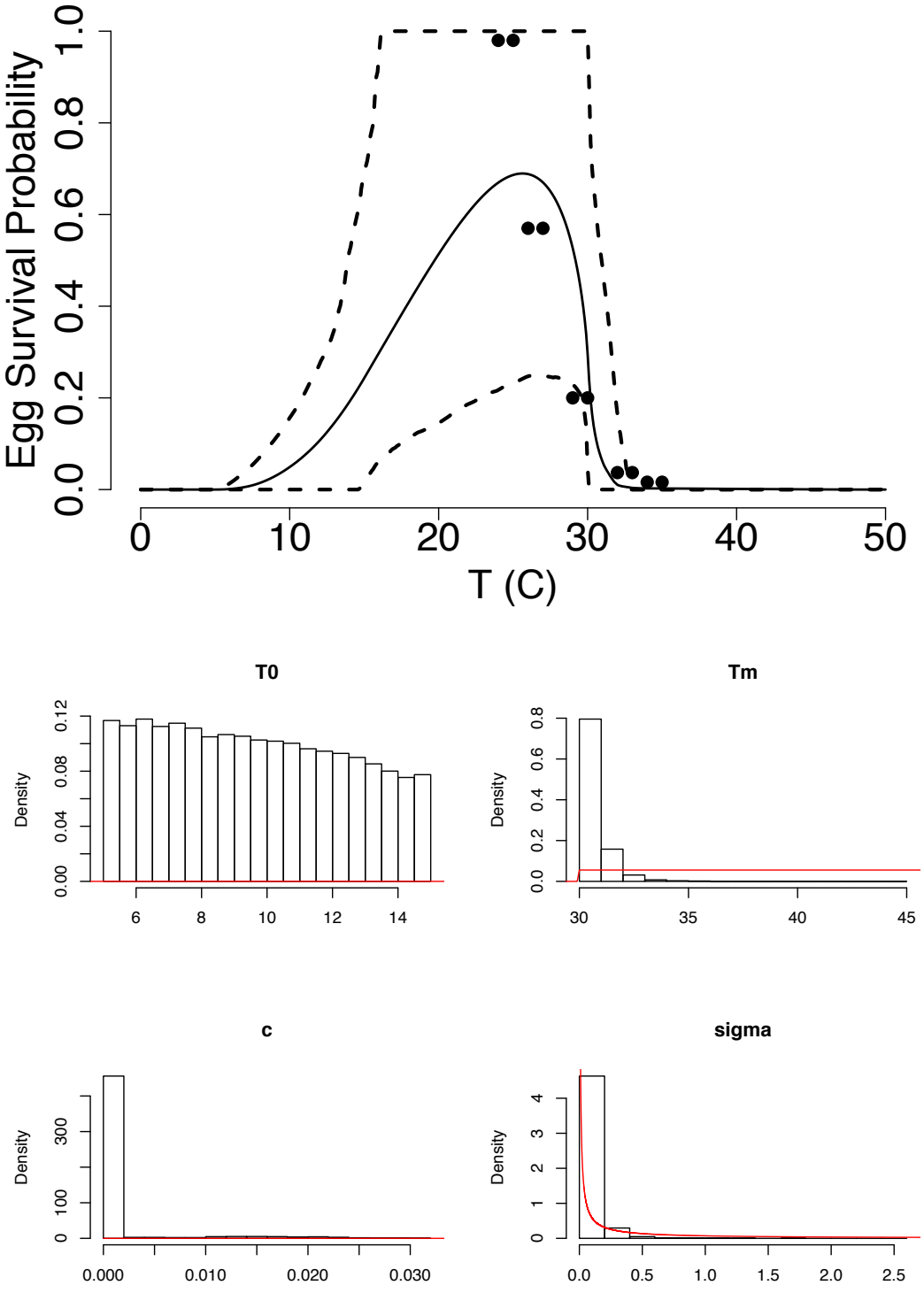

Figure B.22: *Aedes aegypti*: Mean of the posterior distributions of the thermal response curves for the survival probability for eggs p_E in solid line and HPD interval in dashed black. Histograms of the posterior distribution for each parameter of the Brière fit for the probability p_E. The prior distribution for each parameter is plotted in red. The Brière fit is determined by the equation $cT(T - T_0)\sqrt{|T_m - T|}$ using a normal distribution with standard deviation σ.

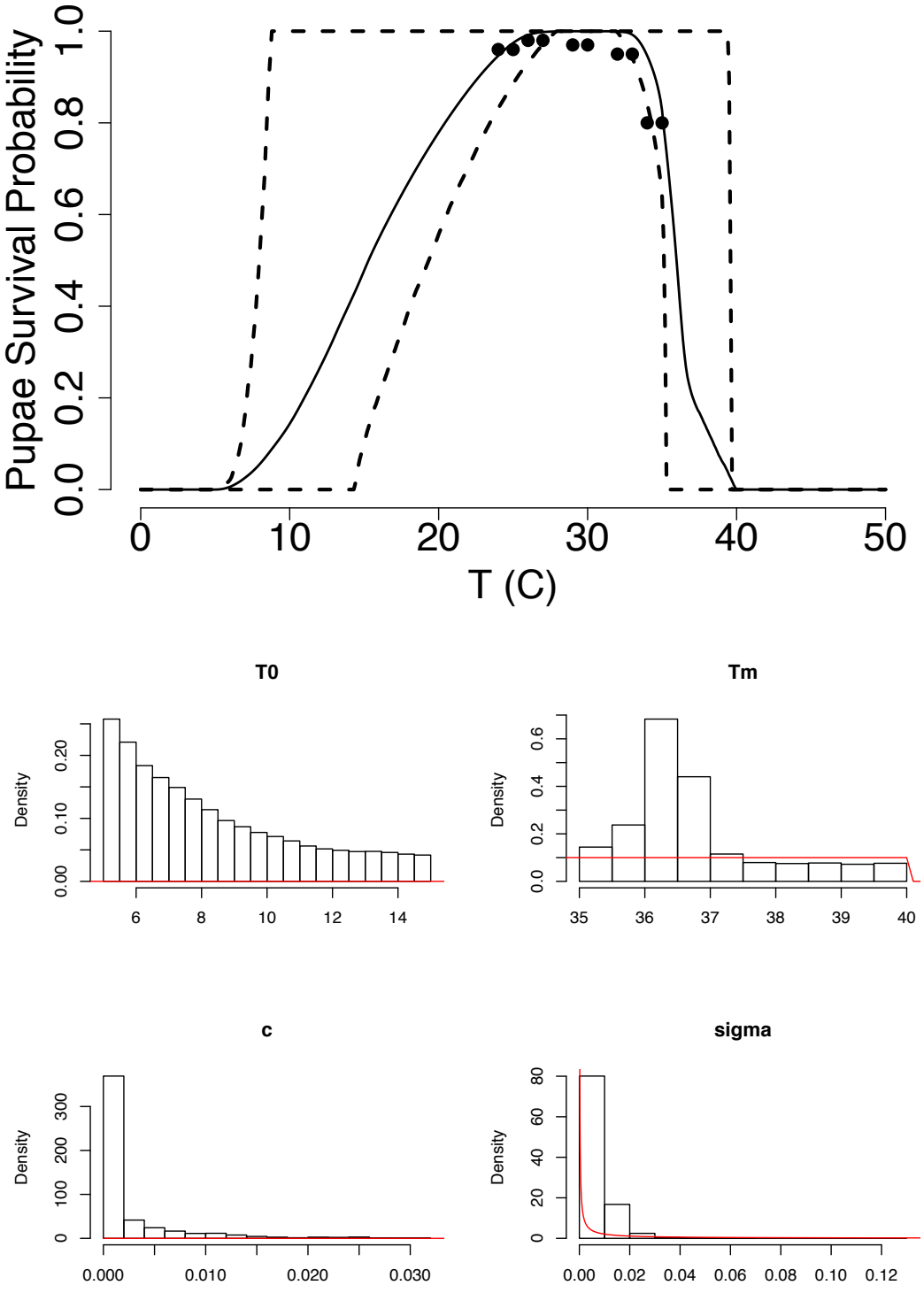

Figure B.23: *Aedes aegypti*: Mean of the posterior distributions of the thermal response curves for the survival probabilities for pupae p_P in solid line and HPD interval in dashed black. Histograms of the posterior distribution for each parameter of the Brière fit for the probability p_P. The prior distribution for each parameter is plotted in red. The Brière fit is determined by the equation $cT(T - T_0)\sqrt{|T_m - T|}$ using a normal distribution with standard deviation σ.

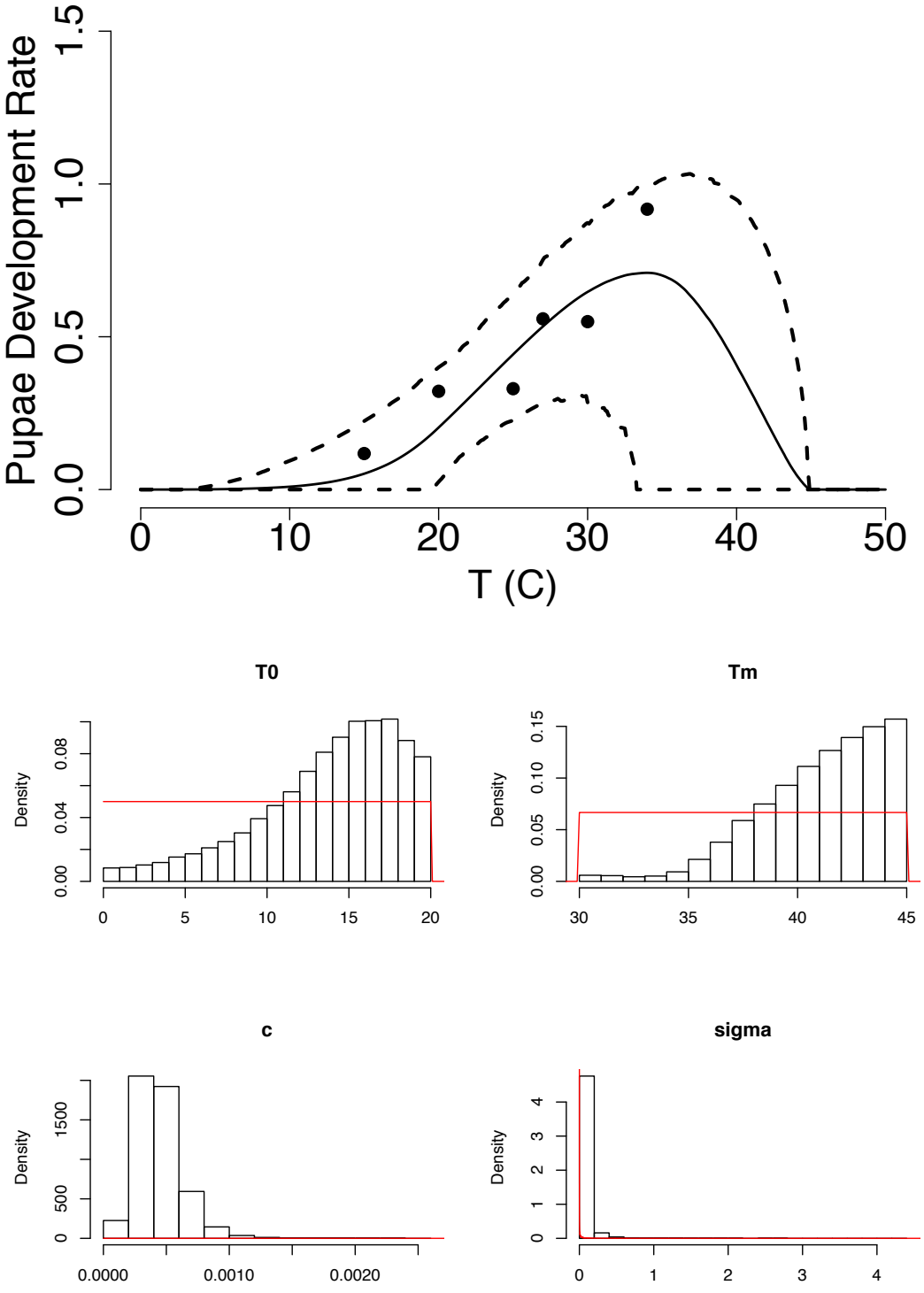

Figure B.24: *Aedes aegypti*: Mean of the posterior distributions of the thermal response curves for the pupal development rate, in solid line and HPD interval in dashed black. Histograms of the posterior distribution for each parameter of the Brière fit for the pupal development rate. The prior distribution for each parameter is plotted in red. The Brière fit is determined by the equation $cT(T - T_0)\sqrt{|T_m - T|}$ using a normal distribution with standard deviation σ.

Model Parameter	Mean Function	Parameters	Prior	Likelihood
Egg Survival Prob. p_E	Brière	T_0	dunif(5,15)	dnorm
		T_m	dunif(30,48)	
		c	dgamma(1,19)	
		τ	dgamma(.1, 0.03)	
Larval Survival Prob. p_L	Brière	T_0	dunif(0,5)	dnorm
		T_m	dunif(30,40)	
		c	dgamma(1,20)	
		τ	dgamma(0.01, 0.03)	
Pupal Survival Prob. p_P	Brière	T_0	dunif(0,5)	dnorm
		T_m	dunif(30,40)	
		c	dgamma(1,20)	
		τ	dgamma(0.01, 0.03)	
Egg Development Rate $lf = 1/\rho_E$	Quadratic	T_0	dunif(0,10)	dnorm
		T_m	dunif(30,45)	
		qd	dgamma(5,1)	
		τ	dgamma(0.001, 0.001)	
Larval Development Rate $1/\rho_L$ instar 1	Brière	T_0	dunif(0, 20)	dnorm
		T_m	dunif(35,45)	
		c	dgamma(1,.1)	
		τ	dgamma(0.001, 0.001)	
Larval Development Rate $1/\rho_L$ instar 2	Brière	T_0	dunif(0, 20)	dnorm
		T_m	dunif(35,45)	
		c	dgamma(1,.1)	
		τ	dgamma(0.001, 0.001)	
Larval Development Rate $1/\rho_L$ instar 3	Brière	T_0	dunif(0, 20)	dnorm
		T_m	dunif(35,45)	
		c	dgamma(1,.1)	
		τ	dgamma(0.001, 0.001)	
Larval Development Rate $1/\rho_L$ instar 4	Brière	T_0	dunif(0, 20)	dnorm
		T_m	dunif(35,45)	
		c	dgamma(1,.1)	
		τ	dgamma(0.001, 0.001)	
Pupal Development Rate $1/\rho_P$ instar 4	Brière	T_0	dunif(0, 20)	dnorm
		T_m	dunif(35,45)	
		c	dgamma(1,.1)	
		τ	dgamma(0.001, 0.001)	

Table B.2: *Aedes albopictus*: Bayesian model values used. For each thermal trait, we specify the likelihood distribution and the priors used for each parameter.

Model Parameter	Mean Function	Parameters	Prior	Likelihood
Egg Survival Prob. p_E	Brière	T_0	dunif(5,15)	dnorm
		T_m	dunif(30,48)	
		c	dgamma(1,19)	
		τ	dgamma(.1, 0.03)	
Egg Survival Prob. p_E	Brière	T_0	dunif(5,15)	dnorm
		T_m	dunif(30,40)	
		c	dgamma(0.001,40)	
		τ	dgamma(.01, 0.000001)	
Larval Development Rate $1/\rho_L$ instar 1	Brière	T_0	dunif(0, 15)	dnorm
		T_m	dunif(30,40)	
		c	dgamma(1,.1)	
		τ	dgamma(0.001, 0.001)	
Larval Development Rate $1/\rho_L$ instar 2	Brière	T_0	dunif(0, 15)	dnorm
		T_m	dunif(30,40)	
		c	dgamma(1,.1)	
		τ	dgamma(0.001, 0.001)	
Larval Development Rate $1/\rho_L$ instar 3	Brière	T_0	dunif(0, 20)	dnorm
		T_m	dunif(30,45)	
		c	dgamma(1,.1)	
		τ	dgamma(0.001, 0.001)	
Larval Development Rate $1/\rho_L$ instar 4	Brière	T_0	dunif(0, 20)	dnorm
		T_m	dunif(30,45)	
		c	dgamma(1,.1)	
		τ	dgamma(0.001, 0.001)	
Pupal Development Rate $1/\rho_P$ instar 4	Brière	T_0	dunif(0, 20)	dnorm
		T_m	dunif(30,45)	
		c	dgamma(1,.1)	
		τ	dgamma(0.001, 0.001)	

Table B.3: *Aedes aegypti*: Bayesian model values used. For each thermal trait, we specify the likelihood distribution and the priors used for each parameter.

Appendix C

Appendix for Chapter 4

C.1 Transmission model for BTV

We use an SIR-SEI type of compartmental model to describe vector-host interactions in transmitting BTV (see Figure 4.2). The host population (H) is divided into susceptible (S), infected (I), and recovered (or immune) (R) classes, while the vector population (V) is divided into susceptible (S_V) and infected (I_V) classes as well as three Exposed (E_V) classes. Here we use three exposed classes in the vector population to incorporate a more realistic length of the extrinsic incubation period. Using three compartments with the exit rate from each compartment being 3 ν, lead to a Gamma distribution for overall midge progression to the infectious class with a mean rate of ν. Increasing the number of compartments used from 3 to a larger number leads to a Gamma distribution with lower variance around the mean [180]. This approach is an alternative to using fixed time delays, which are not suitable when using temperature-dependent parameters. Both host (H) and vector

(V) populations are assumed (and are by definition of the model) constant.

$$\frac{dS}{dt} = -\frac{ab}{H} I_V S \tag{C.1}$$
$$\frac{dI}{dt} = \frac{ab}{H} I_V(t-\tau) S(t-\tau) - dI \tag{C.2}$$
$$\frac{dR}{dt} = dI \tag{C.3}$$
$$\frac{dS_V}{dt} = rV - \frac{ac}{H} I S_V - \mu S_V \tag{C.4}$$
$$\frac{dE_{V1}}{dt} = \frac{ac}{H} I S_V - 3\nu E_{V1} - \mu E_{V1} \tag{C.5}$$
$$\frac{dE_{V2}}{dt} = 3\nu E_{V1} - 3\nu E_{V2} - \mu E_{V2} \tag{C.6}$$
$$\frac{dE_{V3}}{dt} = 3\nu E_{V2} - 3\nu E_{V3} - \mu E_{V3} \tag{C.7}$$
$$\frac{dI_V}{dt} = 3\nu E_{V3} - \mu I_V. \tag{C.8}$$

where

$$H = S + I + R \tag{C.9}$$
$$V = S_V + E_{V1} + E_{V2} + E_{V3} + I_V \tag{C.10}$$

The model's parameters are presented in the Table C.1 below. Note that the

Parameter	Definition	Units
d	Recovery rate of infected hosts	1/day
τ	Host's exposure period	day
r	Vector population's birth rate	1/day
a	Vector biting rate	bites / day
b	Probability that a midge is infected	dimensionless
c	Probability that a midge is infectious	dimensionless
μ	Mortality rate of adult vectors	1/day
ν	Parasite's development rate	1/day

Table C.1: Parameters used in the mathematical model, their description, and units.

parameters τ is the time that a susceptible (S) takes to become infected after receiving a bite from infected vector (I_V). The parameter ν is the inverse of

the Extrinsic Incubation Period of the pathogen (EIP), i.e., $\nu = \dfrac{1}{EIP}$. We define the vector population size to be $V = \dfrac{\lambda}{\mu}$, where λ is the total birth rate of adult midges in the whole population (adults/day), and μ is per-capita adult mortality rate (1/day). This is based on Parham & Michael [74], who derive the expression phenomenologically by treating V as a random variable. Thus, λ is equivalent to rV in the model above, given that $r = \mu$ at disease free equilibrium, and is given by

$$\lambda = \frac{F\ p_E\ p_L\ p_P}{(\rho_E + \rho_L + \rho_P)\ \mu} \tag{C.11}$$

where F is the number of eggs produced by all females in the population per day, $p_{E,L,P}$ are the survival probabilities in the Eggs, Larvae, and Pupae stages, and ρ_E, ρ_L, ρ_P are the development time in each stage. Then, the abundance of the vector becomes,

$$V = \frac{\lambda}{\mu} = \frac{F\ p_E\ p_L\ p_P}{(\rho_E + \rho_L + \rho_P)\ \mu^2} \tag{C.12}$$

C.2 Host recovery rate d sensitivity analysis

Although all ruminants are susceptible to BTV disease, each responds to the infection differently, with sheep being the most susceptible and showing extreme morbidity and mortality. In addition, BTV host recovery depends on the intensity of the infection as well as the time of disease detection, which results in recovery rate variability among hosts. To account for this, we perform a sensitivity analysis on the host recovery rate d by looking at the derivative of R_0 with respect to d as follows:

$$\frac{\partial R_0}{\partial d} = \frac{1}{2}\left(-\frac{V\ g\ f}{d^2\ H\ \mu}\right)\left(\frac{V\ g\ f}{d\ H\ \mu}\right)^{-1/2} = -\frac{1}{2d}\left(R_0^2\right)\left(R_0\right)^{-1} = -\frac{R_0}{2d}. \tag{C.13}$$

Since $\dfrac{\partial R_0}{\partial d} < 0$ always, the basic reproductive ratio R_0 increases as the recovery rate d decreases. Figure C.1 shows different R_0 densities corresponding to different host recovery rate values. Higher lengths of infection $1/d$, i.e.

lower recovery rates d, are associated with higher R_0 densities, meaning that hosts with low recovery rate such as sheep are more challenging to manage as the chance of outbreak for them is more likely.

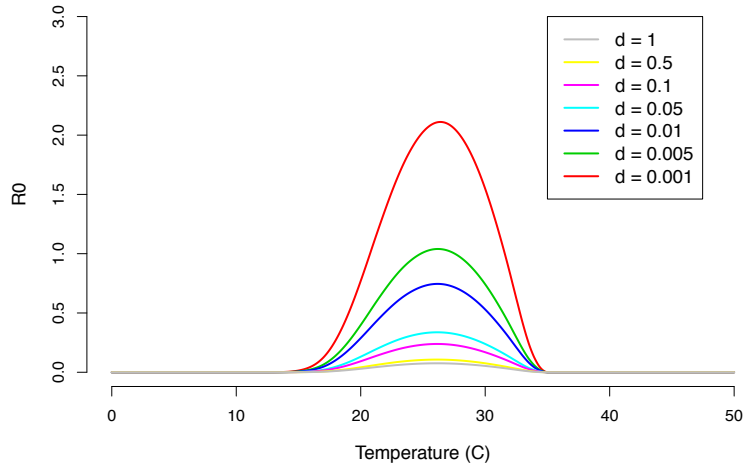

Figure C.1: Host recovery rate d values correspond to different R_0 posterior densities. As d decreases, R_0 density increases meaning that a lower recovery rate correspond to a higher outbreak risk.

C.3 Uncertainty analysis

We investigate the uncertainty caused in each of R_0 components, the midge density V, the functional form f, and the transmission potential g by examining the source of uncertainty within each component. For the midge density, the uncertainty is mainly caused by the adult midge mortality rate μ within a wide temperature range, from 10°C to 32°C. At higher temperatures (>32°C) the uncertainty is caused by the fecundity F.

In the functional form case, the uncertainty is caused by the adult mortality rate μ for temperatures between 18°C and 32°C, this range overlaps with that of the midge density. At lower lower (10-18°C) and higher (32-45°C) temperature ranges, the uncertainty is caused by the pathogen development rate ν. In the transmission potential the overall uncertainty is caused by the biting rate a.

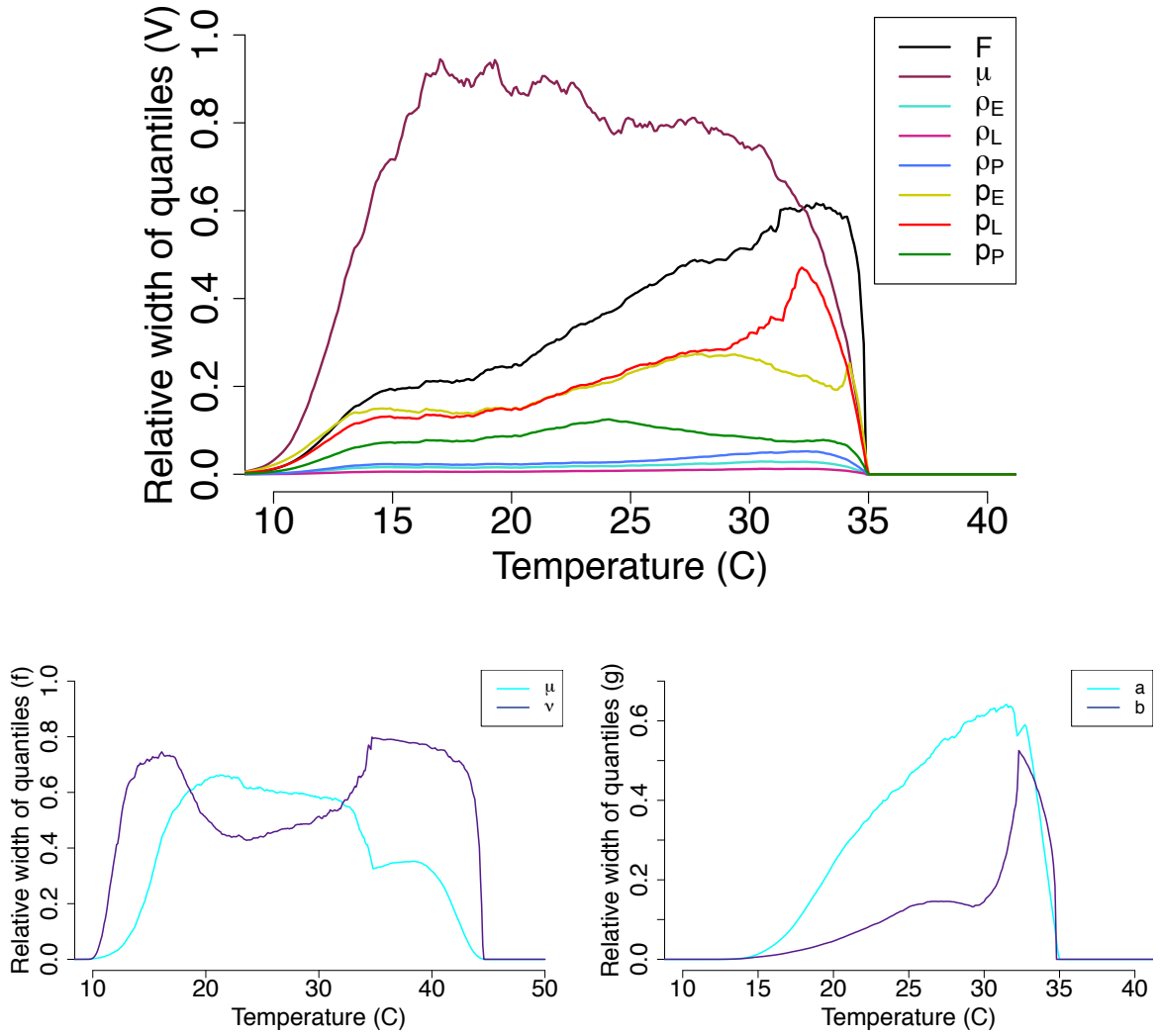

Figure C.2: The source of uncertainty in the midge density V (Top), the functional form f (Bottom-left), and the transmission potential g (Bottom-right) is measured by calculating the relative width of quantiles with each parameter varying with temperature while the remaining parameters are kept constants.

C.4 Bayesian fitting of traits thermal curves

To fit each trait, we chose a unimodal functional form as the mean function. We use normal distributions for most of the data while binomial distributions are used when fitting probability distributions. We used uninformative priors appropriate for the biological description of the data, taking into account the positivity of their values as well as their range. The values in the priors are decided as we go until the appropriate fitting curve is obtained.

Midges biting rate a

The biting rate of adult midges is one of many factors that influence Bluetongue transmission [181]. In order to calculate the biting rate, the time required for female *Culicoides sonorensis* to lay eggs after a blood meal, also known as a gonotrophic period, is required. Biting rate (a) can be approximated by taking the inverse of the gonotrophic cycle duration. Similar to other traits, the biting rate is sensitive to environmental factors, especially, temperature [181] (see Figure C.3 for thermal fit).

Vector competence bc

Vector competence for adult midges is a measure of their ability to transmit the disease. It is genetically determined and heavily influenced by environmental factors such as temperature and humidity [182]. Vector competence (bc) is the product of the probability of a vector getting infected after a blood meal containing a pathogen (c) and the probability of a vector transmiting infection (b). While we were able to find data for b concerning *Culicoides sonorensis* [183], we were unable to find data for c. We assume $c = 0.5$ for all calculations used in this analysis. We did fit a Bayesian model to the parameter b (Figure C.4).

Juvenile survival probability $p_E,\ p_L,\ p_P$

Vaughan et. al. studied the sub-adult life cycle of *Culicoides variipennis* at temperatures of 20 °C, 25 °C, and 28 °C [184]. We define the probability of an egg hatching by using the mean percentage of laid eggs that hatched at each given temperature. We now define the probability of successful larval pupation by collecting the percentage of larva that ended up pupating at each given temperature. We finally define the probability of pupae emerging to become adults, p_P, as the mean percentage of pupae that survive to the adult stage at each given temperature (Figures C.5, C.6, C.7).

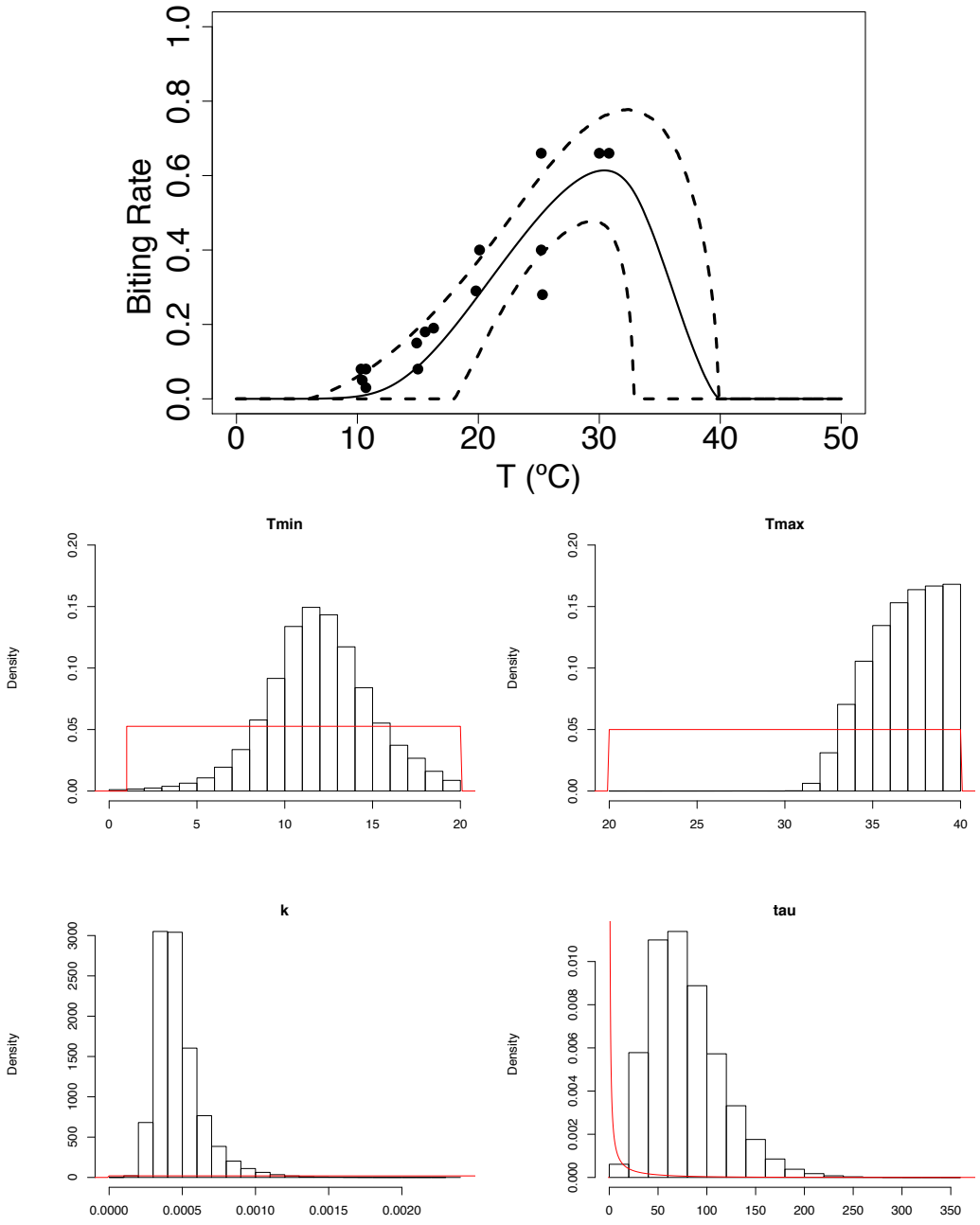

Figure C.3: (Top) The mean trajectory in solid line and HPD interval in dashed black for the biting rate a. (Bottom) Histograms of the posterior distribution for each parameter of the Brière fit for the biting rate a. The prior distribution for each parameter is plotted in red. The Brière fit is determined by the equation $kT(T - T_{Min})\sqrt{T_{Max} - T}$ using a normal distribution with precision τ.

Juvenile development time $\rho_E,\ \rho_L,\ \rho_P$

Egg Development Time is defined as the time in days required for eggs to hatch in a given temperature. *Culicoides variiennis* were studied in a

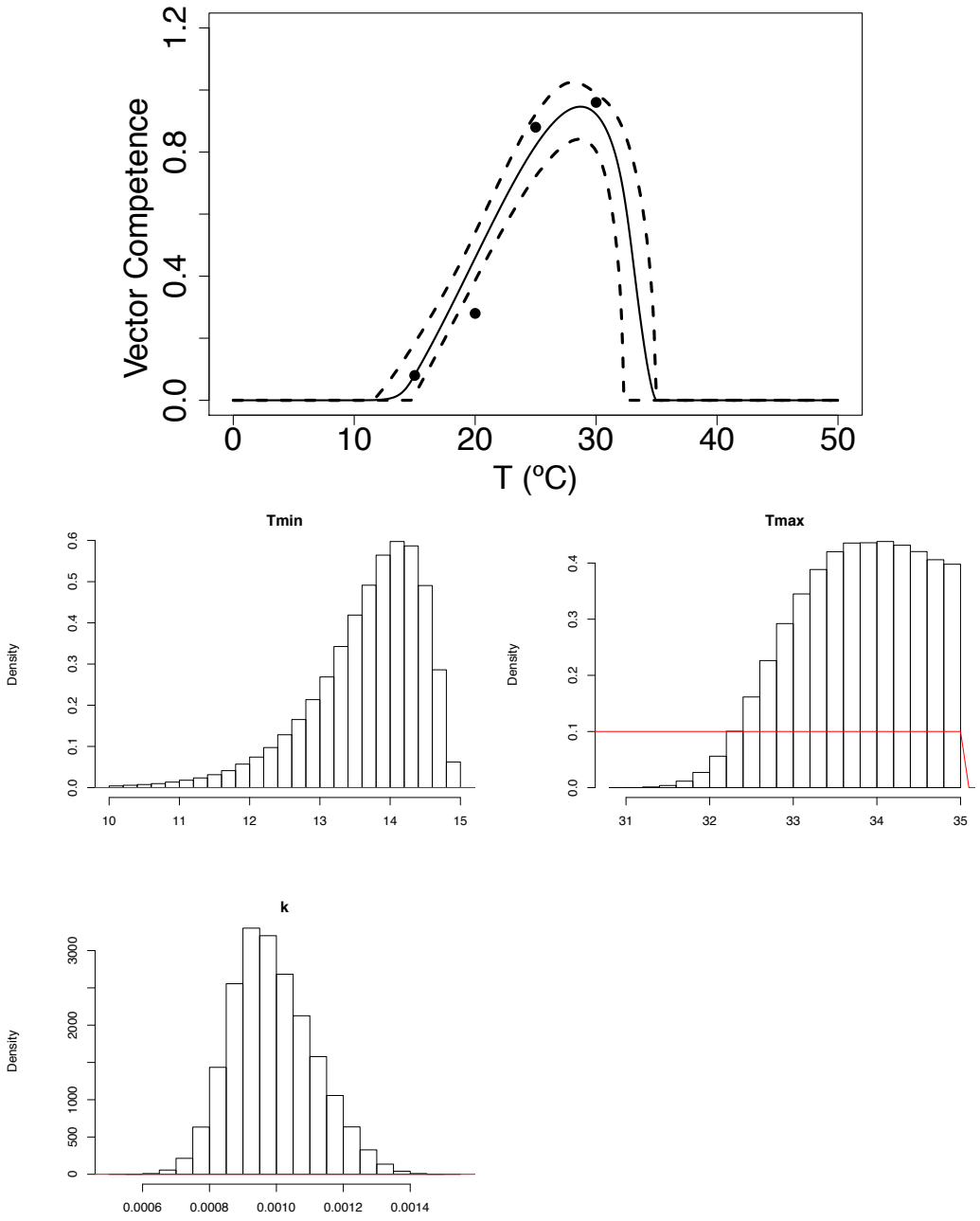

Figure C.4: (Top) The mean trajectory in solid line and HPD interval in dashed black for the probability of a vector transmitting the virus when biting b. (Bottom) Histograms of the posterior distribution for each parameter of the Brière fit for the probability b. The prior distribution for each parameter is plotted in red. The Brière fit is determined by the equation $kT(T - T_{Min})\sqrt{T_{Max} - T}$ using a binomial distribution.

laboratory setting [184]. Larva Development Time is defined as the time in days required for the larva to mature into a pupa in a given temperature. Pupa Development Time is defined as the time in days required for a pupa to mature into adult midges in a given temperature (Figures C.8, C.9, C.10).

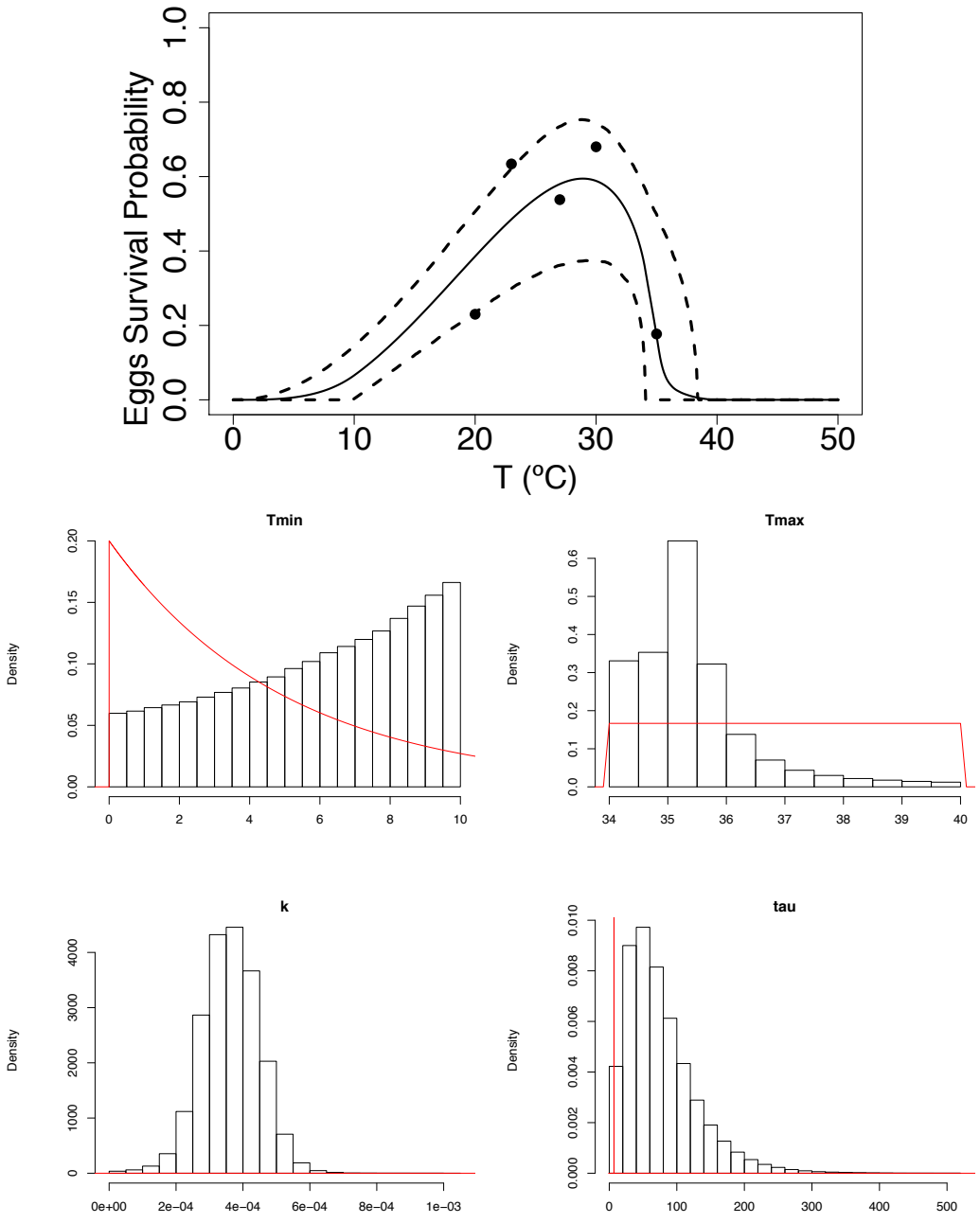

Figure C.5: (Top) The mean trajectory in solid line and HPD interval in dashed black for the egg survival probability p_E. (Bottom) Histograms of the posterior distribution for each parameter of the Brière fit for the probability p_E. The prior distribution for each parameter is plotted in red. The Brière fit is determined by the equation $kT(T - T_{Min})\sqrt{T_{Max} - T}$ using a normal distribution with precision τ.

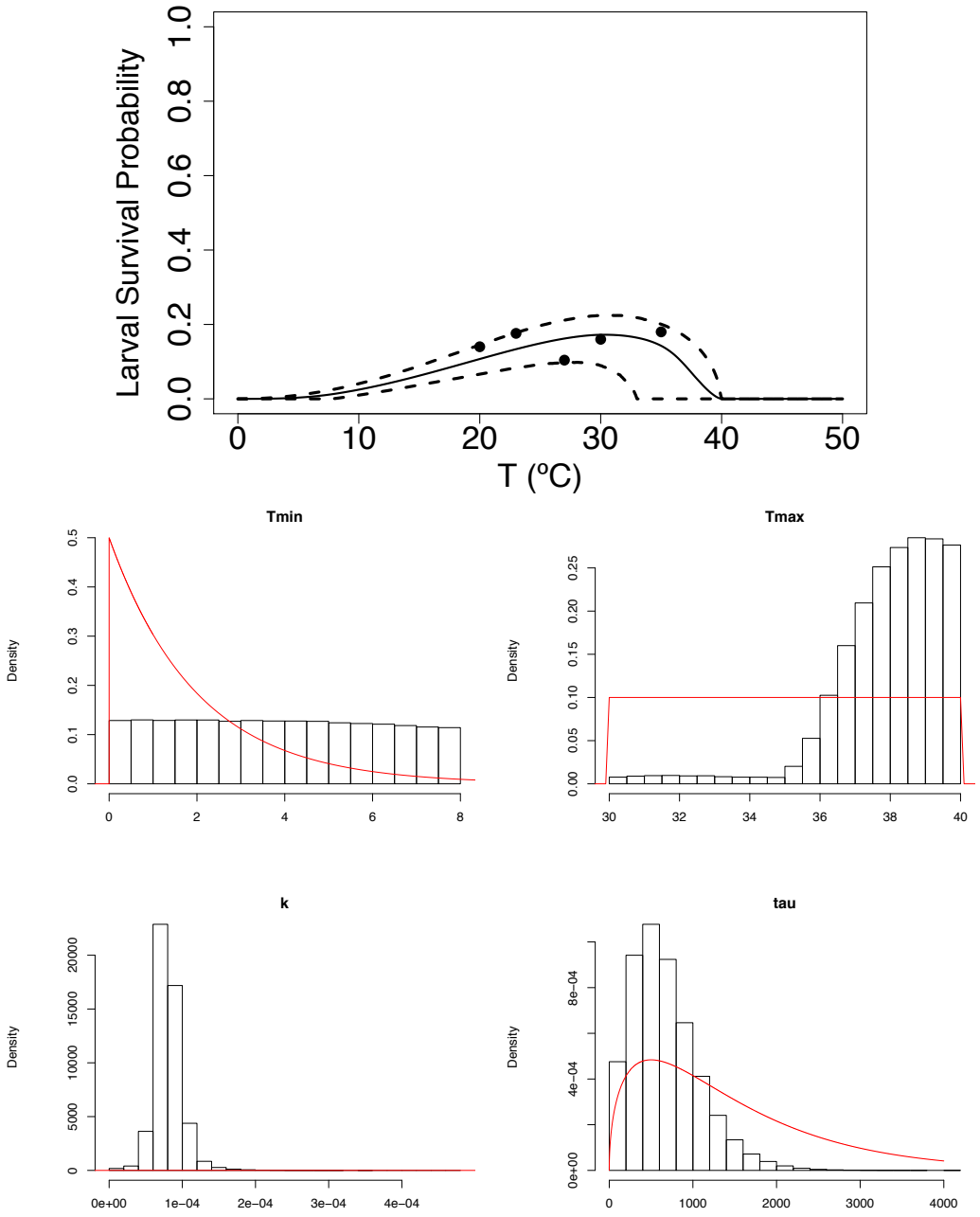

Figure C.6: (Top) The mean trajectory in solid line and HPD interval in dashed black for the larval survival probability p_L. (Bottom) Histograms of the posterior distribution for each parameter of the Brière fit for the probability p_L. The prior distribution for each parameter is plotted in red. The Brière fit is determined by the equation $kT(T - T_{Min})\sqrt{T_{Max} - T}$ using a normal distribution with precision τ.

Fecundity F

The rate at which female midges lay eggs is closely related to the spread of Bluetongue. This rate is typically measured as eggs per female per day. For this study we also utilized fecundity data that was taken over two oviposition

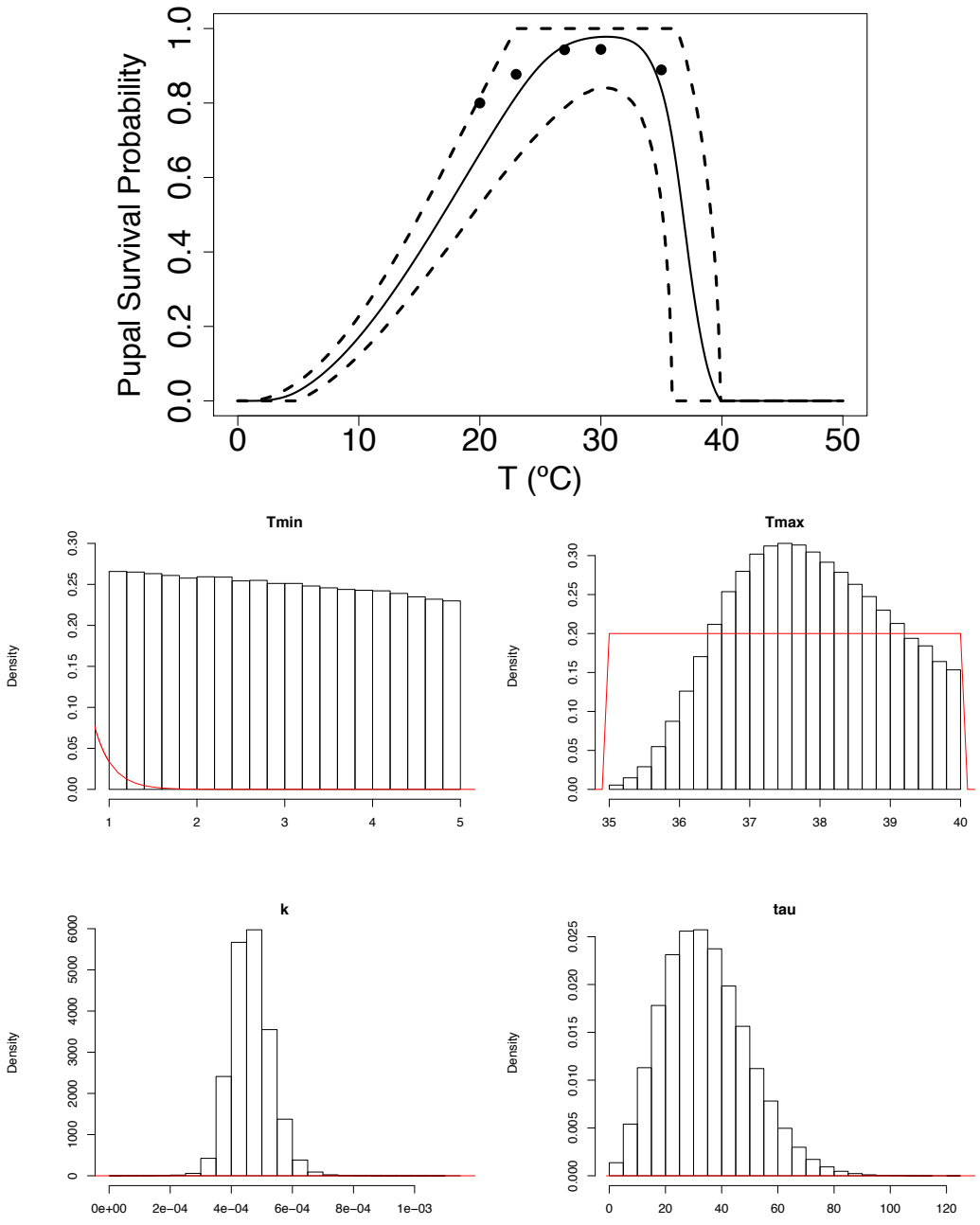

Figure C.7: (Top) The mean trajectory in solid line and HPD interval in dashed black for the pupal survival probability p_P. (Bottom) Histograms of the posterior distribution for each parameter of the Brière fit for the probability p_P. The prior distribution for each parameter is plotted in red. The Brière fit is determined by the equation $kT(T - T_{Min})\sqrt{T_{Max} - T}$ using a normal distribution with precision τ.

cycles and transformed the data (originally eggs per female) by dividing by the median oviposition time [181].

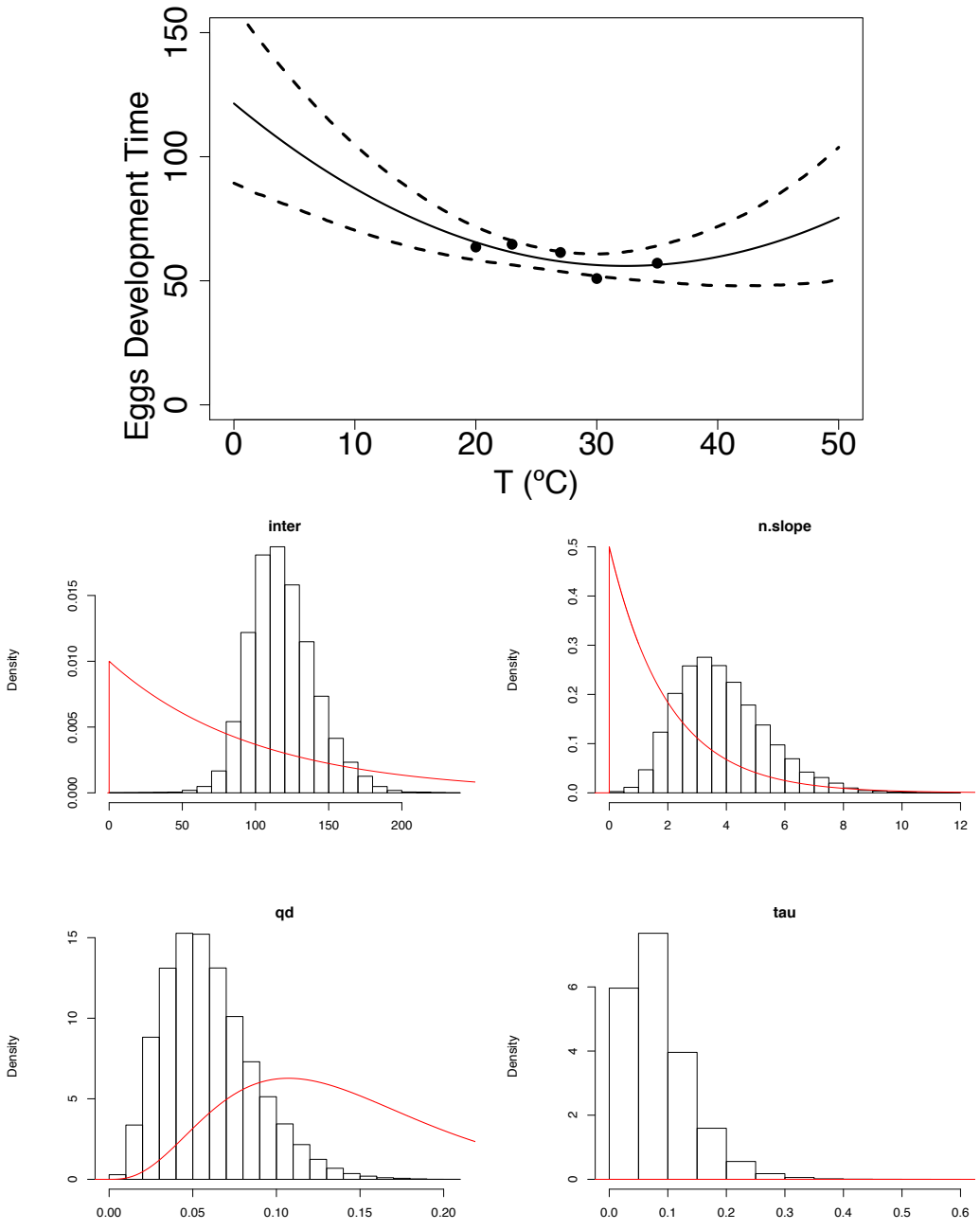

Figure C.8: (Top) The mean trajectory in solid line and HPD interval in dashed black for egg development time ρ_E. (Bottom) Histograms of the posterior distribution for each parameter of the quadratic fit for egg development time ρ_E. The prior distribution for each parameter is plotted in red. The quadratic fit is determined by the equation $inter - n.slope\, T + qd\, T^2$ using a normal distribution with precision τ.

Pathogen development rate ν

Parasite development has been shown to increase with temperature in studies that support the hypothesis that global warming has been cause for latitudi-

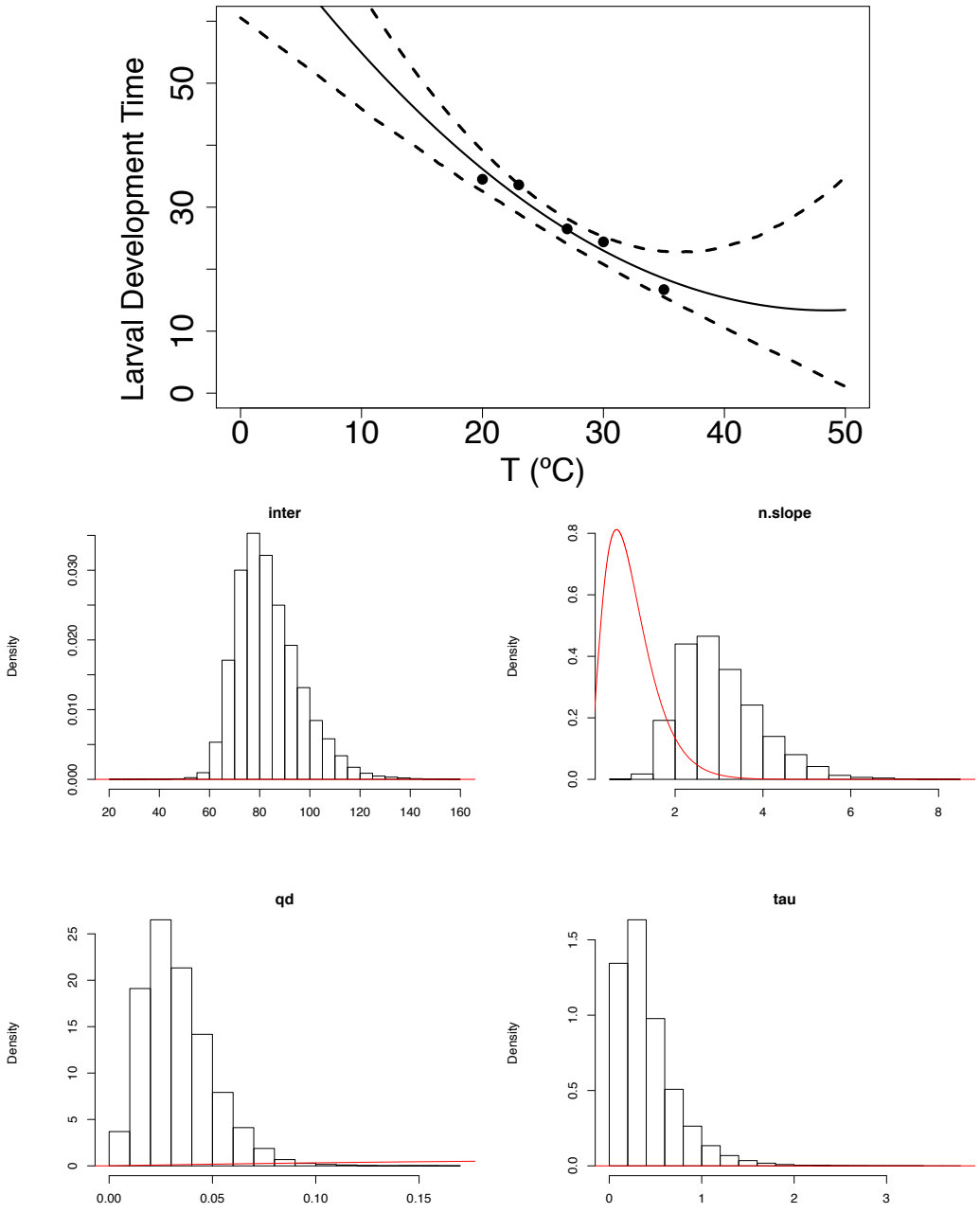

Figure C.9: (Top) The mean trajectory in solid line and HPD interval in dashed black for larval development time ρ_L. (Bottom) Histograms of the posterior distribution for each parameter of the quadratic fit for larval development time ρ_L. The prior distribution for each parameter is plotted in red. The quadratic fit is determined by the equation $inter - n.slope\, T + qd\, T^2$ using a normal distribution with precision τ.

nal shifts which in turn increase the reach of vectors that transmit diseases like bluetongue [185]. In order to investigate this trait's relationship with temperature, we made use of data on Extrinsic Incubation Period (EIP) to create a new parameter: Parasite Development Rate (ν) ($\nu = 1/\text{EIP}$). EIP

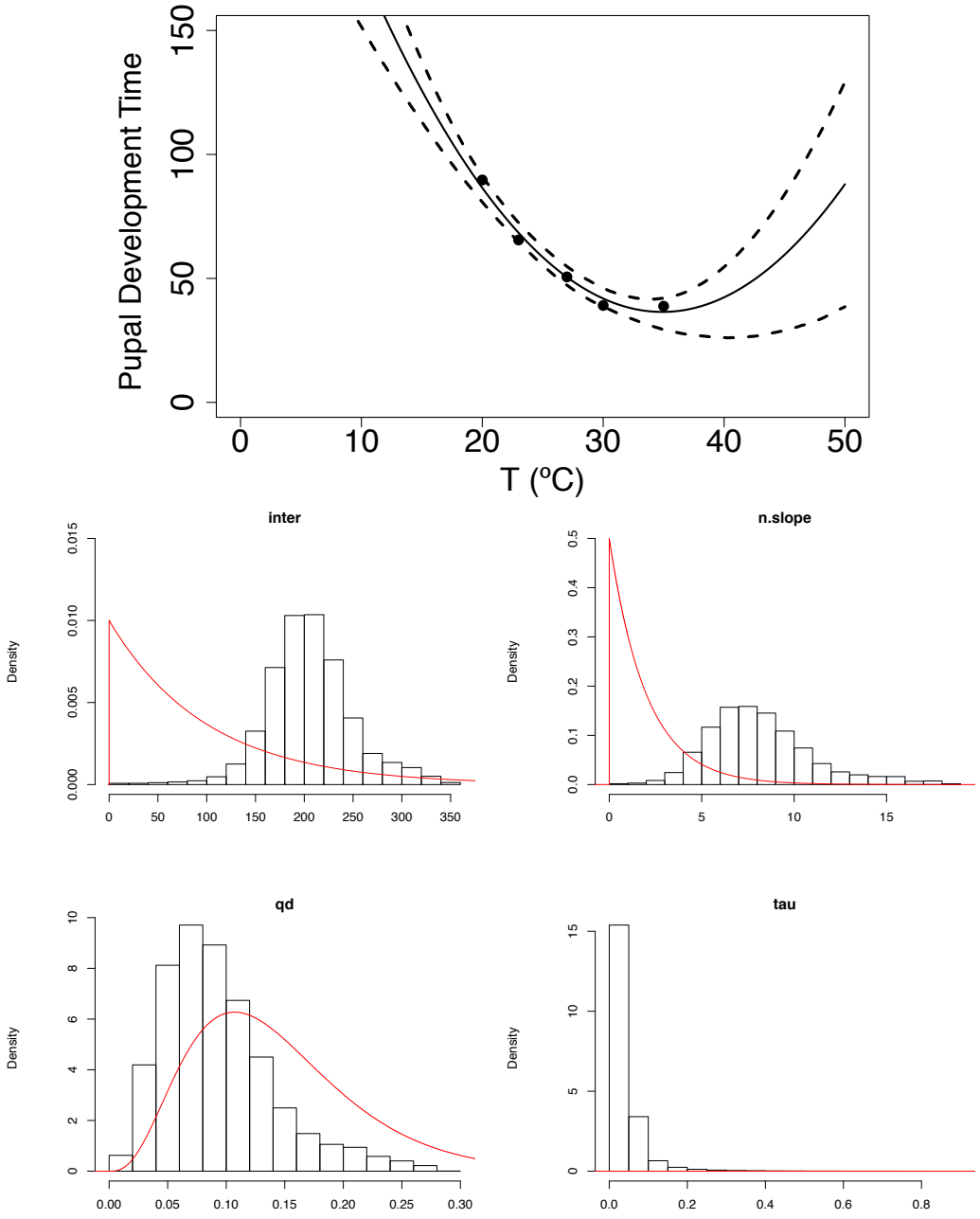

Figure C.10: (Top) The mean trajectory in solid line and HPD interval in dashed black for pupal development time ρ_P. (Bottom) Histograms of the posterior distribution for each parameter of the quadratic fit for pupal development time ρ_P. The prior distribution for each parameter is plotted in red. The quadratic fit is determined by the equation $inter - n.slope\, T + qd\, T^2$ using a normal distribution with precision τ.

is the time between a vector getting infected with a pathogen to the time that the vector itself is able to transmit the pathogen.

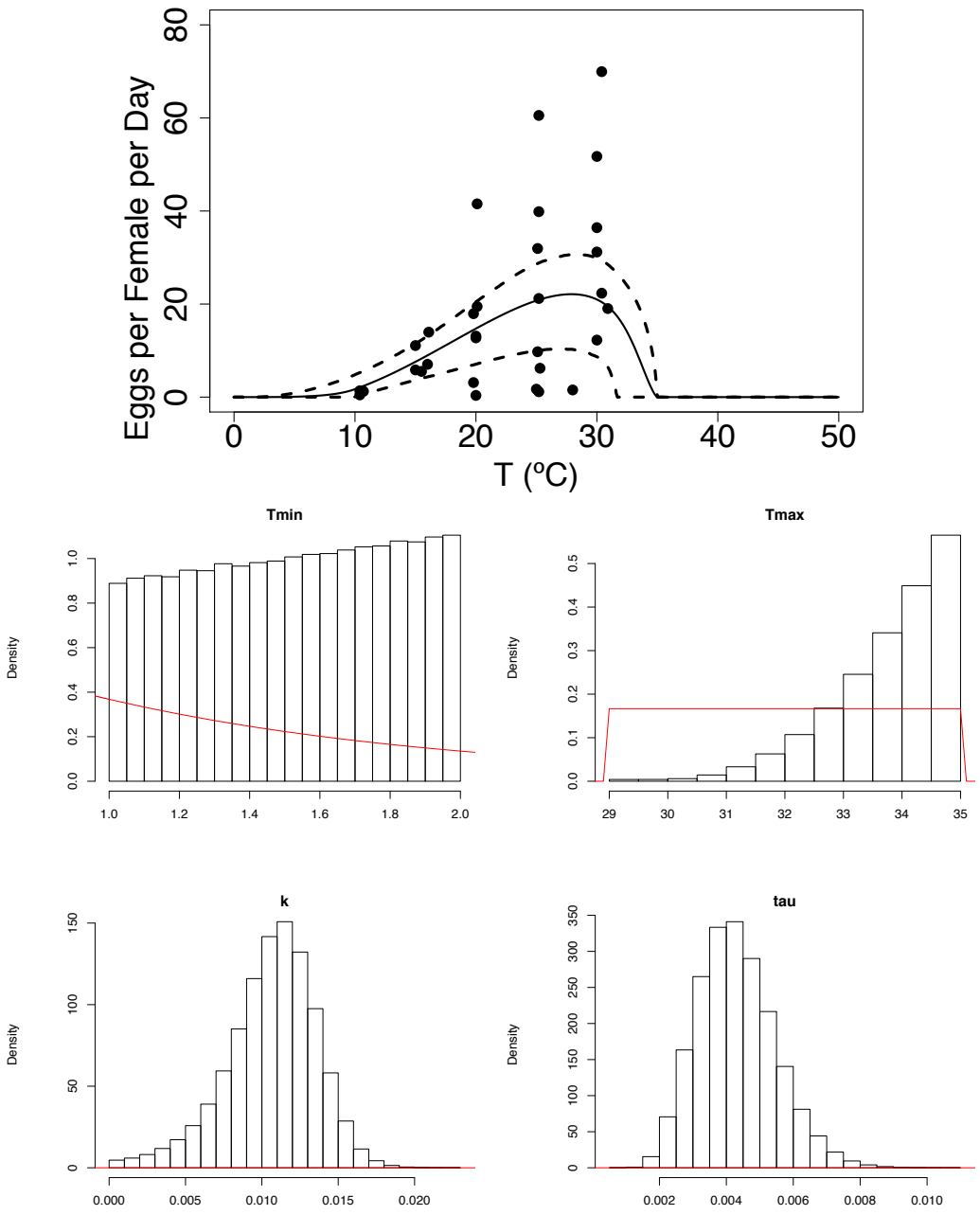

Figure C.11: (Top) The mean trajectory in solid line and HPD interval in dashed black for fecundity F. (Bottom) Histograms of the posterior distribution for each parameter of the Brière fit for fecundity F. The prior distribution for each parameter is plotted in red. The Brière fit is determined by the equation $kT(T - T_{Min})\sqrt{T_{Max} - T}$ using a normal distribution with precision τ.

Adult mortality rate μ

The rate at which midges die over a span of time is known as the mortality rate μ. We define the mortality rate of midges as $\frac{1}{lf}$, where lf represents the lifespan of midges in days, or the probability of survival for the midges.

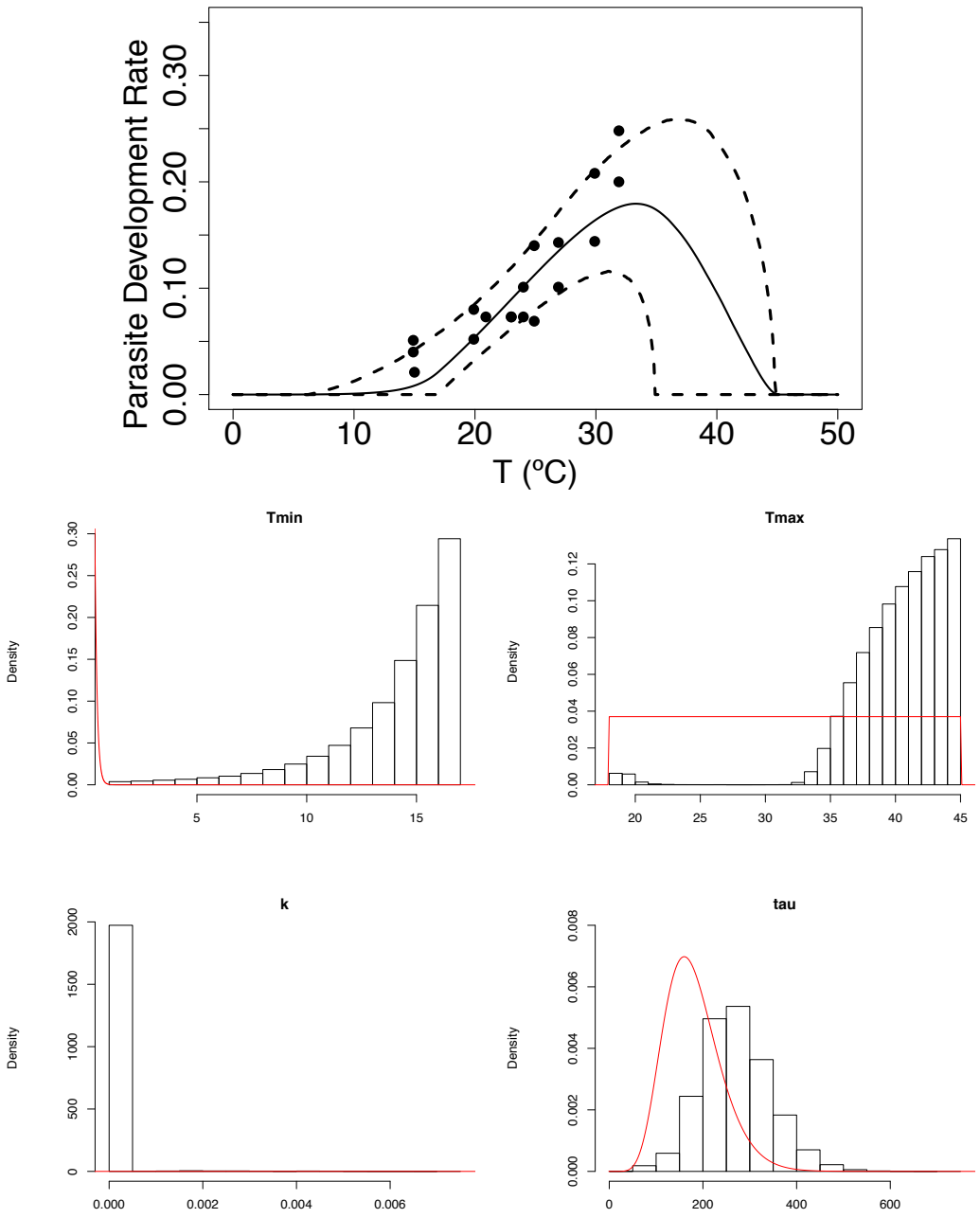

Figure C.12: (Top) The mean trajectory in solid line and HPD interval in dashed black for the parasite development rate ν. (Bottom) Histograms of the posterior distribution for each parameter of the Brière fit for the parasite development rate ν. The prior distribution for each parameter is plotted in red. The Brière fit is determined by the equation $kT(T - T_{Min})\sqrt{T_{Max} - T}$ using a normal distribution with precision τ.

We define mortality rate in the case where lf is the lifespan of midges in days. Mortality rate is also sensitive to environmental factors, especially temperature [181].

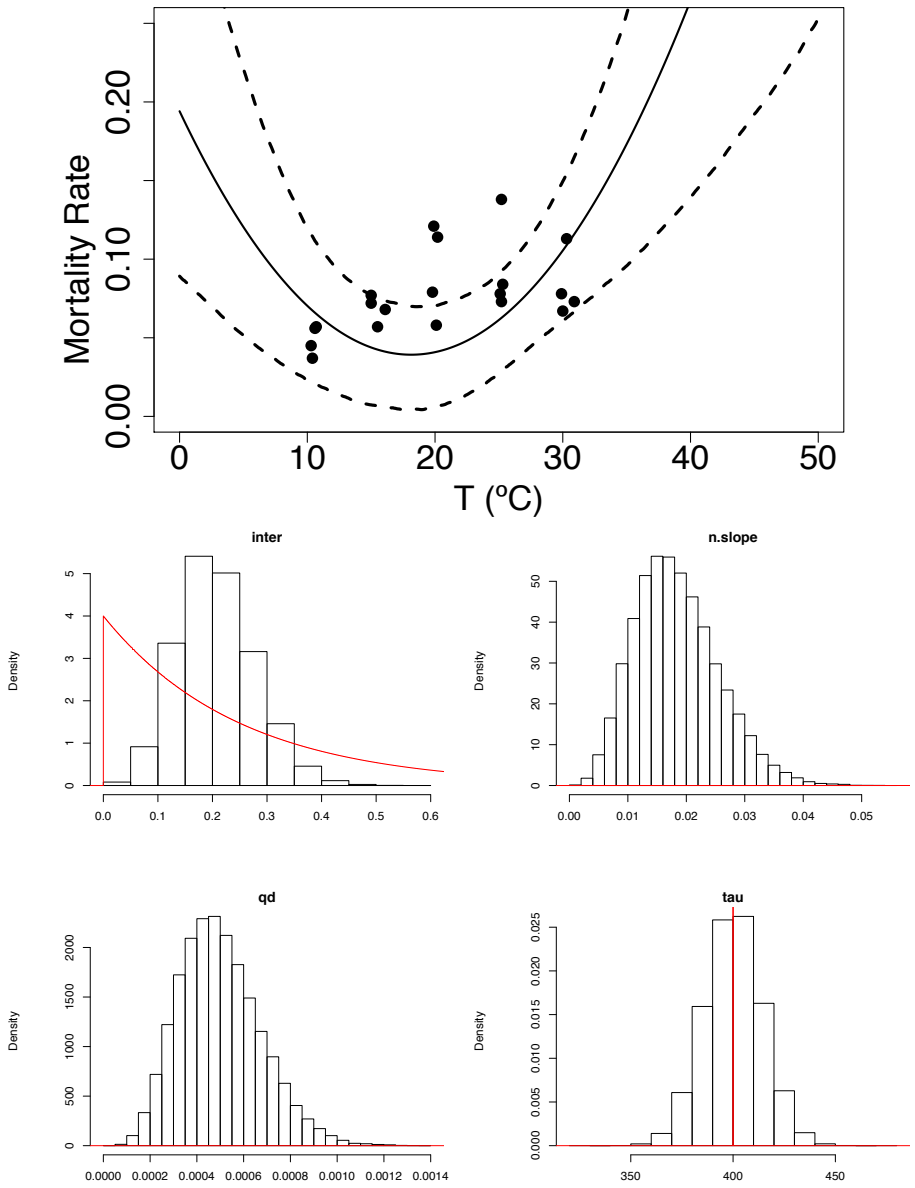

Figure C.13: (Top) The mean trajectory in solid line and HPD interval in dashed black for the mortality rate μ. (Bottom) Histograms of the posterior distribution for each parameter of the quadratic fit for the mortality rate μ. The prior distribution for each parameter is plotted in red. The quadratic fit is determined by the equation $inter - n.slope\ T + qd\ T^2$ using a normal distribution with precision τ.

Thermal traits prior distributions

Table C.2 summarizes all the priors used to fit the thermal curves.

Model Parameter	Mean Function	Parameters	Prior
Biting Rate a	Brière	T_{Min} T_{Max} k τ	dunif(0, 20) dunif(20,40) dgamma(1,20) dgamma(0.01, 0.01)
Transmission probability b	Brière	T_{Min} T_{Max} k	dunif(10,24) dunif(25,35) dgamma(1,10)
Egg Survival Probability p_E	Brière	T_{Min} T_{Max} k τ	dunif(10,20) dunif(35,40) dgamma(1,20) dgamma(7, 5^{-10})
Larval Survival Probability p_L	Brière	T_{Min} T_{Max} k τ	dunif(0,8) dunif(30,40) dgamma(1,20) dgamma(1.5, 0.001)
Pupal Survival Probability p_P	Brière	T_{Min} T_{Max} k τ	dunif(1,5) dunif(35,40) dgamma(1,5) dgamma(10, 0.002)
Egg Development Time ρ_E	Quadratic	inter n.slope qd τ	dgamma(1, 0.01) dgamma(1, 0.5) dgamma(4,28) dnorm(3, 1/800)
Larval Development Time ρ_L	Quadratic	inter n.slope qd τ	dgamma(1, 0.01) dgamma(1, 0.5) dgamma(4,28) dnorm(3, 1/1000)
Pupal Development Time ρ_P	Quadratic	inter n.slope qd τ	dgamma(1, 0.01) dgamma(1, 0.5) dgamma(4,28) dnorm(3, 1/200)
Eggs per Female per Day F	Brière	T_{Min} T_{Max} k τ	dunif(1, 10) dunif(29,35) dgamma(1,1) dgamma(9, 0.0005)
Parasite Development Rate ν	Brière	T_{Min} T_{Max} k τ	dunif(1, 17) dunif(18,45) dgamma(1,10) dgamma(9, 0.05)
Adult Mortality Rate μ	Quadratic	inter n.slope qd τ	dgamma(2,2) dgamma(3,3) dgamma(2,2) dnorm(1000, 1/500)

Table C.2: Prior distributions for each of the parameters for the fitting of the responses for each of the thermal traits considered.

Posterior distributions for all R_0 forms

For all three R_0 posterior distributions we provide posterior distributions for the lower temperature limit, peak temperature, and upper temperature limit.

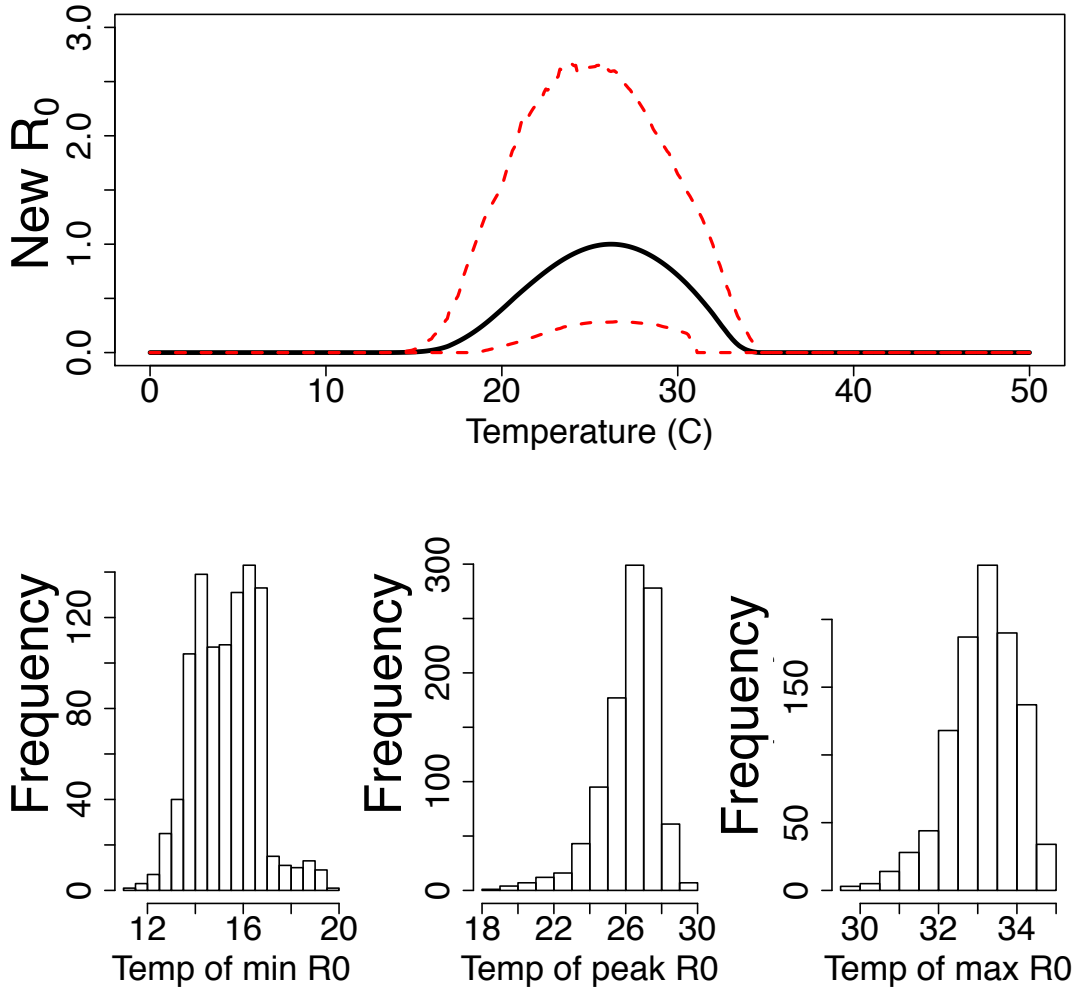

Figure C.14: Minimum, peak and, maximum temepratures posterior densities for the R_0 presented here.

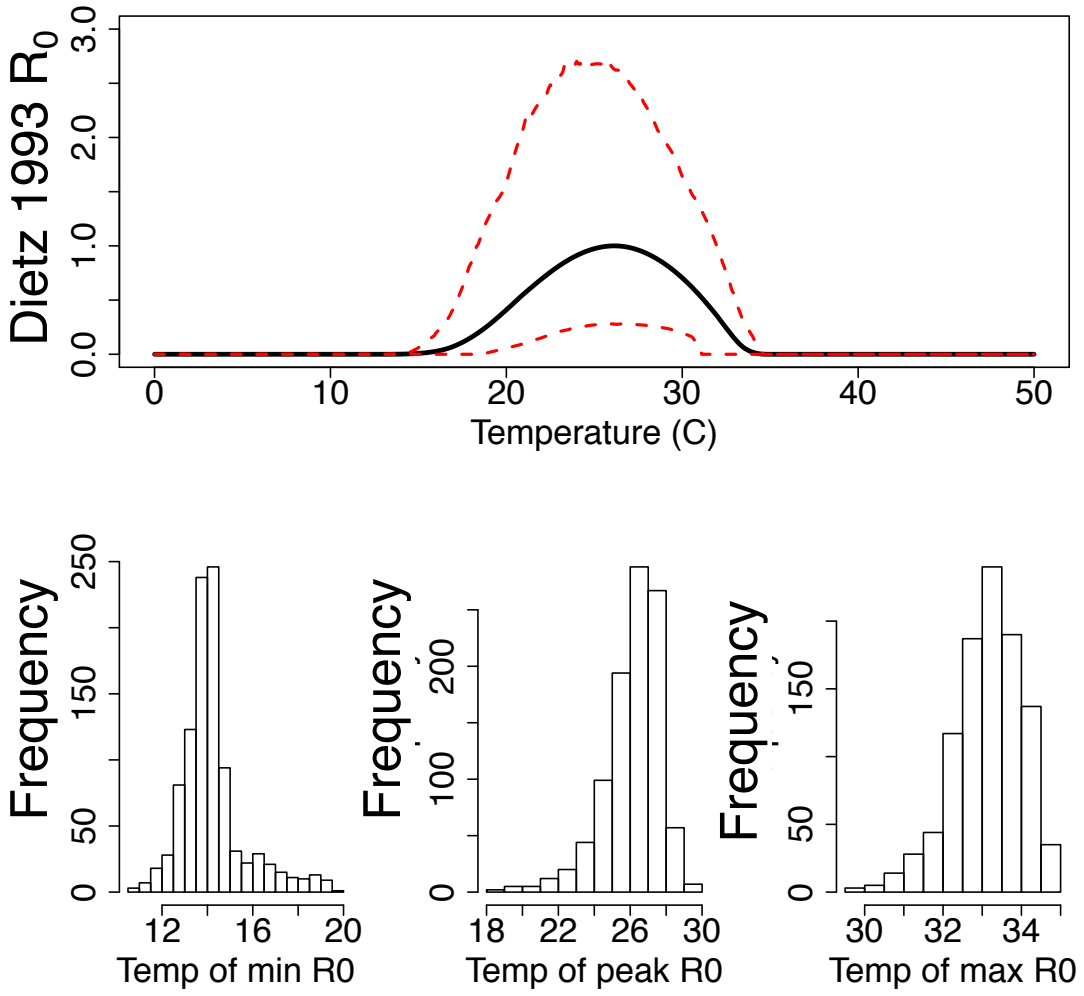

Figure C.15: Minimum, peak and, maximum temepratures posterior densities for Dietz 1993 [130] R_0

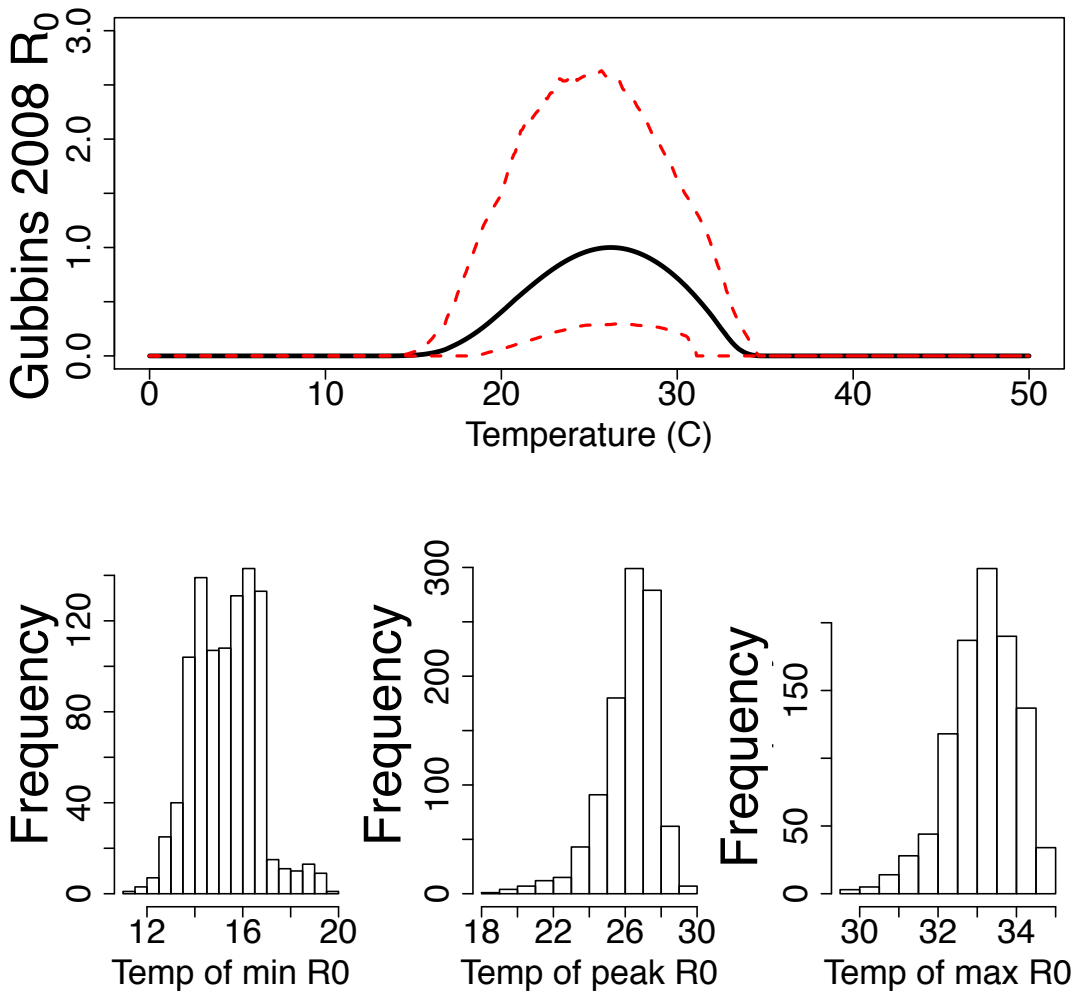

Figure C.16: Minimum, peak and, maximum temepratures posterior densities for Gubbins 2008 [148] R_0

Bibliography

[1] "CDC report: Infectious Diseases,"

[2] A. Pastore y Piontti, N. Perra, L. Rossi, N. Samay, and A. Vespignani, *Infectious disease spreading: from data to models*, pp. 3–10. Cham: Springer International Publishing, 2019.

[3] R. Müller, F. Reuss, V. Kendrovski, and D. Montag, *Vector-Borne Diseases*, pp. 67–90. Cham: Springer International Publishing, 2019.

[4] D. J. Gubler, "Resurgent vector-borne diseases as a global health problem.," *Emerging infectious diseases*, vol. 4, no. 3, p. 442, 1998.

[5] P. Daszak, A. A. Cunningham, and A. D. Hyatt, "Emerging infectious diseases of wildlife–threats to biodiversity and human health," *science*, vol. 287, no. 5452, pp. 443–449, 2000.

[6] R. A. Taylor, E. A. Mordecai, C. A. Gilligan, J. R. Rohr, and L. R. Johnson, "Mathematical models are a powerful method to understand and control the spread of Huanglongbing," *PeerJ*, vol. 4, p. e2642, 2016.

[7] W. O. for Animal Health, "Bluetongue," *World Organisation for Animal Health (OIE)*, 2013.

[8] W. H. Organization *et al.*, "A global brief on vector-borne diseases," 2014.

[9] W. H. Organization, "Vector Borne Diseases," 2016.

[10] S. Funk, M. Salathé, and V. A. Jansen, "Modelling the influence of human behaviour on the spread of infectious diseases: a review," *Journal of the Royal Society Interface*, vol. 7, no. 50, pp. 1247–1256, 2010.

[11] R. Kovats, D. Campbell-Lendrum, A. McMichel, A. Woodward, and J. S. H. Cox, "Early effects of climate change: do they include changes in vector-borne disease?," *Philosophical Transactions of the Royal Society of London B: Biological Sciences*, vol. 356, no. 1411, pp. 1057–1068, 2001.

[12] K. L. Gage, T. R. Burkot, R. J. Eisen, and E. B. Hayes, "Climate and vectorborne diseases," *American journal of preventive medicine*, vol. 35, no. 5, pp. 436–450, 2008.

[13] J. J. McCarthy, *Climate change 2001: impacts, adaptation, and vulnerability: contribution of Working Group II to the third assessment report of the Intergovernmental Panel on Climate Change*. Cambridge University Press, 2001.

[14] S. Altizer, A. Dobson, P. Hosseini, P. Hudson, M. Pascual, and P. Rohani, "Seasonality and the dynamics of infectious diseases," *Ecology letters*, vol. 9, no. 4, pp. 467–484, 2006.

[15] R. C. Reiner, T. A. Perkins, C. M. Barker, T. Niu, L. F. Chaves, A. M. Ellis, D. B. George, A. Le Menach, J. R. Pulliam, D. Bisanzio, *et al.*, "A systematic review of mathematical models of mosquito-borne pathogen transmission: 1970–2010," *Journal of The Royal Society Interface*, vol. 10, no. 81, p. 20120921, 2013.

[16] J. A. Patz and W. K. Reisen, "Immunology, climate change and vectorborne diseases," *Trends in immunology*, vol. 22, no. 4, pp. 171–172, 2001.

[17] E. A. Mordecai, J. M. Cohen, M. V. Evans, P. Gudapati, L. R. Johnson, C. A. Lippi, K. Miazgowicz, C. C. Murdock, J. R. Rohr, S. J. Ryan,

et al., "Detecting the impact of temperature on transmission of Zika, dengue, and chikungunya using mechanistic models," *PLoS neglected tropical diseases*, vol. 11, no. 4, p. e0005568, 2017.

[18] M. K. Butterworth, C. W. Morin, and A. C. Comrie, "An analysis of the potential impact of climate change on dengue transmission in the southeastern United States," *Environmental health perspectives*, vol. 125, no. 4, pp. 579–585, 2016.

[19] A. S. Siraj and T. A. Perkins, "Assessing the population at risk of Zika virus in Asia–is the emergency really over?," *BMJ global health*, vol. 2, no. 3, p. e000309, 2017.

[20] J. H. Huber, M. L. Childs, J. M. Caldwell, and E. A. Mordecai, "Seasonal temperature variation influences climate suitability for dengue, chikungunya, and Zika transmission," *PLoS neglected tropical diseases*, vol. 12, no. 5, p. e0006451, 2018.

[21] R. Kovats, D. Campbell-Lendrum, A. McMichel, A. Woodward, and J. S. H. Cox, "Early effects of climate change: do they include changes in vector-borne disease?," *Philosophical Transactions of the Royal Society of London. Series B: Biological Sciences*, vol. 356, no. 1411, pp. 1057–1068, 2001.

[22] D. Rogers and S. Randolph, "Climate change and vector-borne diseases," *Advances in parasitology*, vol. 62, pp. 345–381, 2006.

[23] V. Chevalier, F. Courtin, H. Guis, A. Tran, and L. Vial, *Climate change and vector-borne diseases*. Springer, 2016.

[24] P. Hunter, "Climate change and waterborne and vector-borne disease," *Journal of applied microbiology*, vol. 94, pp. 37–46, 2003.

[25] D. J. Gubler, P. Reiter, K. L. Ebi, W. Yap, R. Nasci, and J. A. Patz, "Climate variability and change in the United States: potential impacts

on vector-and rodent-borne diseases.," *Environmental health perspectives*, vol. 109, no. Suppl 2, p. 223, 2001.

[26] E. A. Mordecai, K. P. Paaijmans, L. R. Johnson, C. Balzer, T. Ben-Horin, E. Moor, A. McNally, S. Pawar, S. J. Ryan, T. C. Smith, *et al.*, "Optimal temperature for malaria transmission is dramatically lower than previously predicted," *Ecology letters*, vol. 16, no. 1, pp. 22–30, 2013.

[27] E. A. Mordecai, J. M. Cohen, M. V. Evans, P. Gudapati, L. R. Johnson, C. A. Lippi, K. Miazgowicz, C. C. Murdock, J. R. Rohr, S. J. Ryan, *et al.*, "Detecting the impact of temperature on transmission of Zika, dengue, and chikungunya using mechanistic models," *PLoS neglected tropical diseases*, vol. 11, no. 4, p. e0005568, 2017.

[28] P. Reiter, "Weather, vector biology, and arboviral recrudescence," *The arboviruses: epidemiology and ecology*, vol. 1, pp. 245–255, 1988.

[29] W. C. Reeves, J. L. Hardy, W. K. Reisen, and M. M. Milby, "Potential effect of global warming on mosquito-borne arboviruses," *Journal of medical entomology*, vol. 31, no. 3, pp. 323–332, 1994.

[30] P. Reiter, "Global-warming and vector-borne disease in temperate regions and at high altitude," *The Lancet*, vol. 351, no. 9105, pp. 839–840, 1998.

[31] P. R. Grimstad and L. D. Haramis, "Aedes triseriatus (Diptera: Culicidae) and La Crosse virus III. Enhanced oral transmission by nutrition-deprived mosquitoes," *Journal of Medical Entomology*, vol. 21, no. 3, pp. 249–256, 1984.

[32] W. Reisen, H. Lothrop, and J. Hardy, "Bionomics of Culex tarsalis (Diptera: Culicidae) in relation to arbovirus transmission in southeastern California," *Journal of medical entomology*, vol. 32, no. 3, pp. 316–327, 1995.

[33] S. M. Omer and J. Cloudsley-Thompson, "Survival of female Anopheles gambiae Giles through a 9-month dry season in Sudan," *Bulletin of the World Health Organization*, vol. 42, no. 2, p. 319, 1970.

[34] P. Deichstetter, "The Effect of Climate Change on Mosquito-Borne Diseases," *The American Biology Teacher*, vol. 79, no. 3, pp. 169–173, 2017.

[35] W. K. Reisen, "Effect of temperature on Culex tarsalis (Diptera: Culicidae) from the Coachella and San Joaquin valleys of California," *Journal of medical entomology*, vol. 32, no. 5, pp. 636–645, 1995.

[36] C. Mitchell, "Occurrence, biology, and physiology of diapause in overwintering mosquitoes," *The arboviruses: epidemiology and ecology*, vol. 1, pp. 191–218, 1988.

[37] D. A. Focks, E. Daniels, D. G. Haile, and J. E. Keesling, "A simulation model of the epidemiology of urban dengue fever: literature analysis, model development, preliminary validation, and samples of simulation results," *The American journal of tropical medicine and hygiene*, vol. 53, no. 5, pp. 489–506, 1995.

[38] S. H. Paull, D. E. Horton, M. Ashfaq, D. Rastogi, L. D. Kramer, N. S. Diffenbaugh, and A. M. Kilpatrick, "Drought and immunity determine the intensity of West Nile virus epidemics and climate change impacts," *Proc. R. Soc. B*, vol. 284, no. 1848, p. 20162078, 2017.

[39] C. Lansdowne and C. S. Hacker, "The effect of fluctuating temperature and humidity on the adult life table characteristics of five strains of *Aedes aegypti*," *Journal of medical entomology*, vol. 11, no. 6, pp. 723–733, 1975.

[40] D. L. Smith, K. E. Battle, S. I. Hay, C. M. Barker, T. W. Scott, and F. E. McKenzie, "Ross, Macdonald, and a theory for the dynamics and control of mosquito-transmitted pathogens," *PLoS pathogens*, vol. 8, no. 4, p. e1002588, 2012.

[41] W. Martens, T. Jetten, J. Rotmans, and L. Niessen, "Climate change and vector-borne diseases: a global modelling perspective," *Global environmental change*, vol. 5, no. 3, pp. 195–209, 1995.

[42] R. C. Reiner, S. T. Stoddard, B. M. Forshey, A. A. King, A. M. Ellis, A. L. Lloyd, K. C. Long, C. Rocha, S. Vilcarromero, H. Astete, *et al.*, "Time-varying, serotype-specific force of infection of dengue virus," *Proceedings of the National Academy of Sciences*, p. 201314933, 2014.

[43] K. Dietz, "Malaria models," *Advances in Applied Probability*, vol. 3, no. 02, pp. 208–210, 1971.

[44] P. Amarasekare and V. Savage, "A framework for elucidating the temperature dependence of fitness," *The American Naturalist*, vol. 179, no. 2, pp. 178–191, 2011.

[45] O. J. Brady, N. Golding, D. M. Pigott, M. U. Kraemer, J. P. Messina, R. C. Reiner Jr, T. W. Scott, D. L. Smith, P. W. Gething, and S. I. Hay, "Global temperature constraints on *Aedes aegypti* and *Aedes albopictus* persistence and competence for dengue virus transmission," *Parasites & vectors*, vol. 7, no. 1, p. 338, 2014.

[46] P. Amarasekare and R. M. Coutinho, "Effects of temperature on intraspecific competition in ectotherms," *The American Naturalist*, vol. 184, no. 3, pp. E50–E65, 2014.

[47] K. D. Lafferty and E. A. Mordecai, "The rise and fall of infectious disease in a warmer world," *F1000Research*, vol. 5, 2016.

[48] P. M. Schulte, "The effects of temperature on aerobic metabolism: towards a mechanistic understanding of the responses of ectotherms to a changing environment," *Journal of Experimental Biology*, vol. 218, no. 12, pp. 1856–1866, 2015.

[49] S. Lindsay and M. Birley, "Climate change and malaria transmission," *Annals of Tropical Medicine & Parasitology*, vol. 90, no. 5, pp. 573–588, 1996.

[50] E. A. Mordecai, K. P. Paaijmans, L. R. Johnson, C. Balzer, T. Ben-Horin, E. de Moor, A. McNally, S. Pawar, S. J. Ryan, T. C. Smith, *et al.*, "Optimal temperature for malaria transmission is dramatically lower than previously predicted," *Ecology letters*, vol. 16, no. 1, pp. 22–30, 2013.

[51] L. R. Johnson, R. B. Gramacy, J. Cohen, E. Mordecai, C. Murdock, J. Rohr, S. J. Ryan, A. M. Stewart-Ibarra, D. Weikel, *et al.*, "Phenomenological forecasting of disease incidence using heteroskedastic Gaussian processes: A dengue case study," *The Annals of Applied Statistics*, vol. 12, no. 1, pp. 27–66, 2018.

[52] M. A. Robert, R. C. Christofferson, P. D. Weber, and H. J. Wearing, "Temperature impacts on dengue emergence in the United States: Investigating the role of seasonality and climate change," *Epidemics*, p. 100344, 2019.

[53] P. E. Parham and E. Michael, "Modeling the effects of weather and climate change on malaria transmission," *Environmental health perspectives*, vol. 118, no. 5, p. 620, 2010.

[54] D. A. Ewing, C. A. Cobbold, B. Purse, M. Nunn, and S. M. White, "Modelling the effect of temperature on the seasonal population dynamics of temperate mosquitoes," *Journal of theoretical biology*, vol. 400, pp. 65–79, 2016.

[55] O. Diekmann, J. A. P. Heesterbeek, and J. A. Metz, "On the definition and the computation of the basic reproduction ratio R 0 in models for infectious diseases in heterogeneous populations," *Journal of mathematical biology*, vol. 28, no. 4, pp. 365–382, 1990.

[56] O. Diekmann, K. Dietz, and J. Heesterbeek, "The basic reproduction ratio for sexually transmitted diseases: I. Theoretical considerations," *Mathematical biosciences*, vol. 107, no. 2, pp. 325–339, 1991.

[57] F. R. Adler, "The effects of averaging on the basic reproduction ratio," *Mathematical biosciences*, vol. 111, no. 1, pp. 89–98, 1992.

[58] R. Barrera, M. Amador, and A. J. MacKay, "Population dynamics of *Aedes aegypti* and dengue as influenced by weather and human behavior in San Juan, Puerto Rico," *PLoS neglected tropical diseases*, vol. 5, no. 12, p. e1378, 2011.

[59] L. R. Johnson, T. Ben-Horin, K. D. Lafferty, A. McNally, E. Mordecai, K. P. Paaijmans, S. Pawar, and S. J. Ryan, "Understanding uncertainty in temperature effects on vector-borne disease: a Bayesian approach," *Ecology*, vol. 96, no. 1, pp. 203–213, 2015.

[60] L. M. Beck-Johnson, W. A. Nelson, K. P. Paaijmans, A. F. Read, M. B. Thomas, and O. N. Bjørnstad, "The importance of temperature fluctuations in understanding mosquito population dynamics and malaria risk," *Royal Society open science*, vol. 4, no. 3, p. 160969, 2017.

[61] J. I. Blanford, S. Blanford, R. G. Crane, M. E. Mann, K. P. Paaijmans, K. V. Schreiber, and M. B. Thomas, "Implications of temperature variation for malaria parasite development across Africa," *Scientific reports*, vol. 3, p. 1300, 2013.

[62] S. T. Stoddard, H. J. Wearing, R. C. Reiner Jr, A. C. Morrison, H. Astete, S. Vilcarromero, C. Alvarez, C. Ramal-Asayag, M. Sihuincha, C. Rocha, *et al.*, "Long-term and seasonal dynamics of dengue in Iquitos, Peru," *PLoS neglected tropical diseases*, vol. 8, no. 7, p. e3003, 2014.

[63] "The american mosquito control association report: Mosquito borne diseases,"

[64] M. A. Shaukat, S. Ali, B. Saddiq, M. W. Hassan, A. Ahmad, and M. Kamran, "Effective Mechanisms to Control Mosquito Borne Diseases: A Review," *American Journal of Clinical Neurology and Neurosurgery*, vol. 4, no. 1, pp. 21–30, 2019.

[65] R. K. Walsh, C. L. Aguilar, L. Facchinelli, L. Valerio, J. M. Ramsey, T. W. Scott, A. L. Lloyd, and F. Gould, "Regulation of Aedes aegypti population dynamics in field systems: quantifying direct and delayed density dependence," *The American journal of tropical medicine and hygiene*, vol. 89, no. 1, pp. 68–77, 2013.

[66] "Dengue Virus Net: *Aedes aegypti*, *Aedes albopictus*,"

[67] T. W. Scott and A. C. Morrison, "Vector dynamics and transmission of dengue virus: implications for dengue surveillance and prevention strategies," in *Dengue virus*, pp. 115–128, Springer, 2010.

[68] S. P. Brand, K. S. Rock, and M. J. Keeling, "The interaction between vector life history and short vector life in vector-borne disease transmission and control," *PLoS computational biology*, vol. 12, no. 4, p. e1004837, 2016.

[69] N. L. Achee, F. Gould, T. A. Perkins, R. C. Reiner Jr, A. C. Morrison, S. A. Ritchie, D. J. Gubler, R. Teyssou, and T. W. Scott, "A critical assessment of vector control for dengue prevention," *PLoS neglected tropical diseases*, vol. 9, no. 5, p. e0003655, 2015.

[70] R. M. Anderson and R. M. May, *Infectious diseases of humans: dynamics and control*. Oxford university press, 1992.

[71] R. M. Lana, M. M. Morais, T. F. M. de Lima, T. G. de Senna Carneiro, L. M. Stolerman, J. P. C. dos Santos, J. J. C. Cortés, Á. E. Eiras, and C. T. Codeço, "Assessment of a trap based *Aedes aegypti* surveillance program using mathematical modeling," *PloS one*, vol. 13, no. 1, p. e0190673, 2018.

[72] "CDC report: Comparison of Dengue vectors,"

[73] M. Legros, A. L. Lloyd, Y. Huang, and F. Gould, "Density-dependent intraspecific competition in the larval stage of Aedes aegypti (Diptera: Culicidae): revisiting the current paradigm," *Journal of medical entomology*, vol. 46, no. 3, pp. 409–419, 2009.

[74] P. E. Parham and E. Michael, "Modeling the effects of weather and climate change on malaria transmission," *Environmental Health Perspectives*, vol. 118, no. 5, p. 620, 2010.

[75] N. Bacaër, "Approximation of the basic reproduction number R 0 for vector-borne diseases with a periodic vector population," *Bulletin of mathematical biology*, vol. 69, no. 3, pp. 1067–1091, 2007.

[76] N. Bacaër and S. Guernaoui, "The epidemic threshold of vector-borne diseases with seasonality," *Journal of mathematical biology*, vol. 53, no. 3, pp. 421–436, 2006.

[77] M. U. Kraemer, M. E. Sinka, K. A. Duda, A. Q. Mylne, F. M. Shearer, C. M. Barker, C. G. Moore, R. G. Carvalho, G. E. Coelho, W. Van Bortel, *et al.*, "The global distribution of the arbovirus vectors aedes aegypti and ae. albopictus," *elife*, vol. 4, p. e08347, 2015.

[78] L. C. Farnesi, H. C. Vargas, D. Valle, and G. L. Rezende, "Darker eggs of mosquitoes resist more to dry conditions: Melanin enhances serosal cuticle contribution in egg resistance to desiccation in Aedes, Anopheles and Culex vectors," *PLoS neglected tropical diseases*, vol. 11, no. 10, p. e0006063, 2017.

[79] L. E. Munstermann, "Care and maintenance of Aedes mosquito colonies," in *The molecular biology of insect disease vectors*, pp. 13–20, Springer, 1997.

[80] D. L. Denlinger and P. A. Armbruster, "Mosquito diapause," *Annual Review of Entomology*, vol. 59, pp. 73–93, 2014.

[81] T. K. Joy, A. J. Arik, V. Corby-Harris, A. A. Johnson, and M. A. Riehle, "The impact of larval and adult dietary restriction on lifespan, reproduction and growth in the mosquito Aedes aegypti," *Experimental gerontology*, vol. 45, no. 9, pp. 685–690, 2010.

[82] M. Bates *et al.*, *The natural history of mosquitoes.* New York: The Macmillan Co, 1949.

[83] J. D. Wormington and S. A. Juliano, "Sexually dimorphic body size and development time plasticity in Aedes mosquitoes (Diptera: Culicidae)," *Evolutionary ecology research*, vol. 16, p. 223, 2014.

[84] M. Q. Benedict, R. S. Levine, W. A. Hawley, and L. P. Lounibos, "Spread of the tiger: global risk of invasion by the mosquito Aedes albopictus," *Vector-borne and zoonotic Diseases*, vol. 7, no. 1, pp. 76–85, 2007.

[85] M. S. Shocket, S. J. Ryan, and E. A. Mordecai, "Temperature explains broad patterns of Ross River virus transmission," *Elife*, vol. 7, p. e37762, 2018.

[86] C. W. Morin, A. J. Monaghan, M. H. Hayden, R. Barrera, and K. Ernst, "Meteorologically driven simulations of dengue epidemics in San Juan, PR," *PLoS neglected tropical diseases*, vol. 9, no. 8, p. e0004002, 2015.

[87] L. Rueda, K. Patel, R. Axtell, and R. Stinner, "Temperature-dependent development and survival rates of Culex quinquefasciatus and *Aedes aegypti* (Diptera: Culicidae)," *Journal of medical entomology*, vol. 27, no. 5, pp. 892–898, 1990.

[88] A. Mohammed and D. D. Chadee, "Effects of different temperature regimens on the development of *Aedes aegypti* (L.)(Diptera: Culicidae) mosquitoes," *Acta tropica*, vol. 119, no. 1, pp. 38–43, 2011.

[89] J. P. Messina, O. J. Brady, N. Golding, M. U. Kraemer, G. W. Wint, S. E. Ray, D. M. Pigott, F. M. Shearer, K. Johnson, L. Earl, *et al.*, "The current and future global distribution and population at risk of dengue," *Nature microbiology*, p. 1, 2019.

[90] N. A. Honório, R. M. R. Nogueira, C. T. Codeço, M. S. Carvalho, O. G. Cruz, M. d. A. F. M. Magalhães, J. M. G. de Araújo, E. S. M. de Araújo, M. Q. Gomes, L. S. Pinheiro, *et al.*, "Spatial evaluation and modeling of dengue seroprevalence and vector density in Rio de Janeiro, Brazil," *PLoS neglected tropical diseases*, vol. 3, no. 11, p. e545, 2009.

[91] J. Liu-Helmersson, Å. Brännström, M. O. Sewe, J. C. Semenza, and J. Rocklöv, "Estimating Past, Present, and Future Trends in the Global Distribution and Abundance of the Arbovirus Vector Aedes aegypti Under Climate Change Scenarios," *Frontiers in Public Health*, vol. 7, 2019.

[92] E. Koyoc-Cardeña, A. Medina-Barreiro, A. Cohuo-Rodríguez, N. Pavía-Ruz, A. Lenhart, G. Ayora-Talavera, M. Dunbar, P. Manrique-Saide, and G. Vazquez-Prokopec, "Estimating absolute indoor density of Aedes aegypti using removal sampling," *Parasites & vectors*, vol. 12, no. 1, p. 250, 2019.

[93] R. M. Lana, T. G. Carneiro, N. A. Honório, and C. T. Codeço, "Seasonal and nonseasonal dynamics of *Aedes aegypti* in Rio de Janeiro, Brazil: Fitting mathematical models to trap data," *Acta tropica*, vol. 129, pp. 25–32, 2014.

[94] R. M. Lana, M. F. da Costa Gomes, T. F. M. de Lima, N. A. Honório, and C. T. Codeço, "The introduction of dengue follows transportation infrastructure changes in the state of Acre, Brazil: a network-based analysis," *PLoS neglected tropical diseases*, vol. 11, no. 11, p. e0006070, 2017.

[95] M. Heinisch, F. A. Diaz-Quijano, F. Chiaravalloti-Neto, F. G. M. Pancetti, R. R. Coelho, P. dos Santos Andrade, P. R. Urbinatti, R. M. M. S. de Almeida, and T. N. Lima-Camara, "Seasonal and spatial distribution of Aedes aegypti and Aedes albopictus in a municipal urban park in São Paulo, SP, Brazil," *Acta tropica*, vol. 189, pp. 104–113, 2019.

[96] S. Bhatt, P. W. Gething, O. J. Brady, J. P. Messina, A. W. Farlow, C. L. Moyes, J. M. Drake, J. S. Brownstein, A. G. Hoen, O. Sankoh, *et al.*, "The global distribution and burden of dengue," *Nature*, vol. 496, no. 7446, p. 504, 2013.

[97] O. Brady, "Disease Risk: Mapping the emerging burden of dengue," *eLife*, vol. 8, p. e47458, 2019.

[98] K. L. Gage, T. R. Burkot, R. J. Eisen, and E. B. Hayes, "Climate and vectorborne diseases," *American journal of preventive medicine*, vol. 35, no. 5, pp. 436–450, 2008.

[99] P. Reiter, "Climate change and mosquito-borne disease.," *Environmental health perspectives*, vol. 109, no. suppl 1, pp. 141–161, 2001.

[100] C. W. Morin, A. C. Comrie, and K. Ernst, "Climate and dengue transmission: evidence and implications," *Environmental health perspectives*, vol. 121, no. 11-12, pp. 1264–1272, 2013.

[101] A. K. Githeko, S. W. Lindsay, U. E. Confalonieri, and J. A. Patz, "Climate change and vector-borne diseases: a regional analysis," *Bulletin of the World Health Organization*, vol. 78, pp. 1136–1147, 2000.

[102] D. Rogers and S. Randolph, "Climate change and vector-borne diseases," *Advances in parasitology*, vol. 62, pp. 345–381, 2006.

[103] M. Bates, *The nature of natural history*, vol. 1138. Princeton University Press, 2014.

[104] "Bioagents: All about mosquitoes,"

[105] M. J. Turell, M. L. OâĂŹGuinn, D. J. Dohm, and J. W. Jones, "Vector competence of North American mosquitoes (diptera: culicidae) for West Nile virus," *Journal of medical entomology*, vol. 38, no. 2, pp. 130–134, 2001.

[106] L. B. Goddard, A. E. Roth, W. K. Reisen, and T. W. Scott, "Vector competence of California mosquitoes for West Nile virus," *Emerging infectious diseases*, vol. 8, no. 12, p. 1385, 2002.

[107] A. Heitmann, S. Jansen, R. Lühken, M. Leggewie, J. Schmidt-Chanasit, and E. Tannich, "Forced Salivation As a Method to Analyze Vector Competence of Mosquitoes," *Journal of visualized experiments: JoVE*, no. 138, 2018.

[108] "CDC report: Life stages of *Aedes aegypti* and *Aedes albopictus* mosquitoes,"

[109] A. Ponlawat and L. C. Harrington, "Blood feeding patterns of *Aedes aegypti* and *Aedes albopictus* in Thailand," *Journal of medical entomology*, vol. 42, no. 5, pp. 844–849, 2005.

[110] K. P. Paaijmans, S. Blanford, A. S. Bell, J. I. Blanford, A. F. Read, and M. B. Thomas, "Influence of climate on malaria transmission depends on daily temperature variation," *Proceedings of the National Academy of Sciences*, vol. 107, no. 34, pp. 15135–15139, 2010.

[111] L. Xu, L. C. Stige, K.-S. Chan, J. Zhou, J. Yang, S. Sang, M. Wang, Z. Yang, Z. Yan, T. Jiang, *et al.*, "Climate variation drives dengue dynamics," *Proceedings of the National Academy of Sciences*, vol. 114, no. 1, pp. 113–118, 2017.

[112] "CDC report: Dengue Epidemiology,"

[113] J. A. Huwaldt and S. Steinhorst, "Plot digitizer," *URL http://plotdigitizer. sourceforge. net*, 2013.

[114] H. Delatte, G. Gimonneau, A. Triboire, and D. Fontenille, "Influence of temperature on immature development, survival, longevity, fecundity, and gonotrophic cycles of aedes albopictus, vector of chikungunya and dengue in the indian ocean," *Journal of medical entomology*, vol. 46, no. 1, pp. 33–41, 2009.

[115] B. W. Alto and S. A. Juliano, "Temperature effects on the dynamics of aedes albopictus (diptera: Culicidae) populations in the laboratory," *Journal of medical entomology*, vol. 38, no. 4, pp. 548–556, 2001.

[116] D. C. Calado and M. A. Navarro-Silva, "Influência da temperatura sobre a longevidade, fecundidade e atividade hematofágica de aedes (stegomyia) albopictus skuse, 1894 (diptera, culicidae) sob condições de laboratório," *Revista Brasileira de Entomologia*, vol. 46, no. 1, pp. 93–98, 2002.

[117] N. F. Ezeakacha, "Environmental impacts and carry-over effects in complex life cycles: the role of different life history stages," 2015.

[118] F.-Z. Xiao, Y. Zhang, Y.-Q. Deng, S. He, H.-G. Xie, X.-N. Zhou, and Y.-S. Yan, "The effect of temperature on the extrinsic incubation period and infection rate of dengue virus serotype 2 infection in aedes albopictus," *Archives of virology*, vol. 159, no. 11, pp. 3053–3057, 2014.

[119] J. Waldock, N. L. Chandra, J. Lelieveld, Y. Proestos, E. Michael, G. Christophides, and P. E. Parham, "The role of environmental variables on aedes albopictus biology and chikungunya epidemiology," *Pathogens and global health*, vol. 107, no. 5, pp. 224–241, 2013.

[120] B. M. Forshey, C. Guevara, V. A. Laguna-Torres, M. Cespedes, J. Vargas, A. Gianella, E. Vallejo, C. Madrid, N. Aguayo, E. Gotuzzo, *et al.*, "Arboviral etiologies of acute febrile illnesses in western south america, 2000–2007," *PLoS neglected tropical diseases*, vol. 4, no. 8, p. e787, 2010.

[121] "Dengue Forcasting: National Oceanic and Atmospheric Administration,"

[122] M. J. Angilletta Jr and M. J. Angilletta, *Thermal adaptation: a theoretical and empirical synthesis*. Oxford University Press, 2009.

[123] A. I. Dell, S. Pawar, and V. M. Savage, "Systematic variation in the temperature dependence of physiological and ecological traits," *Proceedings of the National Academy of Sciences*, vol. 108, no. 26, pp. 10591–10596, 2011.

[124] M. Bayoh and S. Lindsay, "Effect of temperature on the development of the aquatic stages of anopheles gambiae sensu stricto (diptera: Culicidae)," *Bulletin of entomological research*, vol. 93, no. 5, pp. 375–381, 2003.

[125] J.-F. Briere, P. Pracros, A.-Y. Le Roux, and J.-S. Pierre, "A novel rate model of temperature-dependent development for arthropods," *Environmental Entomology*, vol. 28, no. 1, pp. 22–29, 1999.

[126] L. Joseph, D. B. Wolfson, and R. D. Berger, "Sample size calculations for binomial proportions via highest posterior density intervals," *Journal of the Royal Statistical Society: Series D (The Statistician)*, vol. 44, no. 2, pp. 143–154, 1995.

[127] *R: A Language and Environment for Statistical Computing*.

[128] R. Ross, *The prevention of malaria*. John Murray; London, 1911.

[129] G. Macdonald *et al.*, "The epidemiology and control of malaria.," *The Epidemiology and Control of Malaria.*, 1957.

[130] K. Dietz, "The estimation of the basic reproduction number for infectious diseases," *Statistical methods in medical research*, vol. 2, no. 1, pp. 23–41, 1993.

[131] J. Liu-Helmersson, H. Stenlund, A. Wilder-Smith, and J. Rocklöv, "Vectorial capacity of aedes aegypti: effects of temperature and implications for global dengue epidemic potential," *PloS one*, vol. 9, no. 3, p. e89783, 2014.

[132] O. J. Brady, M. A. Johansson, C. A. Guerra, S. Bhatt, N. Golding, D. M. Pigott, H. Delatte, M. G. Grech, P. T. Leisnham, R. Maciel-de Freitas, *et al.*, "Modelling adult *Aedes aegypti* and *Aedes albopictus*survival at different temperatures in laboratory and field settings," *Parasites & vectors*, vol. 6, no. 1, p. 351, 2013.

[133] A. M. Stewart-Ibarra and R. Lowe, "Climate and non-climate drivers of dengue epidemics in southern coastal ecuador," *The American journal of tropical medicine and hygiene*, vol. 88, no. 5, pp. 971–981, 2013.

[134] C. Calisher and P. Mertens, "Taxonomy of African horse sickness viruses," in *African Horse Sickness*, pp. 3–11, Springer, 1998.

[135] P. Mellor, J. Boorman, and M. Baylis, "Culicoides biting midges: their role as arbovirus vectors," *Annual review of entomology*, vol. 45, no. 1, pp. 307–340, 2000.

[136] E. Wittmann, P. Mellor, and M. Baylis, "Effect of temperature on the transmission of orbiviruses by the biting midge, Culicoides sonorensis," *Medical and veterinary entomology*, vol. 16, no. 2, pp. 147–156, 2002.

[137] S. Gubbins, S. Carpenter, M. Baylis, J. L. Wood, and P. S. Mellor, "Assessing the risk of bluetongue to UK livestock: uncertainty and sensitivity analyses of a temperature-dependent model for the basic reproduction number," *Journal of the Royal Society Interface*, vol. 5, no. 20, pp. 363–371, 2007.

[138] W. J. Tabachnick, C. T. Smartt, and C. R. Connelly, "Bluetongue," *UF IFSAS Extension*, 2008.

[139] A. S. Lear and R. J. Callan, *Overview of Bluetongue*, 2014.

[140] N. J. MacLachlan and A. J. Guthrie, "Re-emergence of bluetongue, African horse sickness, and other Orbivirus diseases," *Veterinary Research*, 2010.

[141] N. Preparedness, A. Incident Coordination Center, Veterinary Services, and P. H. I. Service, *Bluetongue standard operating procedure: an overview of etiology and ecology*, 2016.

[142] K. A. Alexander, N. J. MacLachlan, P. W. Kat, C. House, S. J. O'Brien, N. W. Lerche, M. Sawyer, L. G. Frank, K. Holekamp, L. Smale, J. W. McNutt, M. K. Laurenson, M. G. L. Mills, and B. I. Osburn, "Evidence of natural bluetongue virus infection among african carnivores," *The American journal of tropical medicine and hygiene*, 1994.

[143] M. Jenckel, E. Bréard, C. Schulz, C. Sailleau, C. Viarouge, B. Hoffmann, D. Höper, M. Beer, and S. Zientara, "Complete Coding Genome Sequence of Putative Novel Bluetongue Virus Serotype 27," *Microbiology Resource Announcements*, vol. 3, no. 2, 2015.

[144] USDA, *Veterinary Biological Products*. United States Department of Agriculture, 2019.

[145] USDA, "Orbiviruses Gap Analysis: Bluetongue and Epizootic Hemorrhagic Disease," *Agricultural Research Service*, 2013.

[146] USDA, "U.S. Cattle & Beef Industry Statistics and Information," *Economic Research Service*, 2015.

[147] EC, "Bluetongue seasonally vector free periods," *European Comission*, 2016.

[148] S. Gubbins, S. Carpenter, M. Baylis, J. L. Wood, and P. S. Mellor, "Assessing the risk of bluetongue to UK livestock: uncertainty and sensitivity analyses of a temperature-dependent model for the basic

reproduction number," *Journal of the Royal Society Interface*, vol. 5, no. 20, pp. 363–371, 2007.

[149] J. Turner, R. G. Bowers, and M. Baylis, "Two-host, two-vector basic reproduction ratio (R0) for bluetongue," *PloS one*, vol. 8, no. 1, p. e53128, 2013.

[150] O. Diekmann and J. A. P. Heesterbeek, *Mathematical epidemiology of infectious diseases: model building, analysis and interpretation*, vol. 5. John Wiley & Sons, 2000.

[151] O. Diekmann, J. A. P. Heesterbeek, and M. G. Roberts, "The construction of next-generation matrices for compartmental epidemic models," *Journal of the Royal Society Interface*, p. rsif20090386, 2009.

[152] W. J. Tabachnick, "Culicoides variipennis and bluetongue-virus epidemiology in the united states," *Annual review of entomology*, vol. 41, no. 1, pp. 23–43, 1996.

[153] *`rjags`: Bayesian graphical models using MCMC.*

[154] R. J. Hijmans, S. E. Cameron, J. L. Parra, P. G. Jones, and A. Jarvis, "Very high resolution interpolated climate surfaces for global land areas," *International Journal of Climatology: A Journal of the Royal Meteorological Society*, vol. 25, no. 15, pp. 1965–1978, 2005.

[155] M. Gilbert, G. Nicolas, G. Cinardi, T. P. Van Boeckel, S. Vanwambeke, W. G. R. Wint, and T. P. Robinson, "Global sheep distribution in 2010 (5 minutes of arc)," 2018.

[156] M. Gilbert, G. Nicolas, G. Cinardi, T. P. Van Boeckel, S. O. Vanwambeke, G. W. Wint, and T. P. Robinson, "Global distribution data for cattle, buffaloes, horses, sheep, goats, pigs, chickens and ducks in 2010," *Scientific data*, vol. 5, p. 180227, 2018.

[157] R. J. Hijmans, *raster: Geographic Data Analysis and Modeling*, 2019.

[158] R. J. Hijmans and J. van Etten, *raster: Geographic analysis and modeling with raster data. R package version 2.0–12*, 2012.

[159] R. Bivand, "Lewin-koh, n. maptools: Tools for reading and handling spatial objects. r packag. version 0.9-1. https," *CRAN. R-project. org/package= maptools*, 2017.

[160] R. Bivand, T. Keitt, B. Rowlingson, E. Pebesma, M. Sumner, R. Hijmans, E. Rouault, and M. R. Bivand, "Package ?rgdal?," *Bindings for the Geospatial Data Abstraction Library. Available online: https://cran. r-project. org/web/packages/rgdal/index. html (accessed on 15 October 2017)*, 2015.

[161] S. J. Ryan, A. McNally, L. R. Johnson, E. A. Mordecai, T. Ben-Horin, K. Paaijmans, and K. D. Lafferty, "Mapping physiological suitability limits for malaria in africa under climate change," *Vector-Borne and Zoonotic Diseases*, vol. 15, no. 12, pp. 718–725, 2015.

[162] N. Courtejoie, G. Zanella, and B. Durand, "Bluetongue transmission and control in Europe: A systematic review of compartmental mathematical models," *Preventive veterinary medicine*, 2018.

[163] N. Hartemink, B. Purse, R. Meiswinkel, H. E. Brown, A. De Koeijer, A. Elbers, G.-J. Boender, D. Rogers, and J. Heesterbeek, "Mapping the basic reproduction number (R0) for vector-borne diseases: a case study on bluetongue virus," *Epidemics*, vol. 1, no. 3, pp. 153–161, 2009.

[164] R. A. Taylor, S. J. Ryan, C. A. Lippi, D. G. Hall, H. A. Narouei-Khandan, J. R. Rohr, and L. R. Johnson, "Predicting the fundamental thermal niche of crop pests and diseases in a changing world: a case study on citrus greening," *Journal of Applied Ecology*, vol. 56, no. 8, pp. 2057–2068, 2019.

[165] A. E. Jones, J. Turner, C. Caminade, A. E. Heath, M. Wardeh, G. Kluiters, P. J. Diggle, A. P. Morse, and M. Baylis, "Bluetongue risk

under future climates," *Nature Climate Change*, vol. 9, no. 2, p. 153, 2019.

[166] L. H. Franklinos, K. E. Jones, D. W. Redding, and I. Abubakar, "The effect of global change on mosquito-borne disease," *The Lancet Infectious Diseases*, 2019.

[167] S. Blagica and S. Jovana, "Risk Management and Risk Communication in the Case of Vector-Borne Disease: Case of Macedonia–Risk Management in VBDs," in *Global Applications of One Health Practice and Care*, pp. 159–173, IGI Global, 2019.

[168] K.-s. Kim, "Current Challenges in the Development of Vaccines and Drugs Against Emerging Vector-borne Diseases," *Current medicinal chemistry*, 2019.

[169] C. Caminade, K. M. McIntyre, and A. E. Jones, "Impact of recent and future climate change on vector-borne diseases," *Annals of the New York Academy of Sciences*, vol. 1436, no. 1, p. 157, 2019.

[170] R. Müller, F. Reuss, V. Kendrovski, and D. Montag, "Vector-Borne Diseases," in *Biodiversity and Health in the Face of Climate Change*, pp. 67–90, Springer, 2019.

[171] S. Paz, "Effects of climate change on vector-borne diseases: an updated focus on West Nile virus in humans," *Emerging Topics in Life Sciences*, vol. 3, no. 2, pp. 143–152, 2019.

[172] B. T. Grenfell, A. P. Dobson, H. Moffatt, *et al.*, *Ecology of infectious diseases in natural populations*, vol. 7. Cambridge University Press, 1995.

[173] R. M. Anderson and R. M. May, "Population biology of infectious diseases: Part i," *Nature*, vol. 280, no. 5721, p. 361, 1979.

[174] R. M. May and R. M. Anderson, "Population biology of infectious diseases: Part ii," *Nature*, vol. 280, no. 5722, p. 455, 1979.

[175] J. M. Heffernan, R. J. Smith, and L. M. Wahl, "Perspectives on the basic reproductive ratio," *Journal of the Royal Society Interface*, vol. 2, no. 4, pp. 281–293, 2005.

[176] K. Dietz, "The estimation of the basic reproduction number for infectious diseases," *Statistical methods in medical research*, vol. 2, no. 1, pp. 23–41, 1993.

[177] H. J. Wearing, P. Rohani, and M. J. Keeling, "Appropriate models for the management of infectious diseases," *PLoS medicine*, vol. 2, no. 7, p. e174, 2005.

[178] L. C. Monteiro, J. R. de Souza, and C. M. de Albuquerque, "Eclosion rate, development and survivorship of *Aedes albopictus* (Skuse)(Diptera: Culicidae) under different water temperatures," *Neotropical entomology*, vol. 36, no. 6, pp. 966–971, 2007.

[179] F. A. Verhoef, G. J. Venter, and C. W. Weldon, "Thermal limits of two biting midges, Culicoides imicola Kieffer and C. bolitinos Meiswinkel (Diptera: Ceratopogonidae)," *Parasites & vectors*, vol. 7, no. 1, p. 384, 2014.

[180] A. L. Lloyd, "Realistic distributions of infectious periods in epidemic models: changing patterns of persistence and dynamics," *Theoretical Population Biology*, vol. 60, no. 1, pp. 59–71, 2001.

[181] T. J. Lysyk and T. Danyk, "Effect of temperature on life history parameters of adult Culicoides sonorensis (Diptera: Ceratopogonidae) in relation to geographic origin and vectorial capacity for bluetongue virus," *Journal of Medical Entomology*, vol. 44, no. 5, pp. 741–751, 2007.

[182] B. Mullens, A. Gerry, T. Lysyk, and E. Schmidtmann, "Environmental effects on vector competence and virogenesis of bluetongue virus in Culicoides: interpreting laboratory data in a field context," *Vet Ital*, vol. 40, no. 3, pp. 160–166, 2004.

[183] S. Carpenter, A. Wilson, J. Barber, E. Veronesi, P. Mellor, G. Venter, and S. Gubbins, "Temperature dependence of the extrinsic incubation period of orbiviruses in Culicoides biting midges," *PloS one*, vol. 6, no. 11, p. e27987, 2011.

[184] J. Vaughan and E. Turner Jr, "Development of immature Culicoides variipennis (Diptera: Ceratopogonidae) from Saltville, Virginia, at constant laboratory temperatures," *Journal of medical entomology*, vol. 24, no. 3, pp. 390–395, 1987.

[185] C. D. Harvell, C. E. Mitchell, J. R. Ward, S. Altizer, A. P. Dobson, R. S. Ostfeld, and M. D. Samuel, "Climate warming and disease risks for terrestrial and marine biota," *Science*, vol. 296, no. 5576, pp. 2158–2162, 2002.